

# User manual for software “HIFU beam”

**Simulator of acoustic fields generated  
by HIFU single element transducers  
and annular arrays in a flat-layered  
medium imitating biological tissues**



Laboratory for Industrial and Medical Ultrasound

July 2021

# Contents

---

1. Introduction .....	3
<i>Overview</i> .....	3
<i>History, Credits, and Contributors</i> .....	3
<i>License</i> .....	5
2. Installation .....	6
3. Table of symbols.....	8
4. Numerical model .....	11
<i>Governing equations</i> .....	11
<i>Parabolic approximation of diffraction</i> .....	13
<i>Wide angle parabolic approximation</i> .....	15
<i>Setting a boundary condition in the ‘KZK’ mode. Equivalent source model.</i> .....	19
<i>Setting a boundary condition in the ‘WAPE’ mode</i> .....	20
<i>Realization of multi-layer medium with a power law absorption</i> .....	21
5. Setting parameters for simulation .....	23
<i>First step: Propagation equation selection</i> .....	23
<i>Second step: Acoustic source –single-element transducer or annular array</i> .....	23
<i>Third step: Propagation in a multi-layer medium</i> .....	30
<i>Fourth step: Setting the grid and output domain parameters</i> .....	32
6. Examples of numerical simulations .....	34
<i>Single-element focused transducer, propagation in water</i> .....	34
<i>‘WAPE’ vs. ‘KZK’: certain differences in calculation details</i> .....	42
<i>Examples of scripts to plot results directly from .mat files</i> .....	43
<i>Ring-shaped array, propagation in water</i> .....	45
<i>Single-element spherical HIFU source, multi-layered medium</i> .....	48
7. Appendix: numerical methods and algorithms .....	51
<i>Boundary Conditions for the Radial Coordinate (PML)</i> .....	51
<i>Diffraction operator</i> .....	52
<i>Nonlinear operator</i> .....	55
<i>Absorption</i> .....	55
8. References and links .....	56

# Introduction

---

## Overview

The “HIFU beam” is a MATLAB application combined with a binary executable designed for numerical simulation of acoustic fields generated by HIFU single element transducers and annular arrays in a flat-layered medium imitating biological tissues. The numerical models incorporated in the simulator are based on one-way propagation equations, either a KZK-type (Khokhlov-Zabolotskaya-Kuznetsov) equation or a one-way Westervelt-type equation, which account for both linear and nonlinear wave propagation of radially symmetric ultrasound beams in homogeneous and layered media with thermoviscous or power law acoustic absorption.



The differences between the two available modes, ‘KZK’ and ‘WAPE’ (abbreviation from Wide-Angle Parabolic Equation), are the approximations used when solving the diffraction operator and setting the boundary conditions to the models. The KZK equation accounts for diffraction in a parabolic approximation and the boundary condition is set in the initial plane using either the nominal geometric parameters of the source or using an equivalent source model. Wide-angle Padé approximations are used for solving the diffraction operator in the Westervelt-type equation with the boundary condition set on the spherical surface of the source. The core functionality of simulations is provided by finite-difference numerical schemes.

A graphical user interface to the application has been designed to ensure both flexibility and user friendliness. The interface uses MATLAB GUI functionality to set user-defined input parameters to the numerical model, to run simulations, and to read and visualize output data. The computational engine is compiled to a binary file from FORTRAN 2003 source code. The binary code has been optimized for speed, accuracy, and parallel execution on multi-core processors. The “HIFU beam” project is still under development and its functionality is still evolving. We hope that feedback from user community can help us to make it better.

## History, Credits, and Contributors

The “HIFU beam” application has been developed within the Laboratory for Industrial and Medical Ultrasound (LIMU) at Moscow State University. Prior to the appearance of this software, several KZK solvers for axially symmetric acoustic beams were known. Some of them, such as the KZK Texas Code, were published, others were developed and used privately in different laboratories worldwide.

A private KZK equation solver has been under development since 2001 in the scientific group of Vera Khokhlova and Oleg Sapozhnikov at Moscow State University.<sup>1</sup> Several generations of PhD and MS students of LIMU have contributed to further development of this private version. The main contributors are Svetlana Kashcheeva,<sup>2</sup> Elena Filonenko,<sup>3</sup> Anatoliy Ponomarev,<sup>4</sup> Olga Georg (Bessonova),<sup>5,6,7</sup> Mikhail Averiyarov,<sup>8</sup> Maria Karzova,<sup>9</sup> Pavel Rosnitskiy,<sup>10,11,12</sup> and Petr Yuldashev (see sections “People” and “Alumni” at our website <https://limu.msu.ru/?language=en>).

Since 2015, we started to enhance the KZK equation with an equivalent source model<sup>10,11,12</sup> in order to increase the accuracy of the parabolic approximation when simulating strongly focused beams. More accurate, but much more computationally extensive 3D models based on the one-way version of the Westervelt equation was developed by Petr Yuldashev<sup>13</sup> and then applied to simulating strongly nonlinear fields from various high power sources.<sup>14,15,16,17,18</sup> Later, Petr developed a code to resolve the diffraction operator in the one-way Westervelt equation using wide-angle approximations based on Padé expansions.<sup>19</sup> This simplified the algorithm and made it possible to accurately account for diffraction effects in a sufficiently large range of diffraction angles using finite-difference methods, similar to those used in solving the KZK equation.

However, as it often happens with numerical codes, our private versions were not organized and not documented sufficiently to be presented to a wider user community. The idea behind the “HIFU beam” program was to create a new piece of software to represent the valuable experience of LIMU on simulating the KZK and wide-angle parabolic equations in a structured and documented form.

The overall development of the “HIFU beam” complex has been driven by Petr Yuldashev, Vera Khokhlova, Oleg Sapozhnikov, Pavel Rosnitskiy, and Maria Karzova since 2015. Various versions of the code have been successfully validated through modeling and measuring nonlinear fields generated by various HIFU transducers in collaborative studies performed with our colleagues from the Center for Industrial and Medical Ultrasound of the Applied Physics Laboratory, University of Washington in Seattle: Michael Averkiou<sup>4</sup> Michael Bailey,<sup>20, 21, 22, 23</sup> Michael Canney,<sup>21,22,23</sup> Wayne Kreider,<sup>24</sup> Tatiana Khokhlova,<sup>23,24</sup> Adam Maxwell,<sup>11</sup> and Lawrence Crum.<sup>4,20,21,22,23</sup>

Without breaking the tradition, the FORTRAN (2003 standard) programming language was chosen for realization of the computational engine. Since the MATLAB system is widely used in the scientific community to create GUI and text interfaces to different solvers, we also followed this choice. Petr Yuldashev developed software architecture and implemented all source codes both on MATLAB and FORTRAN. We are grateful to our collaborators and students who have contributed to this project through suggestions, usage feedback, and bug reports.

### *Major publication*

P.V. Yuldashev, M.M. Karzova, W. Kreider, P.B. Rosnitskiy, O.A. Sapozhnikov, V.A. Khokhlova. “HIFU beam”: a simulator for predicting axially symmetric nonlinear acoustic fields generated by focused transducers in a layered medium. IEEE Transactions on Ultrasonics, Ferroelectrics, and Frequency Control, April 20 2021. DOI: 10.1109/TUFFC.2021.3074611

## License

**Russian patent:** № 2017613572, obtained on 6<sup>th</sup> of February 2017

**Authors:** Petr V. Yuldashev, Vera A. Khokhlova, Oleg A. Sapozhnikov, Pavel B. Rosnitsky, and Maria M. Karzova

Формы № 43 ИР, КД, ТП-2011

**ФЕДЕРАЛЬНАЯ СЛУЖБА ПО ИНТЕЛЛЕКТУАЛЬНОЙ СОБСТВЕННОСТИ (РОСПАТЕНТ)**

Березинский наб., 30, корп. 1, Москва, Г-89, ГСП-3, 125993. Телефон (8-495) 240-60-15. Факс (8-495) 531-63-18

На № 29-2017 от 03.02.2017  
Наш № 2017301146

При перепечатке следует сослаться на наш № и сообщить дату получения настоящей корреспонденции от 22.03.2017

119991,  
Москва,  
ГСП-1, Ленинские горы, 1, МГУ, Фонд  
«Национальное интеллектуальное  
развитие»

24.03.2017  
304-2017

### УВЕДОМЛЕНИЕ о государственной регистрации

Ставим Вас в известность о том, что программа для ЭВМ: Программа с графической оболочкой для расчета нелинейных ультразвуковых пучков, создаваемых мощными одноэлементными излучателями и кольцевыми решетками

(21) по заявке № 2017610934/69

(22) Дата поступления заявки 06.02.2017

(71) Заявитель(и) Федеральное государственное бюджетное образовательное учреждение высшего образования «Московский государственный университет имени М.В.Ломоносова» (МГУ) (RU)

внесена в Реестр программ для ЭВМ, регистрационный № 2017613572 от 22.03.2017

Приложение: свидетельство о государственной регистрации на 1 л. в 1 экз.

Начальник отдела правового  
обеспечения предоставления  
государственных услуг

Судкин В.И. (499)240-33-42



Терещенко Д.Г.

РОССИЙСКАЯ ФЕДЕРАЦИЯ

**СВИДЕТЕЛЬСТВО**  
о государственной регистрации программы для ЭВМ  
№ 2017613572

Программа с графической оболочкой для расчета нелинейных ультразвуковых пучков, создаваемых мощными одноэлементными излучателями и кольцевыми решетками

Правообладатель: Федеральное государственное бюджетное образовательное учреждение высшего образования «Московский государственный университет имени М.В.Ломоносова» (МГУ) (RU)

Авторы: см. на обороте

Заявка № 2017610934  
Дата поступления 06 февраля 2017 г.  
Дата государственной регистрации  
в Реестре программ для ЭВМ 22 марта 2017 г.

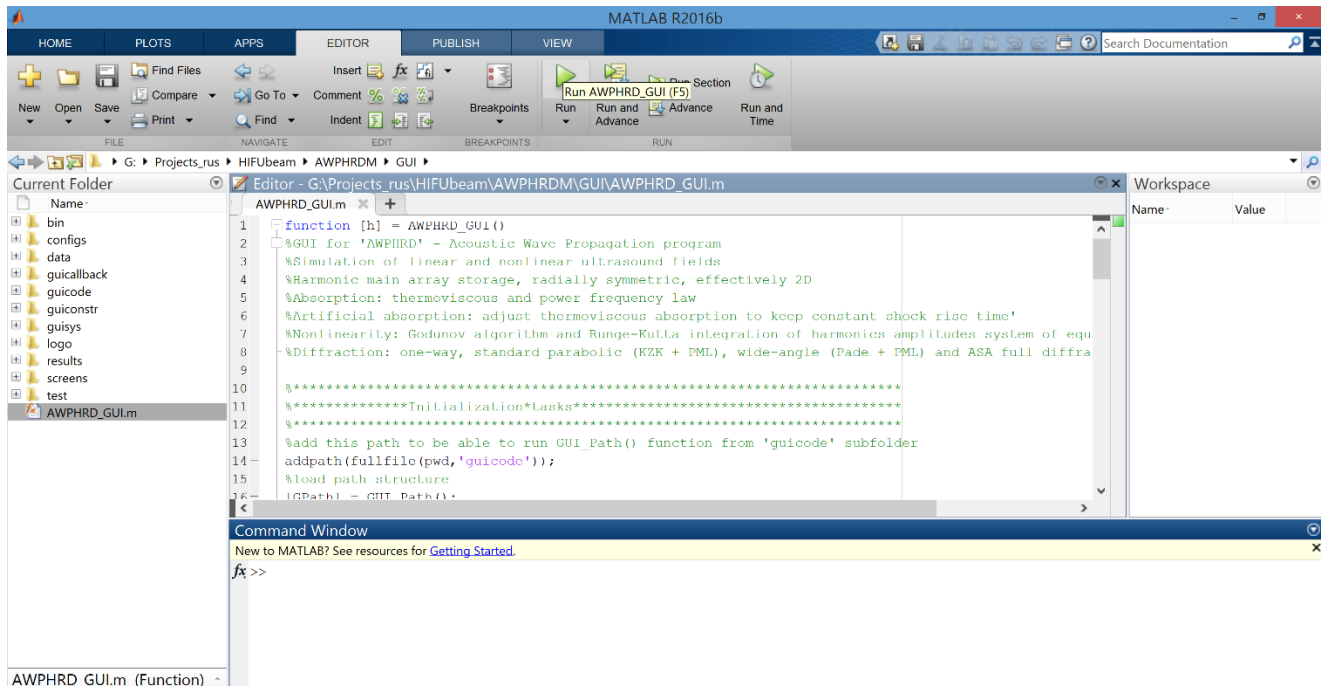
Руководитель Федеральной службы  
по интеллектуальной собственности

Г.П. Ильин

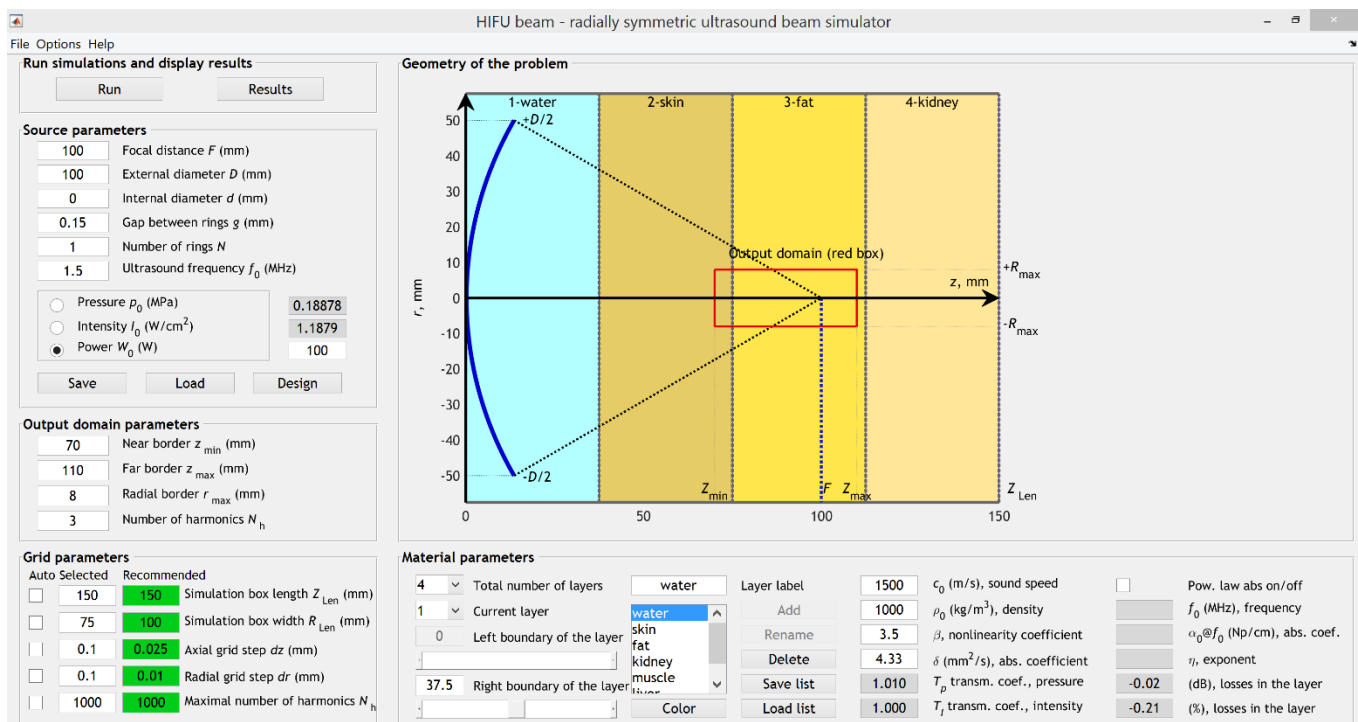
Авторы: **Юлдашев Петр Викторович (RU), Хохлова Вера Александровна (RU), Сапожников Олег Анатольевич (RU), Росницкий Павел Борисович (RU), Карзова Мария Михайловна (RU)**

# Installation

The software “HIFU beam” comprises two folders named “AWPHRDM” and “MatlabLibrary”. Both should be downloaded and placed into the same directory. Then the user should open MATLAB and choose directory where both folders are located as its ‘current folder’. Finally, a file ‘AWPHRD\_GUI.m’ should be run in MATLAB from the folder ‘GUI’ located inside the ‘AWPHRDM’ folder.

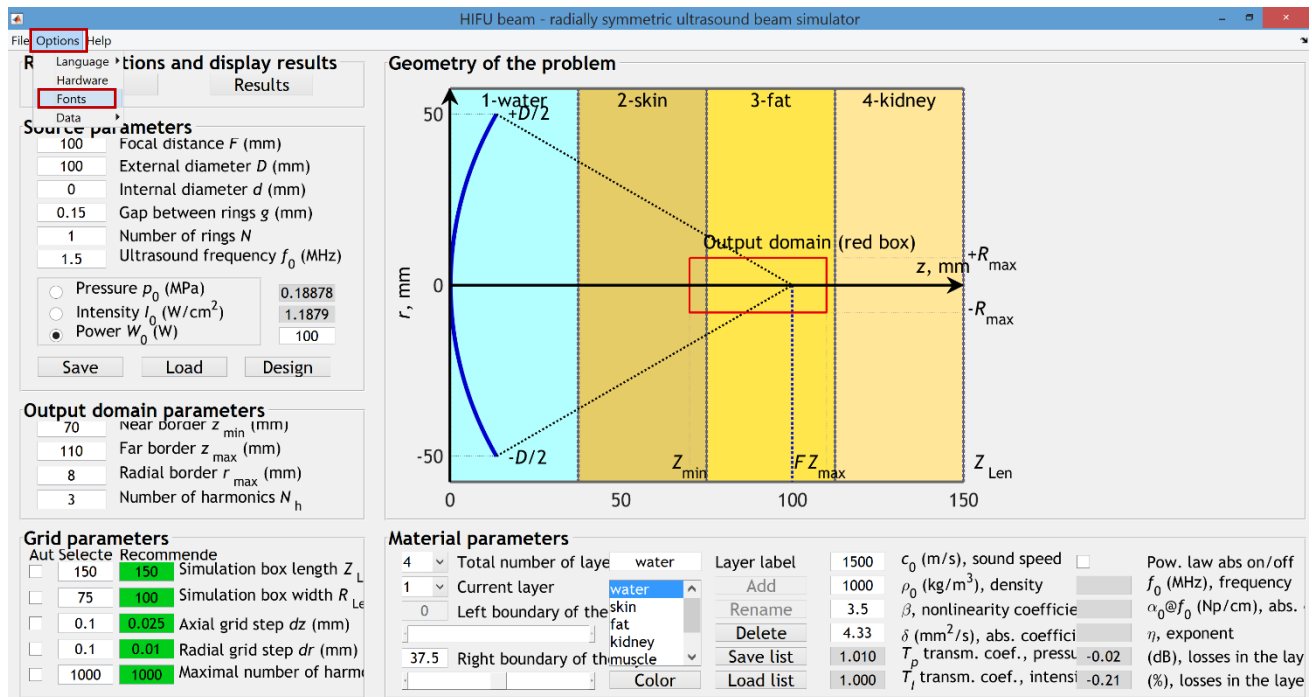


After starting the ‘AWPHRD\_GUI.m’ file in MATLAB, the working interface appears:





If you see that the font size is too large or too small, adjust the font settings by clicking ‘Options’→‘Fonts’ in the main menu and choose appropriate font size for every interface element. Example is given below:



After changing font size for ‘Label text’ on 9 and for other interface elements on 10, the whole interface window should fit the screen perfectly:

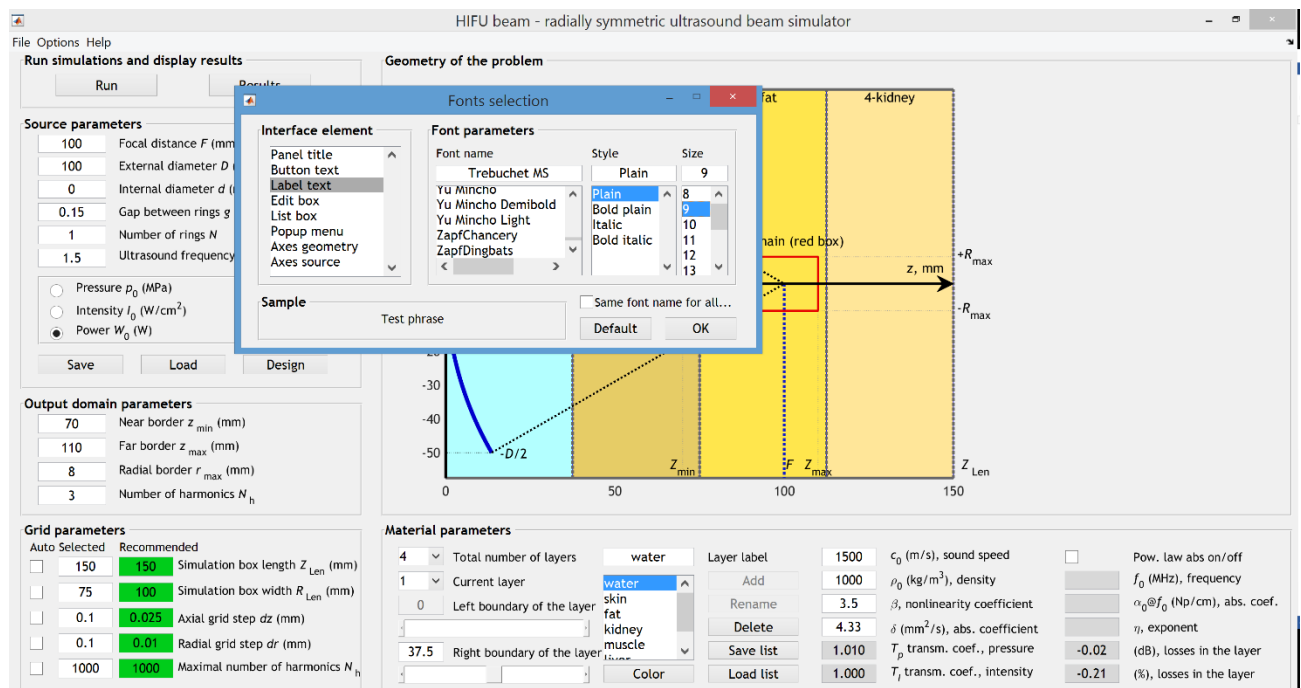


## Table of symbols

Symbol	Description
$p'$	acoustic pressure
$z$	spatial coordinate along the beam axis
$x, y$	spatial coordinates perpendicular to $z$ -axis
$r$	radial coordinate perpendicular to $z$ -axis
$t$	time
$\Delta$	$\Delta = \partial^2/\partial x^2 + \partial^2/\partial y^2 + \partial^2/\partial z^2$ , Laplace operator
$\Delta_{\perp}$	$\Delta_{\perp} = \partial^2/\partial x^2 + \partial^2/\partial y^2 = \partial^2/\partial r^2 + r^{-1} \partial/\partial r$ , transverse Laplace operator
$\rho_0$	ambient density
$c_0$	isentropic sound speed
$\beta$	nonlinearity coefficient
$\delta$	diffusivity of sound
$L'_a(p')$	linear operator describing power law absorption
$\mathbf{u}'$	vibrational velocity
$f$	wave frequency
$\tau$	$\tau = t - z/c_0$ , retarded time
$p$	acoustic pressure in the retarded coordinate system
$\omega$	$\omega = 2\pi f$ , angular frequency
$p_n$	acoustic pressure amplitude of the $n$ th harmonic of the fundamental frequency $\omega$ in the Fourier expansion: $p(\tau, r, z) = \sum_{n=-\infty}^{\infty} p_n(r, z) e^{-in\omega\tau}$
$L_a(p)$	linear operator describing power law absorption in the retarded coordinate system
$\tilde{L}_a(p_n)$	linear operator describing power law absorption in the retarded coordinate system in the frequency domain
$k$	$k = \omega/c_0$ , wavenumber corresponding to angular frequency $\omega$
$p'_\omega$	$p'_\omega = \int p' e^{i\omega t} dt$ , particular Fourier component of acoustic pressure at the angular frequency $\omega$
$p_\omega$	$p'_\omega(r, z) = p_\omega(r, z) \exp(ikz)$ , slowly varying complex pressure amplitude at angular frequency $\omega$ in the retarded coordinate system. Can be found also as $p_\omega = \int p e^{i\omega\tau} d\tau$ .
$\hat{L}$	$\hat{L} = \frac{\Delta_{\perp}}{k^2} = \frac{1}{k^2} \left( \frac{\partial^2}{\partial r^2} + \frac{1}{r} \frac{\partial}{\partial r} \right)$ , differential operator
$\hat{Q}^2$	$\hat{Q}^2 = 1 + \hat{L} = 1 + \frac{1}{k^2} \left( \frac{\partial^2}{\partial r^2} + \frac{1}{r} \frac{\partial}{\partial r} \right)$ , differential operator
$q_n$	real coefficients of Taylor expansion
$\hat{A}$	$\hat{A} = \exp \left[ ik\Delta z \left( \sqrt{1 + \hat{L}} - 1 \right) \right]$ , propagator of one-way full diffraction equation



$a_n, b_n$	coefficients of the Padé approximation
$(N, N)$	order of the Padé approximation
$\hat{A}_{NN}$	$\hat{A}_{NN} = \left( \sum_{n=0}^N a_n \hat{L}^n \right) / \left( \sum_{n=0}^N b_n \hat{L}^n \right)$ , Padé approximation of the order $(N, N)$ of the propagator $\hat{A}$
$\alpha_1 \dots \alpha_N$	roots of the polynomial $\sum_{n=0}^N a_n \hat{L}^n = 0$
$\beta_1 \dots \beta_N$	roots of the polynomial $\sum_{n=0}^N b_n \hat{L}^n = 0$
$\mu_n$	$\mu_n = -1/\alpha_n$
$\nu_n$	$\nu_n = -1/\beta_n$
$F$	Radius of curvature of the source
$D$	external diameter of the source projection to the plane $z = 0$
$p_0$	pressure amplitude at the source surface
$f_0$	ultrasound frequency of the source
$\omega_0$	$\omega_0 = 2\pi f_0$ , ultrasound angular frequency of the source
$k_0$	$k_0 = \omega_0/c_0$ , wavenumber at the source angular frequency $\omega_0$
F-number	ratio of focal length to diameter of the source: $F\text{-number} = F / D$
$D_p, F_p, p_0^p$	diameter, focal distance, and initial pressure amplitude of the equivalent source, respectively
$p'_{\omega, n}$	complex pressure amplitude at angular frequency $\omega$ for the incident wave in the $n$ -th layer
$p'_{\omega, r}$	complex pressure amplitude at angular frequency $\omega$ for the reflected wave
$\rho_n, c_n$	density and sound speed in the $n$ -th layer, respectively
$u'_{\omega, zn}$	$z$ -projection of vibrational velocity at angular frequency $\omega$ for the incident wave in the $n$ -th layer
$u'_{\omega, zr}$	$z$ -projection of vibrational velocity at angular frequency $\omega$ for the reflected wave
$T_p$	transmission coefficient for pressure from one layer to another one
$T_I$	transmission coefficient for intensity from one layer to another one
$\alpha_0$	absorption coefficient for biological tissue at the frequency $\omega_0$
$\alpha$	absorption coefficient at the frequency $\omega$
$\eta$	exponent in the absorption power law
$c(\omega)$	frequency-dependent phase velocity in tissue
$\Delta c$	deviation of phase velocity in tissue induced by dispersion from the reference value of the sound speed: $\Delta c = c(\omega) - c_0$
$d$	internal diameter of the source (diameter of the central opening)
$N$	number of rings of an annular array
$g$	gap between rings
$W_0$	acoustic power of the source
$I_0$	intensity at the source surface

$\lambda$	wavelength
$\varphi$	focusing angle
$h$	depth of a spherical bowl
$S_{\text{full}}$	total surface area of a spherical cup
$h_{\text{ext}}$	bowl depth corresponding to the external diameter $D$
$h_{\text{int}}$	bowl depth corresponding to the internal diameter $d$
$S_{\text{act}}$	active surface area of the source
$p_{\text{F}}$	pressure amplitude at the focus
$K_{\text{p}}$	focusing gain defined as a ratio of the pressure amplitude at the focus $p_{\text{F}}$ to the initial pressure amplitude $p_0$ at the source assuming propagation in non-absorbing medium
$K_{\text{p,abs}}$	focusing gain with account for absorption losses
$Z_{\text{Len}}$	simulation box length
$R_{\text{Len}}$	simulation box width
$dz$	axial grid step
$dr$	radial grid step
$N_{\text{h}}$	maximum number of harmonics
$z_{\text{min}}$	proximal border of the output domain
$z_{\text{max}}$	distant border of the output domain
$r_{\text{max}}$	radial border of the output domain
$p_{+}$	peak positive pressure (level of the pressure maximum in the waveform)
$p_{-}$	peak negative pressure (level of the pressure minimum in the waveform)
$A_{\text{sh}}$	shock amplitude (pressure jump at the shock front)
$r_{\text{PML}}$	radial coordinate where perfectly matched layer (PML) begins
$w$	$w = R_{\text{Len}} - r_{\text{PML}}$ , thickness of the PML
$\sigma(r)$	positive attenuation function in the PML
$\tilde{r}$	$\tilde{r} = r + \int_{r_{\text{PML}}}^r \frac{i\sigma(r')}{\omega} dr'$ , complex radial coordinate for the PML
$S(r)$	$S(r) = 1 + \frac{i\sigma(r)}{\omega}$ , stretch factor for the PML
$\bar{S}(r)$	$\bar{S}(r) = 1 + \frac{1}{r} \int_{r_{\text{PML}}}^r \frac{i\sigma(r')}{\omega} dr'$ , coordinate transformation factor for the PML

## Numerical model

Here we describe governing equations used in the “HIFU beam” software, setting boundary conditions to the numerical models, and realization of multi-layer propagation medium. In a current Version 1.0 there are two modes, ‘KZK’ and ‘WAPE’, which are based on numerical simulations of the KZK equation and of the one-way Westervelt-type equation with account for diffraction effects using wide-angle parabolic approximation, respectively.

### Governing equations

#### 3D Westervelt equation

In nonlinear acoustics, the basic equation that governs propagation of nonlinear acoustic waves in arbitrary directions is the Westervelt equation, which takes into account nonlinearity, diffraction, and thermoviscous absorption:

$$\Delta p' - \frac{1}{c_0^2} \frac{\partial^2 p'}{\partial t^2} = -\frac{\beta}{\rho_0 c_0^4} \frac{\partial^2 p'^2}{\partial t^2} - \frac{\delta}{c_0^4} \frac{\partial^3 p'}{\partial t^3} - L'_a(p'). \quad (1)$$

Here  $p'$  is the acoustic pressure,  $\Delta p' = \partial^2 p' / \partial x^2 + \partial^2 p' / \partial y^2 + \partial^2 p' / \partial z^2$  is the Laplacian,  $z$  is the spatial coordinate along the beam axis,  $x$  and  $y$  are spatial coordinates perpendicular to  $z$ ,  $t$  is time. Parameters  $\rho_0$ ,  $c_0$ ,  $\beta$ , and  $\delta$  are ambient (or equilibrium) density, isentropic sound speed, nonlinearity coefficient, and diffusivity of sound of the medium, respectively. Additional linear operator  $L'_a(p')$  describes the power law absorption and corresponding dispersion, which are observed in biological tissues.

In the retarded coordinate system,  $\tau = t - z / c_0$ , the Eq. (1) can be rewritten as:

$$\frac{\partial^2 p}{\partial \tau \partial z} = \frac{c_0}{2} \Delta p + \frac{\beta}{2 \rho_0 c_0^3} \frac{\partial^2 p^2}{\partial \tau^2} + \frac{\delta}{2 c_0^3} \frac{\partial^3 p}{\partial \tau^3} + L_a(p), \quad (2)$$

where  $p$  is the acoustic pressure and  $L_a(p)$  is the operator describing the power law absorption and dispersion, in the retarded coordinate system, respectively. Note that the Westervelt Eq. (1) is valid for adiabatic flow and neglects Lagrangian energy density


$\frac{\rho_0 \mathbf{u}'^2}{2} - \frac{p'^2}{2 \rho_0 c_0^2}$  in the nonlinear term, where  $\mathbf{u}'$  is the vibrational velocity.


Simulation of the three-dimensional Westervelt Eq. (2) is numerically challenging and only few scientific groups have numerical codes for these simulations. Thus, simplified models are more commonly used by scientific community for simulating high-intensity ultrasonic fields. In “HIFU beam”, we provide simulators of these commonly used simplified equations, not the general full-wave 3D Westervelt equation. Below we shortly derive governing equations used in “HIFU beam” sequentially simplifying the Westervelt Eq. (2).


## 2D radially symmetric Westervelt equation in the time domain


Since typical HIFU single-element transducers and annular arrays have radially symmetric geometry, one can use two-dimensional radially symmetric form of the Eq. (2):

$$\frac{\partial^2 p}{\partial \tau \partial z} = \frac{c_0}{2} \left( \frac{\partial^2 p}{\partial z^2} + \frac{\partial^2 p}{\partial r^2} + \frac{1}{r} \frac{\partial p}{\partial r} \right) + \frac{\beta}{2\rho_0 c_0^3} \frac{\partial^2 p^2}{\partial \tau^2} + \frac{\delta}{2c_0^3} \frac{\partial^3 p}{\partial \tau^3} + L_a(p). \quad (3)$$

  
**Diffraction**  
*(full diffraction)*

  
**Nonlinearity**

  
**Thermo-  
viscous  
absorption**

  
**Power law  
absorption  
and  
dispersion**

where  $r$  is the radial coordinate.

In the frequency domain, the pressure is represented in the form of Fourier series expansion of harmonic components:  $p(\tau, r, z) = \sum_{n=-\infty}^{\infty} p_n(r, z) e^{-in\omega\tau}$ , where  $p_n(r, z)$  is a discrete Fourier harmonic of the acoustic pressure at angular frequency  $n\omega$ ,  $\omega = 2\pi f$  and  $f$  is frequency. According to this, Eq. (3) can be rewritten in the frequency domain as:

$$\frac{\partial p_n}{\partial z} = \frac{ic_0}{2n\omega} \Delta p_n - \frac{i\beta n\omega}{2\rho_0 c_0^3} \left( 2 \sum_{m=1}^{\infty} p_m^* p_{n+m} + \sum_{m=1}^{n-1} p_m p_{n-m} \right) - \frac{\delta n^2 \omega^2}{2c_0^3} p_n + \tilde{L}_a(p_n). \quad (4)$$


Here, constant component of acoustic pressure field is assumed equal to zero,  $p_n^*$  denotes the complex conjugate harmonic amplitude, and  $\tilde{L}_a(p_n)$  is a linear operator for power law absorption and dispersion represented in a frequency domain and described in the section ‘*Realization of multi-layer medium with a power law absorption*’.

In simulations, both time-domain and frequency-domain representations of the acoustic field are used.<sup>6,13,15</sup> From numerical point of view, the simulation of Eq. (3) is significantly complicated by the second derivative of the pressure with respect to the coordinate  $z$ :  $\frac{\partial^2 p}{\partial z^2}$ . Neglecting this term means that the pressure  $p(\tau, r, z)$  slowly changes as a function of  $z$ . This assumption leads to the KZK equation.

## 2D radially symmetric KZK equation (mode ‘KZK’) in time domain

The first mode ‘KZK’ available in the “HIFU beam” software is a solver of the KZK-type (Khokhlov-Zabolotskaya-Kuznetsov) equation. The KZK equation describes nonlinear acoustic beams in thermoviscous medium which accounts for diffraction effects in the parabolic approximation. For radially symmetric acoustic beams the KZK equation is:

$$\frac{\partial^2 p}{\partial \tau \partial z} = \frac{c_0}{2} \left( \frac{\partial^2 p}{\partial r^2} + \frac{1}{r} \frac{\partial p}{\partial r} \right) + \frac{\beta}{2\rho_0 c_0^3} \frac{\partial^2 p^2}{\partial \tau^2} + \frac{\delta}{2c_0^3} \frac{\partial^3 p}{\partial \tau^3} + L_a(p). \quad (5)$$



Diffraction (in parabolic approximation)      Nonlinearity      Thermo-viscous absorption      Power law absorption and dispersion

In the frequency domain, Eq. (5) can be rewritten as:

$$\frac{\partial p_n}{\partial z} = \frac{ic_0}{2n\omega} \Delta_{\perp} p_n - \frac{i\beta n\omega}{2\rho_0 c_0^3} \left( 2 \sum_{m=1}^{\infty} p_m^* p_{n+m} + \sum_{m=1}^{n-1} p_m p_{n-m} \right) - \frac{\delta n^2 \omega^2}{2c_0^3} p_n + \tilde{L}_a(p_n), \quad (6)$$

where  $\Delta_{\perp}$  is the transverse Laplacian.

The only difference between the KZK, Eq. (5), and the Westervelt, Eq. (3), equations is in their diffraction operators. The diffraction operator of the Westervelt Eq. (3) contains an extra pressure derivative of the second order with respect to  $z$  in comparison with the KZK Eq. (5). This difference reflects the fact that diffraction operator of the Westervelt equation exactly corresponds to the linear wave equation, while the KZK uses small diffraction angle approximation. It results in different accuracy of these two models in the case of focused beams. Obviously, for high focusing angles, the Westervelt equation is more accurate than the KZK equation. It is possible, however, to modify source boundary condition to the KZK equation to increase its accuracy. For this purpose, an equivalent source model is used and is described in the subsection ‘Setting a boundary condition in the ‘KZK’ mode’ later in this section.

### Parabolic approximation of diffraction

The linearized version of the Westervelt Eq. (1) is derived from the linear wave equation by assuming nonlinear and thermoviscous absorption coefficients are equal to zero and only describing the diffraction effects:

$$\frac{\partial^2 p'}{\partial z^2} + \frac{\partial^2 p'}{\partial r^2} + \frac{1}{r} \frac{\partial p'}{\partial r} - \frac{1}{c_0^2} \frac{\partial^2 p'}{\partial t^2} = 0. \quad (7)$$

The solution to the linearized wave equation, Eq. (7), can be derived for a complex pressure amplitude of the specified Fourier harmonic  $p'_{\omega}$  with an angular frequency  $\omega$ :

$$p'_{\omega}(\omega, r, z) = \int p'(t, r, z) e^{i\omega t} dt. \quad (8)$$

Substituting Eq. (8) into the wave Eq. (7) yields the classical Helmholtz equation for the complex pressure amplitude  $p'_{\omega}$ :

$$\frac{\partial^2 p'_{\omega}}{\partial z^2} + \frac{\partial^2 p'_{\omega}}{\partial r^2} + \frac{1}{r} \frac{\partial p'_{\omega}}{\partial r} + k^2 p'_{\omega} = 0, \quad (9)$$

where  $k = \omega / c_0$  is the wavenumber. If the differential operators  $\hat{L}$  and  $\hat{Q}$  are introduced as:

$$\hat{L} = \frac{\Delta_{\perp}}{k^2} = \frac{1}{k^2} \left( \frac{\partial^2}{\partial r^2} + \frac{1}{r} \frac{\partial}{\partial r} \right), \quad (10)$$

and

$$\hat{Q}^2 = 1 + \hat{L} = 1 + \frac{\Delta_{\perp}}{k^2} = 1 + \frac{1}{k^2} \left( \frac{\partial^2}{\partial r^2} + \frac{1}{r} \frac{\partial}{\partial r} \right), \quad (11)$$

then the Helmholtz equation can be written in the operator form as follows:

$$\frac{\partial^2 p'_{\omega}}{\partial z^2} + k^2 \hat{Q}^2 p'_{\omega} = 0. \quad (12)$$

In the case of a homogeneous propagation medium, the wavenumber  $k$  doesn't depend on  $z$  coordinate. Therefore, the Helmholtz equation can be factored into two propagation equations:

$$\begin{aligned} \frac{\partial p'_{\omega}}{\partial z} + ik \hat{Q} p'_{\omega} &= 0, \\ \frac{\partial p'_{\omega}}{\partial z} - ik \hat{Q} p'_{\omega} &= 0, \end{aligned} \quad (13)$$

each of which corresponds to acoustic beams traveling in either the negative or the positive directions of the axis  $z$ .

To derive a parabolic approximation of the diffraction operator, one considers only one-way propagation in the positive direction of  $z$  axis:

$$\frac{\partial p'_{\omega}}{\partial z} = ik \hat{Q} p'_{\omega} \quad (14)$$

and represents the operator  $\hat{Q}$  via operator  $\hat{L}$  using formal Taylor expansion:

$$\hat{Q} = \sqrt{1 + \hat{L}} = 1 + \sum_{n=1}^{\infty} q_n \hat{L}^n, \quad (15)$$

where real numbers  $q_n$  are coefficients of Taylor series of square-root function.

The parabolic approximation of the one-way Helmholtz equation is obtained when only the first order term is retained in the Taylor expansion of the operator  $\hat{Q}$ :

$$\hat{Q} \approx 1 + \hat{L} / 2. \quad (16)$$



The pressure amplitude in Eq. (12) can be represented as a product of slowly varying complex amplitude in the retarded coordinate system  $p_\omega$  and an oscillating function at carrier frequency  $\exp(ikz)$ :

$$p'_\omega(r, z) = p_\omega(r, z) \exp(ikz), \quad (17)$$

the parabolic diffraction Eq. (14) in the operator form is:

$$\frac{\partial p_\omega}{\partial z} = \frac{ik}{2} \hat{L} p_\omega. \quad (18)$$

Substitution of the operator  $\hat{L}$  yields the parabolic diffraction equation in its standard form:

$$\frac{\partial p_\omega}{\partial z} = \frac{i}{2k} \Delta_\perp p_\omega = \frac{i}{2k} \frac{1}{r} \frac{\partial}{\partial r} \left( r \frac{\partial p_\omega}{\partial r} \right). \quad (19)$$

### Wide angle parabolic approximation

‘WAPE’ (abbreviation from Wide-Angle Parabolic Equation) mode in the “HIFU beam” software is based on more accurate approximation of the diffraction operator, Eq. (15). Retaining higher-order terms in the expansion, Eq. (15), yields more accurate wide-angle parabolic approximation equations. However, from numerical point of view, there is a disadvantage in using such expansions because they include higher-order spatial derivatives that complicates numerical schemes and their solutions. In practice, the approximate equation is constructed in a different way.

If the operator  $\hat{Q}$  does not depend on the propagation distance  $z$ , which is true for homogeneous propagation medium, the commutator of two operators  $\left[ \partial/\partial z, \hat{Q} \right]$  is equal to zero. In this case the second derivative of the pressure with respect to  $z$  is calculated using the one-way full diffraction propagation Eq. (14):

$$\frac{\partial^2 p'_\omega}{\partial z^2} = \frac{\partial}{\partial z} \frac{\partial p'_\omega}{\partial z} = \frac{\partial}{\partial z} (ik \hat{Q} p'_\omega) = ik \hat{Q} \frac{\partial p'_\omega}{\partial z} = ik \hat{Q} ik \hat{Q} p'_\omega = (ik \hat{Q})^2 p'_\omega. \quad (20)$$

Similarly, for  $n$ -th derivative of the complex pressure amplitude  $p'_\omega$  the result is:

$$\frac{\partial^n p'_\omega}{\partial z^n} = (ik \hat{Q})^n p'_\omega. \quad (21)$$

Using the derivatives, Eq. (21), the Taylor expansion of the pressure field at  $z + \Delta z$ :

$$p'_\omega(z + \Delta z) = p'_\omega(z) + \frac{1}{1!} (ik \hat{Q})^1 p'_\omega(z) \Delta z + \dots + \frac{1}{n!} (ik \hat{Q})^n p'_\omega(z) \Delta z^n + \dots$$

can be expressed as:

$$p'_\omega(z + \Delta z) = \left[ 1 + \frac{1}{1!} (ik\Delta z \hat{Q})^1 + \dots + \frac{1}{n!} (ik\Delta z \hat{Q})^n + \dots \right] p'_\omega(z). \quad (22)$$

Note that infinite sum in the parenthesis is the Taylor expansion of the operator  $\exp[ik\Delta z \hat{Q}]$ . Thus, solution of the propagation Eq. (14) can be represented as

$$p'_\omega(z + \Delta z) = \exp[ik\Delta z \hat{Q}] p'_\omega(z). \quad (23)$$

For slowly varying amplitude  $p_\omega$ , ( $p'_\omega(r, z) = p_\omega \exp(ikz)$ ), the Eq. (22) transforms to:

$$p_\omega(z + \Delta z) = \exp[ik\Delta z (\hat{Q} - 1)] p_\omega(z) = \exp\left[ik\Delta z \left(\sqrt{1 + \hat{L}} - 1\right)\right] p_\omega(z). \quad (24)$$

According to this derived Eq. (24), the pressure field  $p_\omega(z + \Delta z)$  at the distance  $z + \Delta z$  is obtained from the pressure field  $p_\omega(z)$  at the distance  $z$  by an action of the propagation operator  $\hat{A}$  (called *propagator*) in the exponential form:

$$\hat{A} = \exp\left[ik\Delta z \left(\sqrt{1 + \hat{L}} - 1\right)\right], \quad (25)$$

which is a function of the operator  $\hat{L}$  and the parameter  $ik\Delta z$ . Note that the propagator  $\hat{A}$  gives the exact solution of the full diffraction one-way propagation Eq. (14) for a homogeneous medium.

The propagator  $\hat{A}$ , similarly to the operator  $\hat{Q}$ , can be approximated by the first several terms in the Taylor series expansion. However, as it was mentioned above, such representation is not practical. Therefore, the propagator is more often represented as a rational function: the ratio of two polynomials of the degree  $N$ , which is also called *the Padé* or *the split-step Padé approximation*.

The Padé approximation of the order  $(N, N)$  of the propagator  $\hat{A}$  is  $\hat{A}_{NN}$ :

$$\hat{A} \approx \hat{A}_{NN} = \frac{a_0 + a_1 \hat{L} + \dots + a_N \hat{L}^N}{b_0 + b_1 \hat{L} + \dots + b_N \hat{L}^N} = \frac{\sum_{n=0}^N a_n \hat{L}^n}{\sum_{n=0}^N b_n \hat{L}^n}. \quad (26)$$

The coefficients  $a_n$  and  $b_n$  of the Padé approximation can be obtained from coefficients of the Taylor expansion of the propagator  $\hat{A}$  up to the  $2N$  terms inclusively:

$$\hat{A} \approx \sum_{l=0}^{2N} q_l \hat{L}^l. \quad (27)$$

Equating Padé approximation and Taylor expansion:

$$\sum_{n=0}^N a_n \hat{L}^n = \sum_{l=0}^{2N} q_l \hat{L}^l \sum_{n=0}^N b_n \hat{L}^n, \quad (28)$$

equations for the coefficients can be obtained by relating coefficients with equal powers of the operator  $\hat{L}$  on the left and right hand sides of Eq. (28). Setting the coefficients  $a_0$  and  $b_0$  equal to unity, one obtains the following system of linear algebraic equations:

$$\begin{cases} a_n = q_n + \sum_{l=1}^n b_l q_{n-l}, & 0 \leq n \leq N \\ 0 = q_n + \sum_{l=1}^N b_l q_{n-l}, & N+1 \leq n \leq 2N. \end{cases} \quad (29)$$

First, the second line of this system is solved for the coefficients  $b_n$  in a matrix form of these linear equations. Then the first line yields values of the coefficients  $a_n$ .

If  $\alpha_1 \dots \alpha_N$  are roots of the polynomial  $\sum_{n=0}^N a_n \hat{L}^n$  and  $\beta_1 \dots \beta_N$  are roots of the polynomial  $\sum_{n=0}^N b_n \hat{L}^n$ , then the approximate propagator  $\hat{A}_{NN}$  can be factorized to:

$$\hat{A}_{NN} = \frac{a_N \prod_{n=1}^N (\hat{L} - \alpha_n)}{b_N \prod_{n=1}^N (\hat{L} - \beta_n)} = \frac{a_N \prod_{n=1}^N \alpha_n (-1)^N \prod_{n=1}^N (-\hat{L} / \alpha_n + 1)}{b_N \prod_{n=1}^N \beta_n (-1)^N \prod_{n=1}^N (-\hat{L} / \beta_n + 1)}. \quad (30)$$

According to Vieta's formulas:

$$\begin{aligned} \prod_{n=1}^N \alpha_n (-1)^N &= \frac{a_0}{a_N} = \frac{1}{a_N}, \\ \prod_{n=1}^N \beta_n (-1)^N &= \frac{b_0}{b_N} = \frac{1}{b_N}, \end{aligned} \quad (31)$$

one obtains:

$$\hat{A}_{NN} = \frac{\prod_{n=1}^N \left( -\frac{\hat{L}}{\alpha_n} + 1 \right)}{\prod_{n=1}^N \left( -\frac{\hat{L}}{\beta_n} + 1 \right)}. \quad (32)$$

Denoting  $\mu_n = -1/\alpha_n$  and  $\nu_n = -1/\beta_n$ , the Padé approximated operator is finally written as:

$$\hat{A}_{NN} = \frac{\prod_{n=1}^N (1 + \mu_n \hat{L})}{\prod_{n=1}^N (1 + \nu_n \hat{L})}. \quad (33)$$

Substituting the Padé approximation of the propagator  $\hat{A}$  from Eq. (33) to the propagation Eq. (24), we obtain the wide-angle parabolic equation:

$$p_{\omega}(z + \Delta z) = \frac{\prod_{n=1}^N (1 + \mu_n \hat{L})}{\prod_{n=1}^N (1 + \nu_n \hat{L})} p_{\omega}(z) \quad (34)$$

or

$$\prod_{n=1}^N (1 + \nu_n \hat{L}) p_{\omega}(z + \Delta z) = \prod_{n=1}^N (1 + \mu_n \hat{L}) p_{\omega}(z). \quad (35)$$

This equation can be solved iteratively for  $n = 1 \dots N$ :

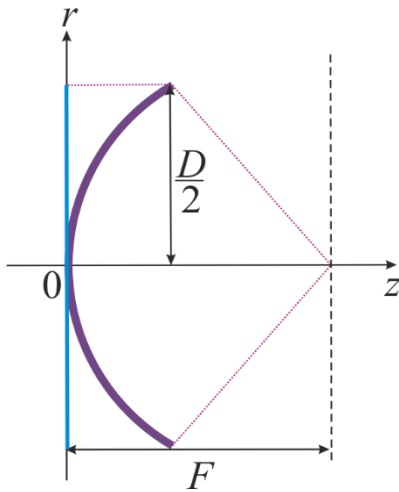
$$(1 + \nu_n \hat{L}) \tilde{p}_{\omega}^n(z + \Delta z) = (1 + \mu_n \hat{L}) \tilde{p}_{\omega}^n(z), \quad (36)$$

where  $\tilde{p}_{\omega}^1(z) = p_{\omega}(z)$ ,  $\tilde{p}_{\omega}^{n+1}(z) = \tilde{p}_{\omega}^n(z + \Delta z)$ ,  $\tilde{p}_{\omega}^N(z + \Delta z) = p_{\omega}(z + \Delta z)$ . Thus, to obtain the solution at the next step  $z + \Delta z$ ,  $N$  equations of the same type should be solved. The larger is the number  $N$ , the better approximation of the initial propagator, Eq. (25) is achieved by Eq. (33). In the simulator “HIFU beam”, the value of  $N = 3$  is used, which means the 6<sup>th</sup> order of accuracy in the Taylor expansion.

In summary, the ‘WAPE’ mode differs from the ‘KZK’ mode by more accurate approximation of the diffraction operator: the 6<sup>th</sup> order approximation instead of the first order approximation of standard parabolic equation. This more accurate approximation uses split-step Padé approximation of the propagator in the one-way propagation equation.

Historically, more accurate approximations than the parabolic one in solving diffraction operator are called ‘wide-angle parabolic approximation’. This term means that the solution of such approximation is valid for larger angles of diffraction than the parabolic approximation yields. Despite the fact that the word ‘parabolic’ is wrong here since the approximation of the dispersion relation of the Helmholtz equation (circle of radius  $k$ ) is not parabolic, we follow this historical term and abbreviate it as ‘WAPE’.

## Setting a boundary condition in the ‘KZK’ mode. Equivalent source model.



In the KZK model the boundary condition is set on the plane

The boundary condition to the radially symmetric KZK Eq. (4) is usually set on the plane  $z=0$  as the pressure amplitude distribution at the source operating with angular frequency  $\omega_0$ :

$$p_{\omega_0}(r, z=0) = \begin{cases} p_0 \exp\left(-i \frac{k_0 r^2}{2F}\right), & r \leq \frac{D}{2} \\ 0, & r > \frac{D}{2}. \end{cases} \quad (37)$$

Here  $F$  is the focal distance of the source,  $D$  is the source diameter as shown in the figure,  $p_0$  is the pressure amplitude at the source surface,  $k_0 = \omega_0/c_0$  is

the wavenumber at a source angular frequency  $\omega_0$ . However, it is well known that with an increase in the focusing angle of the source, the solution to this standard parabolic model starts to deviate from the solution to the full diffraction problem, obtained, for example, in the form of the Rayleigh integral.<sup>25,26</sup>

To extend the applicability limits of the parabolic approximation, we recommend that “HIFU beam” users in the ‘KZK’ mode modify the boundary condition, Eq. (37), to the form of an equivalent source. The basic principles of building the equivalent source model are described in detail in Refs. [10,11]. Here, we briefly summarize the equivalent source, how to obtain its parameters, and the relevant formulae.

The equivalent source is a flat source with parameters that are obtained from the parameters of the real spherical source so that the simulated acoustic field provides minimum difference between the solutions to the parabolic and full diffraction models in the focal region. This matching is achieved by varying the diameter, focal distance, and pressure amplitude in the boundary condition, Eq. (37), as compared to those of the real spherically curved source. In other words, the parameters of the equivalent source are slightly different from parameters of the real source, but its acoustic field in the focal region is in a good agreement (i.e. equivalent) to the real one.

Different approaches can be used to obtain the parameters of the equivalent source for setting the boundary conditions to the KZK equation in order to produce the effects of strong focusing.<sup>21,27</sup> A procedure for finding parameters of the equivalent source used in the software “HIFU beam” is based on matching pressure amplitudes at the focus and positions of the first diffraction zeros of the main focal lobe at the beam axis for solutions obtained with the parabolic model and with the Rayleigh integral. Analytic expressions were obtained for  $(F\text{-number})_p = F_p / D_p$ , focal distance  $F_p$ , and

initial pressure amplitude  $p_0^p$  of the equivalent source as functions of F-number =  $F / D$ ,  $F$ , and  $p_0$  of the spherically focused source:

$$\begin{cases} \frac{F_p}{D_p} = 0.5 \frac{1}{\sqrt{2\pi}} \left( \frac{\sigma_1 \sigma_2}{\sigma_1 - \sigma_2} \right)^{1/2}, \\ k_0 F_p = -\frac{2\sigma_1 \sigma_2}{\sigma_1 + \sigma_2}, \\ p_0^p = 4 \left( \frac{F_p}{D_p} \right)^2 p_0 \frac{F}{F_p} \left( 2 - \sqrt{4 - \left( \frac{D}{F} \right)^2} \right), \end{cases} \quad (38)$$

where

$$\sigma_{1,2} = 4\pi \left( \frac{D}{F} \right) \frac{k_0 F (\mp k_0 F - \pi) \sqrt{4(F/D)^2 - 1} \mp 2(F/D) \left[ (k_0 F)^2 \pm 3\pi k_0 F + 2\pi^2 \right]}{(k_0 F)^2 + 16\pi(\pi \pm k_0 F)(F/D)^2}. \quad (39)$$

It can be shown that the values of the diameter  $D_p$  and the focal distance  $F_p$  always exceed the corresponding values of  $D$  and  $F$ , and the difference between them increases with an increase in the focusing angle of the source.

Note that the parabolic model and the proposed equivalent source method of setting the boundary condition at the initial plane can be used not only for a single spherically focused transducer that vibrates uniformly, but also for sources with slightly nonuniform amplitude distribution and multi-element phased arrays with circular piston elements distributed over a spherical cup. In such cases, the initial pressure amplitude  $p_0^p$ , focal distance  $F_p$ , and the diameter  $D_p$  of the equivalent source should be chosen numerically to obtain the best agreement between the axial solution of the parabolic equation and the calculated or measured field on the axis of the real source.

### *Setting a boundary condition in the ‘WAPE’ mode*

In the ‘WAPE’ mode, the user directly sets parameters of the real HIFU spherical source. The boundary condition in a form of pressure amplitude distribution in the initial plane is obtained in two steps. First, the program uses the Rayleigh integral to calculate acoustic pressure distribution in the plane located in the middle between the edge of the source and the focus, assuming a uniform distribution of the normal component of the vibrational velocity at the source surface. Then, the obtained pressure amplitude distribution is back-propagated to the plane  $z = 0$  using the linear WAPE and further is used as a boundary condition. In contrast to the ‘KZK’ mode, in the ‘WAPE’ mode the pressure amplitude distribution at the initial plane has a nonuniform pattern along the



radial coordinate and is notably different from the rectangular distributions of the parabolic model.

Various methods can be used to choose the location of the plane between the source and the focus or to backpropagate the field for setting a boundary condition on the initial plane  $z = 0$ . For example, the plane can be chosen not at the half distance to the focus, but closer to it. For back-propagation, the angular spectrum method or the Rayleigh integral can be employed. The specific choice of such procedure implemented in the “HIFU beam” software is not critical.

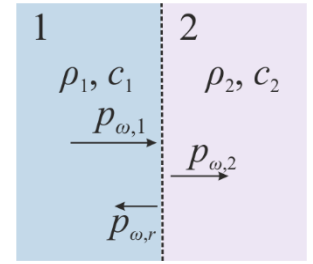
Our general recommendation is to use ‘WAPE’ mode if you do not have strict preferences to obtain results using the KZK equation because it provides a more accurate solution in the nearfield of the source.

### *Realization of multi-layer medium with a power law absorption*

#### *Boundary conditions between two layers*

The simulator “HIFU beam” allows the user to imitate propagation through biological tissue layers by using a model of flat-layered medium. The user may set up to 10 different layers. Acoustic conditions at the interface between two plane layers with different acoustic properties are the following:

$$\begin{aligned} p'_{\omega,1} + p'_{\omega,r} &= p'_{\omega,2}, \\ u'_{\omega,z1} + u'_{\omega,zr} &= u'_{\omega,z2}, \end{aligned} \quad (40) \quad \text{Transmission through layers}$$



where  $p'_{\omega,1}$  is the complex amplitude at the angular frequency  $\omega$  of the incident wave propagating in the first layer with density  $\rho_1$  and sound speed  $c_1$ ;  $p'_{\omega,r}$  is the complex amplitude of the reflected wave propagating in the same layer;  $p'_{\omega,2}$  is the amplitude of the transmitted wave propagating in the second layer with density  $\rho_2$  and sound speed  $c_2$ ; and  $u'_{\omega,z1}, u'_{\omega,zr}, u'_{\omega,z2}$  are z-components of vibrational velocities at the angular frequency  $\omega$  for the corresponding layers. The first condition is the equality of pressure, and the second one is the medium continuity condition. Since acoustic oscillation velocity is related to the pressure gradient as  $\rho \partial \mathbf{u}' / \partial t = -\nabla p'$ , for Fourier harmonic amplitudes the relation is:

$$u'_{\omega,z} = \frac{1}{i\rho\omega} \frac{\partial p'_{\omega}}{\partial z} \quad (41)$$

and the interface equations are rewritten as:

$$\begin{aligned} p'_{\omega,1} + p'_{\omega,r} &= p'_{\omega,2}, \\ \frac{1}{\rho_1} \frac{\partial p'_{\omega,1}}{\partial z} + \frac{1}{\rho_1} \frac{\partial p'_{\omega,r}}{\partial z} &= \frac{1}{\rho_2} \frac{\partial p'_{\omega,2}}{\partial z}. \end{aligned} \quad (42)$$

These conditions should be satisfied at all points of the interface between the two layers. In the current Version 1.0 of the software the transmission coefficient  $T_p$  for

pressure from one layer to another one is approximated by the transmission coefficient for a plane wave propagating perpendicular to the interface between the layers:

$$T_p = \frac{p_{\omega,2}}{p_{\omega,1}} = \frac{2\rho_2 c_2}{\rho_2 c_2 + \rho_1 c_1}. \quad (43)$$

### Power law absorption in layers

In equations (4) and (6), which describe nonlinear propagation of focused axially symmetric acoustic beam in thermoviscous medium, there is an additional operator  $\tilde{L}_a(p_n)$  accounting for the power law of absorption typical for biological tissues. Since such absorption is calculated in a frequency domain, we did not write an explicit formula for  $L_a(p)$  in the time domain in Eqs. (3), (5). In the frequency domain, the operator  $\tilde{L}_a(p_n)$  governs both the absorption and dispersion. Absorption is described according to the power law:

$$\alpha(\omega) = \alpha_0 \left( \frac{\omega}{\omega_0} \right)^\eta. \quad (44)$$

Here  $\alpha_0$  is the absorption coefficient for biological tissue at the source frequency  $\omega_0$ , while  $\alpha$  is the absorption coefficient at the frequency  $\omega$ ,  $\eta$  is the exponent in the absorption law and is typically close to unity for biological tissues. Dispersion is described by frequency-dependent phase velocity  $c(\omega)$  in tissue introduced in accordance with the local dispersion relationship:<sup>28,29,30</sup>

$$\frac{\Delta c}{c_0} = \frac{c(\omega) - c_0}{c_0} = \begin{cases} -\frac{c_0 \alpha_0}{\omega_0} \tan\left(\frac{\pi}{2} \eta\right) \left[ \left( \frac{\omega}{\omega_0} \right)^{\eta-1} - 1 \right], & \eta \neq 1 \\ \frac{2c_0 \alpha_0}{\pi \omega_0} \ln\left( \frac{\omega}{\omega_0} \right), & \eta = 1. \end{cases} \quad (45)$$

As soon as the absorption coefficient  $\alpha(\omega)$  and phase velocity  $c(\omega)$  are determined for each angular frequency, the pressure amplitude of each frequency component  $p_\omega$  in the frequency domain is obtained taking into account  $k(\omega) = \omega/c \approx \omega(1 - \Delta c/c_0)/c_0$  as:

$$p_\omega(z + \Delta z) = p_\omega(z) \exp\left( i\omega \frac{\Delta c(\omega)}{c_0^2} \Delta z \right) \exp[-\alpha(\omega) \Delta z]. \quad (46)$$

Thus, in the equations (4) and (6) the operator  $\tilde{L}_a(p_n)$  is:

$$\tilde{L}_a(p_n) = \left[ i\omega \frac{\Delta c(n\omega)}{c_0^2} - \alpha(n\omega) \right] p_n. \quad (47)$$

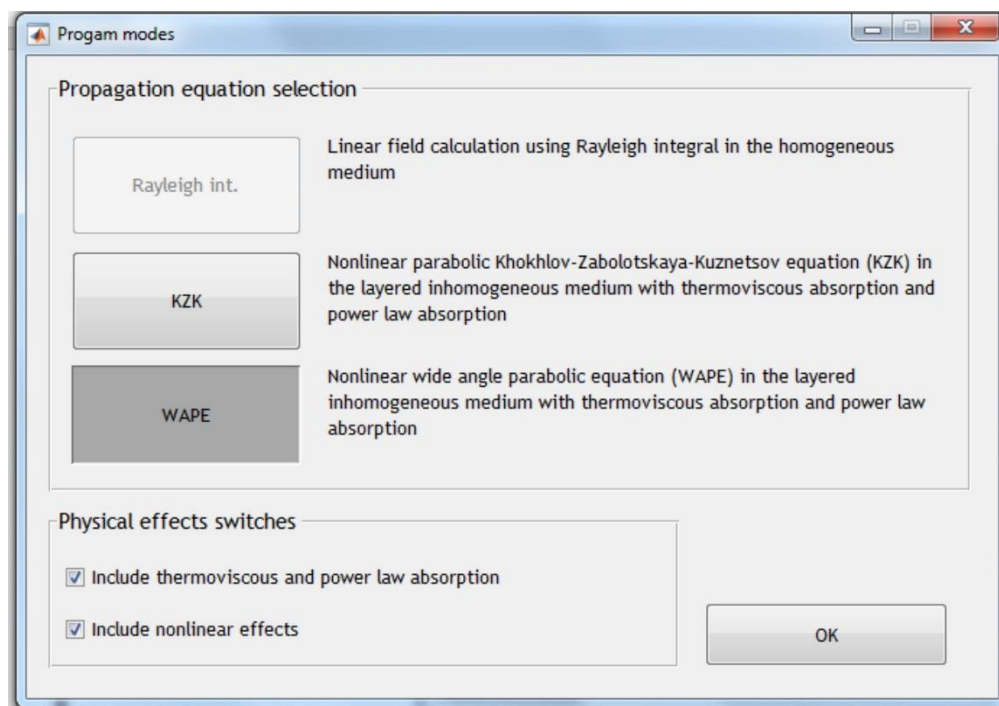
Finally, the pressure  $p$  is reconstructed in the time domain from all frequency components using the Fourier transform.

## Setting parameters for simulation

This section is intended to help the user to correctly set the input data for the simulator. We tried to organize the interface in an intuitive manner. Detailed description of all steps in setting parameters in the “HIFU beam” simulator is given here.

### *First step: Propagation equation selection*

First step is the choice of the solver - either the ‘KZK’ or ‘WAPE’ mode. The difference between the choices is the approximation used when solving the diffraction operator. If the user has no preferences, we recommend using ‘WAPE’ mode because it is more accurate than the ‘KZK’ mode. The user should also decide whether to include thermoviscous and/or power law absorption, as well as nonlinear effects. If there is no preference or the degree of nonlinear effects is unknown, the user should check that all effects are included.



*‘WAPE’ mode is on; absorption and nonlinear effects are taken into account.*

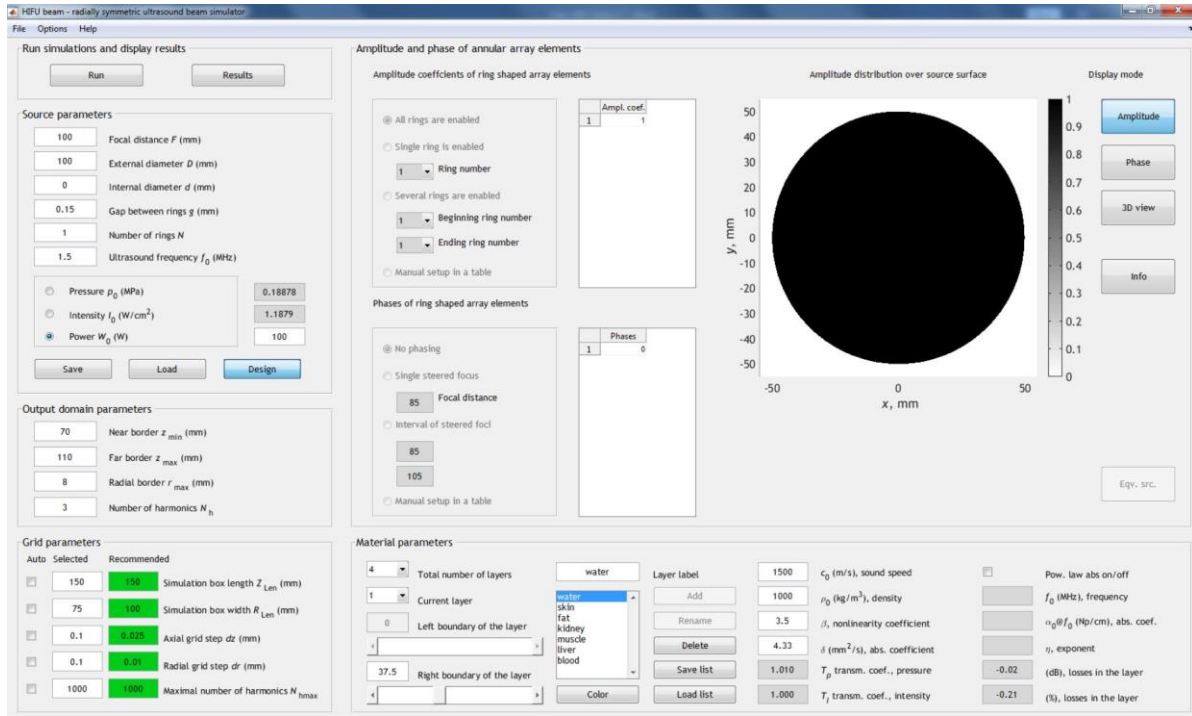
### *Second step: Acoustic source –single-element transducer or annular array*

The software “HIFU beam” provides possibilities in customizing the acoustic source parameters with the limitation of its axial symmetry. Acoustic sources available for simulation in “HIFU beam” can be divided into two choices: a single-element circular transducer (with or without an opening at the apex of the spherical cup) and a multi-element annular array with any given amplitude and phase distribution on the elements. Consider here the realizations of both possibilities.

### Single-element focused HIFU transducer: 'WAPE' mode

A single-element focused HIFU transducer can be implemented in both the 'KZK' and 'WAPE' modes. Since we recommend simulation in 'WAPE' mode as more accurate and simpler in use, we first describe setting the single element source parameters in this mode.

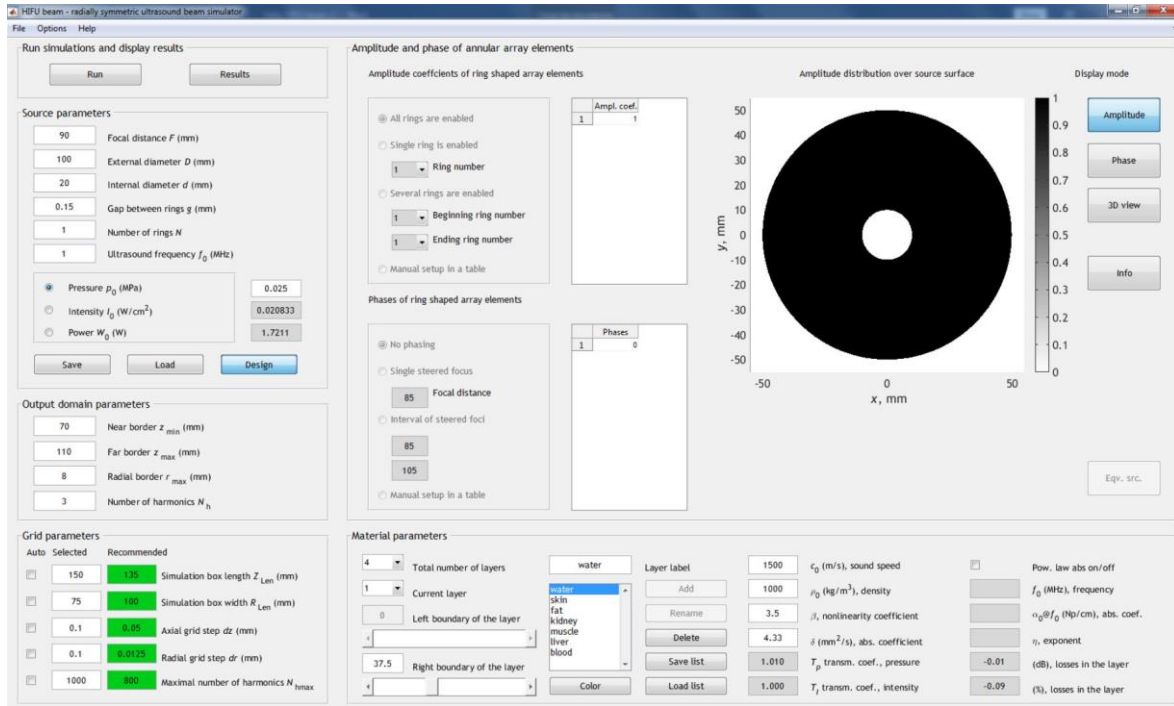
After choosing the 'WAPE' mode and clicking on 'Design' push button in a box 'Source parameters', the user will see this interface:



Interface in 'WAPE' mode. Option 'Design' in the box 'Source parameters' is active.

For the single-element HIFU source the user should provide the following parameters: the focal distance  $F$ , external diameter  $D$ , internal diameter  $d$  (only if the source has an opening at the apex, otherwise it equals to zero), and ultrasound frequency  $f_0$ . The number of rings  $N$  should be set to 1; in this case technical gap between the rings  $g$  is ignored. The dimensions of all parameters are given in parentheses. The user can set either the power  $W_0$  of the source, the intensity  $I_0$ , or the characteristic pressure amplitude  $p_0$  on the source surface to control the source output. Note that these parameters are related to each other: the power  $W_0$  is the intensity  $I_0$  integrated over the active surface of the source; pressure amplitude  $p_0$  is related to intensity  $I_0$  through acoustic parameters  $\rho_0$  and  $c_0$  of the closest to the source material layer:  $p_0 = \sqrt{2I_0\rho_0c_0}$ .

For example, a single-element circular HIFU transducer with the focal distance of 90 mm, the external diameter of 100 mm, the diameter of the central opening 20 mm (internal diameter), and frequency of 1 MHz should be set in this manner:



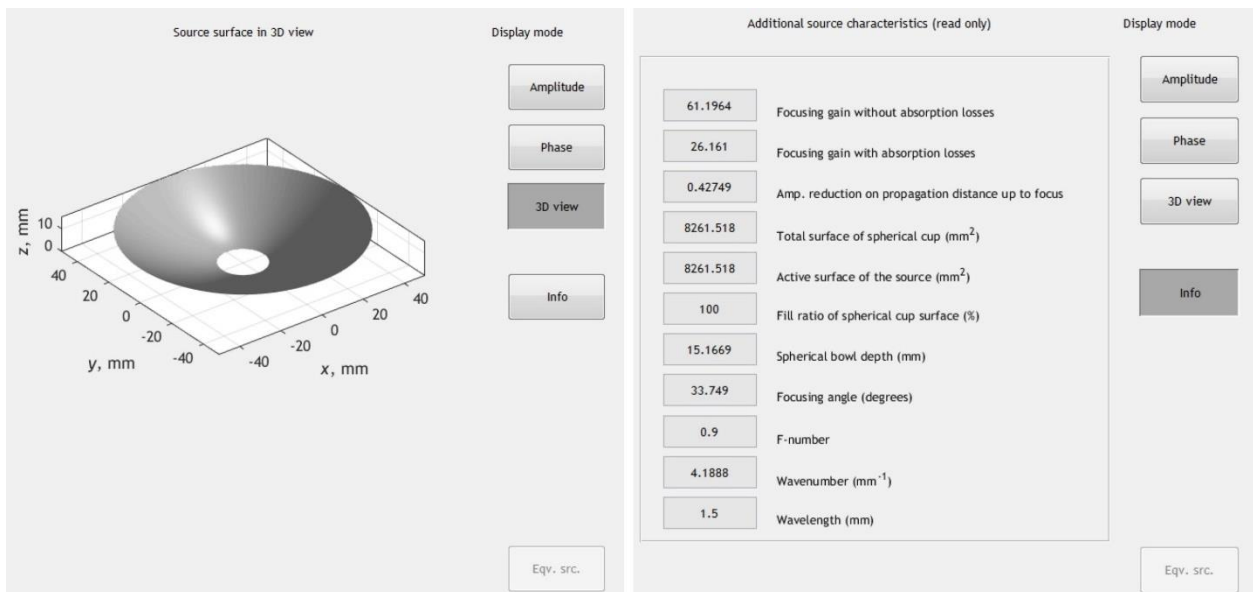
Interface in 'WAPE' mode. Single-element HIFU source with the following parameters:  $F = 90$  mm,  $D = 100$  mm,  $d = 20$  mm, and  $f_0 = 1$  MHz is set. Display mode is 'Amplitude'.

To visualize the source geometry and to see additional source characteristics calculated based on the set ones, there are display modes named 'Amplitude', 'Phase', '3D view', and 'Info' in the upper right corner of the interface. 'Info' mode displays the following characteristics (the listing order is changed to simplify each parameter description):

Characteristics in the 'Info' mode	Description
Wavelength ( $\lambda$ )	$\lambda = c_0 / f_0$ , where $c_0$ is sound speed in the closest to the source layer
Wavenumber ( $k$ )	$k = 2\pi / \lambda$
F-number	F-number = $F / D$
Focusing angle ( $\varphi$ )	$\varphi = \arcsin(D / 2F)$
Spherical bowl depth ( $h$ )	Calculated based on only external diameter $D$ as: $h = F(1 - \cos \varphi)$
Total surface of the spherical cup ( $S_{\text{full}}$ )	Surface of the spherical bowl between internal and external diameters: $S_{\text{full}} = 2\pi F(h_{\text{ext}} - h_{\text{int}})$ , where $h_{\text{ext}}$ is bowl depth for the external diameter $D$ and $h_{\text{int}}$ is bowl depth corresponded to internal diameter $d$
Active surface area of the source ( $S_{\text{act}}$ )	Surface area of the active part of the source. If the source has no gaps between elements, active surface area equals to the total surface area
Filling factor of the spherical cup surface (%)	Ratio of the active surface area to the total surface area of the source.

Focusing gain without absorption losses ( $K_p$ )	Ratio of the pressure amplitude at the focus $p_F$ to the initial pressure amplitude $p_0$ assuming propagation in non-absorbing medium: $K_p = p_F / p_0 = k(h_{\text{ext}} - h_{\text{int}})$ . If the source is a ring-shaped array, it is the sum of focusing gains calculated for all rings.
Focusing gain with absorption losses ( $K_{p,\text{abs}}$ )	<p>This focusing gain accounts for absorption in layers located between the source and the focus. If there is only one layer, <math>K_{p,\text{abs}}</math> is calculated as follows:</p> $K_{p,\text{abs}} = K_p \exp\left(-\frac{\delta\omega_0^2}{2c_0^3} F\right) \exp(-\alpha(\omega_0)F),$ <p>where the first exponent describes thermoviscous absorption, while the second exponent describes power law absorption (if it is included by the user into the model). For several layers the formula is similar, but each exponent is calculated on its layer width <math>\Delta z_i</math> and with layer's parameters <math>\delta_i</math>, <math>c_{0i}</math>, and <math>\alpha_i</math>:</p> $K_{p,\text{abs}} = K_p \prod_i \exp\left(-\frac{\delta_i\omega_0^2}{2c_{0i}^3} \Delta z_i\right) \exp(-\alpha_i(\omega_0)\Delta z_i).$
Amp. reduction on propagation distance up to the focus	Amplitude reduction is calculated as the ratio of the pressure amplitude at the focus $p_F$ in non-absorbing medium to the pressure amplitude at the focus in the user-defined layered medium, i.e., it is $K_p / K_{p,\text{abs}}$ .

In the following figure one can see how ‘3D view’ and ‘Info’ modes look like.



On the left - ‘3D view’ mode is active. On the right - ‘Info’ mode is active.

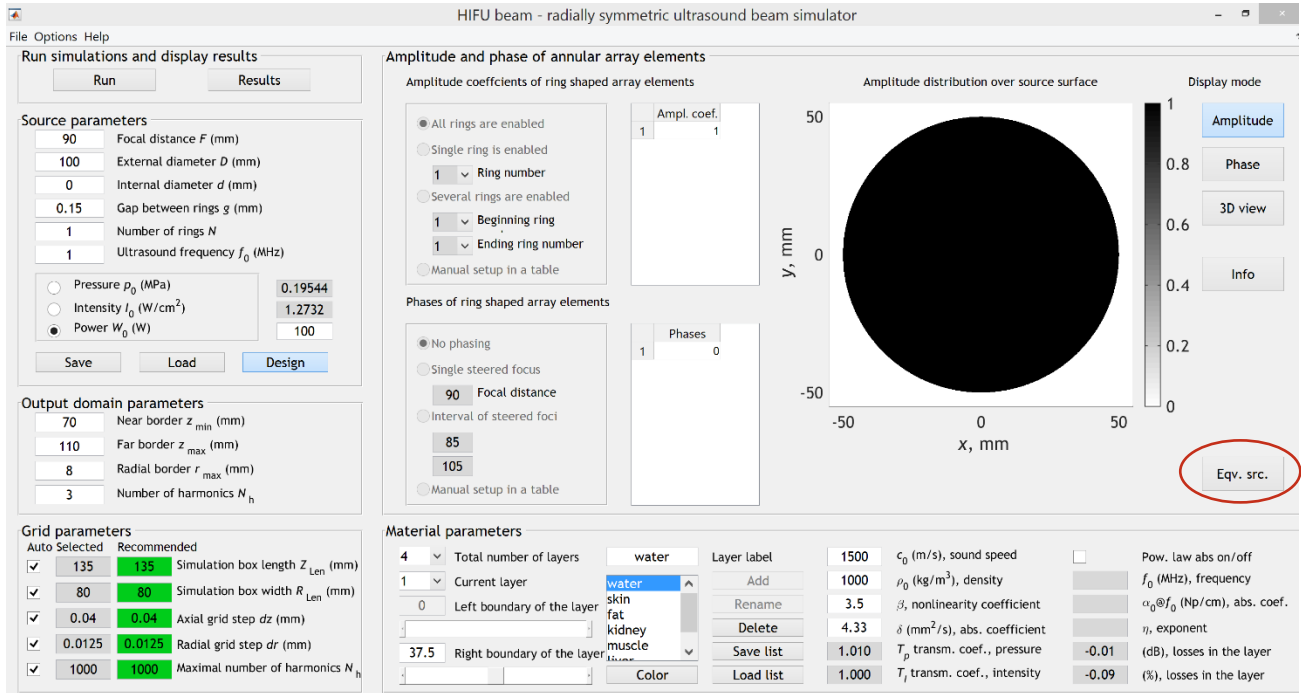


## Single-element focused HIFU transducer: 'KZK' mode

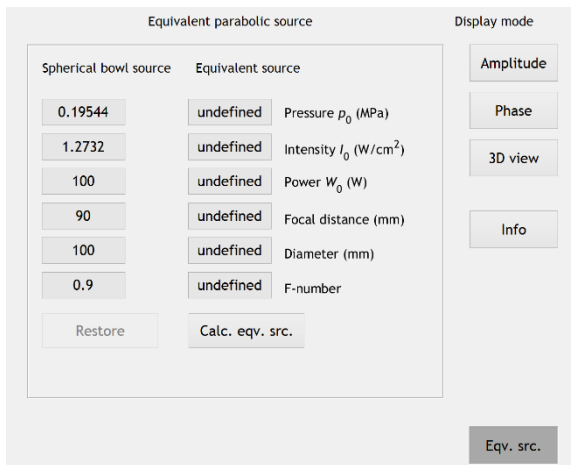
When working in the 'KZK' mode, the user should remember that the boundary condition in the KZK equation is set on the plane (see section 'Setting a boundary condition in the 'KZK' mode. Equivalent source model.'). and thus the data assigned by the user in the box 'Source parameters' will be interpreted by the KZK model as set on the plane  $z = 0$ .

An option of using equivalent source model is applicable in the software *only for* the spherical single-element HIFU transducer *without an opening at the apex*.

Let's consider the source with parameters similar to the previously considered ones but without an opening:  $F = 90$  mm,  $D = 100$  mm, and  $f_0 = 1$  MHz. In the 'KZK' mode button 'Eqv.src.' becomes active.



Interface in the 'KZK' mode. Single element HIFU source with the following parameters  $F = 90$  mm,  $D = 100$  mm, and  $f_0 = 1$  MHz is set. Mode 'Eqv. src.' is active for applying.



Box 'Equivalent parabolic source' is open.

After clicking on the push button 'Eqv.src.', a box 'Equivalent parabolic source' appears. For defining parameters of the equivalent source user should click 'Calc. eqv.src.' button. Eq. (38) will be used in the software for this procedure. Calculated geometrical parameters of the equivalent source usually have larger values than the initial ones assigned by user.

For HIFU transducers with an opening at the apex for insertion of a diagnostic ultrasound probe, the button 'Eqv.src.' is not active and the indicated external and internal diameters of the source will be set in the plane.

HIFU beam - radially symmetric ultrasound beam simulator

File Options Help

Run simulations and display results

Run Results

Source parameters

98.2744 Focal distance  $F$  (mm)

114.0638 External diameter  $D$  (mm)

0 Internal diameter  $d$  (mm)

0.15 Gap between rings  $g$  (mm)

1 Number of rings  $N$

1 Ultrasound frequency  $f_0$  (MHz)

☐ Pressure  $p_0$  (MPa) 0.17912

☐ Intensity  $I_0$  (W/cm<sup>2</sup>) 1.0695

☒ Power  $W_0$  (W) 109.2838

Save Load Design

Output domain parameters

70 Near border  $z_{min}$  (mm)

110 Far border  $z_{max}$  (mm)

8 Radial border  $r_{max}$  (mm)

3 Number of harmonics  $N_h$

Grid parameters

Auto Selected Recommended

✓ 147.4116 147.4116 Simulation box length  $Z_{Len}$  (mm)

✓ 91.251 91.251 Simulation box width  $R_{Len}$  (mm)

✓ 0.04 0.04 Axial grid step  $dz$  (mm)

✓ 0.0125 0.0125 Radial grid step  $dr$  (mm)

✓ 1000 1000 Maximal number of harmonics  $N_h$

Amplitude and phase of annular array elements

Amplitude coefficients of ring shaped array elements

☒ All rings are enabled

☐ Single ring is enabled

1 Ring number

☐ Several rings are enabled

1 Beginning ring

1 Ending ring number

☐ Manual setup in a table

Phases of ring shaped array elements

☒ No phasing

☐ Single steered focus

98.274 Focal distance

☐ Interval of steered foci

85

105

☐ Manual setup in a table

Material parameters

4 Total number of layers

1 Current layer

0 Left boundary of the layer

37.5 Right boundary of the layer

water Layer label

1500  $c_0$  (m/s), sound speed

1000  $\rho_0$  (kg/m<sup>3</sup>), density

3.5  $\beta$ , nonlinearity coefficient

4.33  $\delta$  (mm<sup>2</sup>/s), abs. coefficient

1.010  $T_p$  transm. coef., pressure

1.000  $T_i$  transm. coef., intensity

1500  $c_0$  (m/s), sound speed

1000  $\rho_0$  (kg/m<sup>3</sup>), density

3.5  $\beta$ , nonlinearity coefficient

4.33  $\delta$  (mm<sup>2</sup>/s), abs. coefficient

1.010  $T_p$  transm. coef., pressure

1.000  $T_i$  transm. coef., intensity

Equivalent parabolic source

Spherical bowl source

0.19544

1.2732

100

90

100

0.9

Restore

Equivalent source

0.17912 Pressure  $p_0$  (MPa)

1.0695 Intensity  $I_0$  (W/cm<sup>2</sup>)

109.2838 Power  $W_0$  (W)

98.2744 Focal distance (mm)

114.0638 Diameter (mm)

0.86157 F-number

Calc. eqv. src.

Display mode

Amplitude

Phase

3D view

Info

Eqv. src.

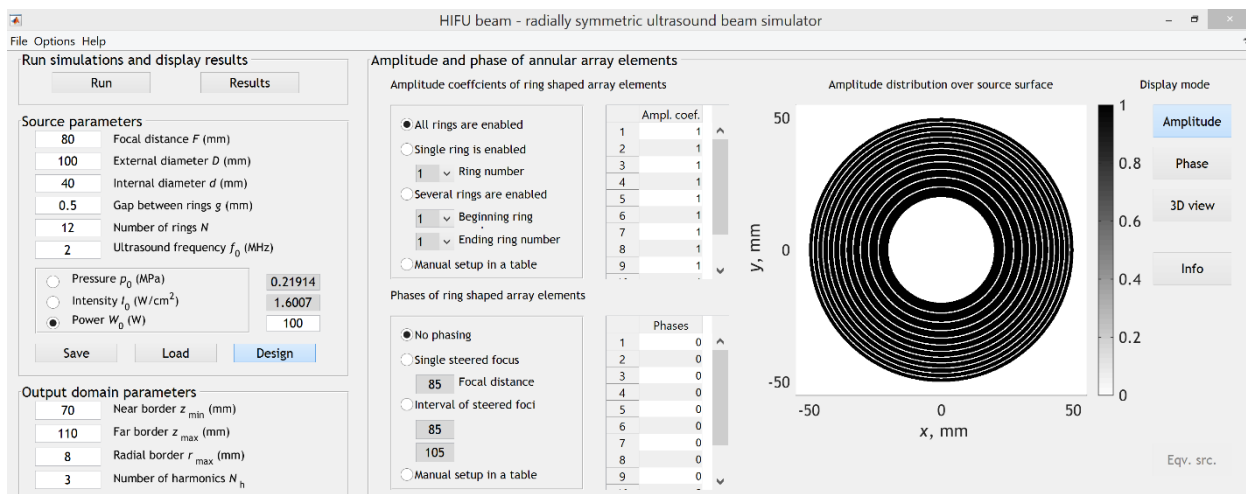
Setting equivalent source as a boundary condition in the ‘KZK’ mode.

## Multi-element annular array

The functional of the software to set multi-element ring-shaped arrays is quite extensive: available options are to switch on/off different rings of the array, to set manually phases and amplitudes for each ring, and to set a point for axial steering or an interval of steered foci to produce an elongated focus.

Here, a demonstration of the ring-shaped array settings is presented for ‘WAPE’ mode. In the ‘KZK’ mode the adjusting is similar, but the user should pay attention that in this case the array parameters will be set on the plane, not on a spherical segment.

Setting the number of rings  $N$  and technical gap  $g$  between them leads to dividing the surface of a spherical bowl into  $N$  rings of *equal area* spaced apart by a gap distance.



Setting 12-elements-ring-shaped array in the ‘WAPE’ mode. Technical gap is 0.5 mm.

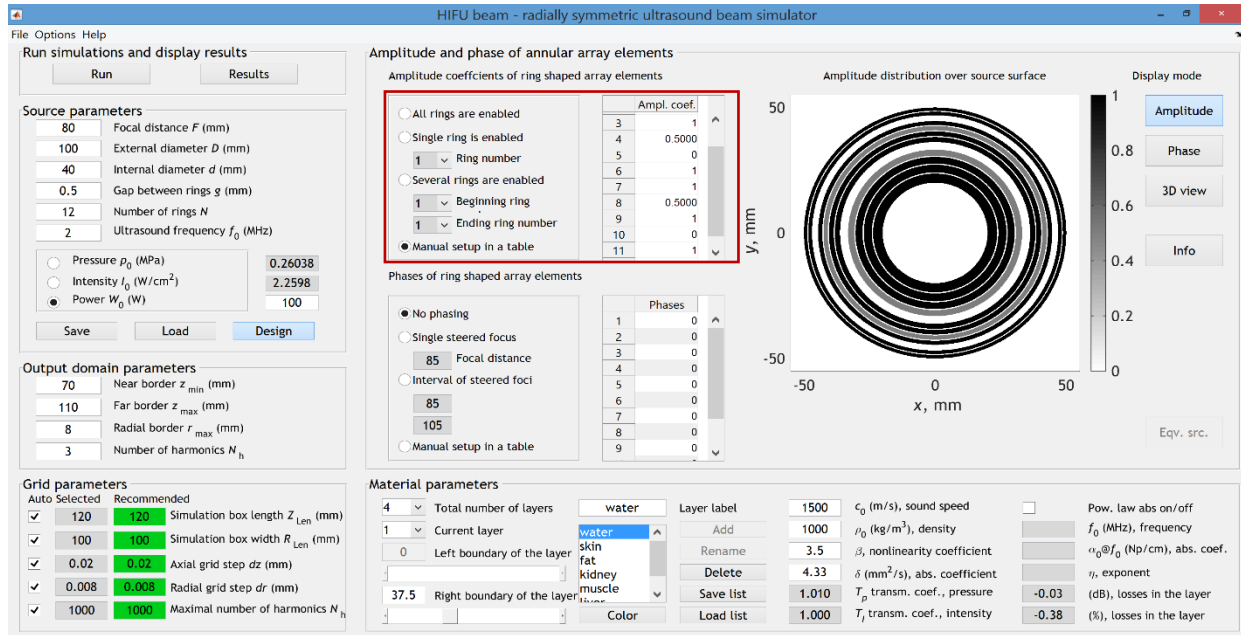
The parameters of each ring are configured in the box ‘Amplitude and phase of annular array elements’. User can adjust the amplitude and phase of each ring

separately. In particular, selected rings can be turned off by setting to zero the amplitude coefficient.

In the box ‘Amplitude coefficients of ring shape array elements’ there are four options:

- ‘All rings are enabled’. In this option, all rings are turned on, amplitude coefficients are equal to unity for all rings.
- ‘Single ring is enabled’. The number of the only emitting ring is selected, the rest will be inoperative.
- ‘Several rings are enabled’. User specifies the beginning and ending ring number of the working section of the array.
- ‘Manual setup in a table’. User manually sets the amplitude coefficients for each of the rings. In this case, setting zero amplitude will mean that the ring does not vibrate.

Below is an example of an interface with manual setup of the amplitude coefficients for a 12-element ring-shaped annular array with the 5<sup>th</sup> and the 10<sup>th</sup> rings off and the 4<sup>th</sup> and 8<sup>th</sup> rings emitting at half of the amplitude.



Manual setup of the amplitude coefficients for a 12-element ring-shaped array in ‘WAPE’ mode.

The element phase settings are adjusted in the box ‘Phases of ring shaped array elements’. Options are:

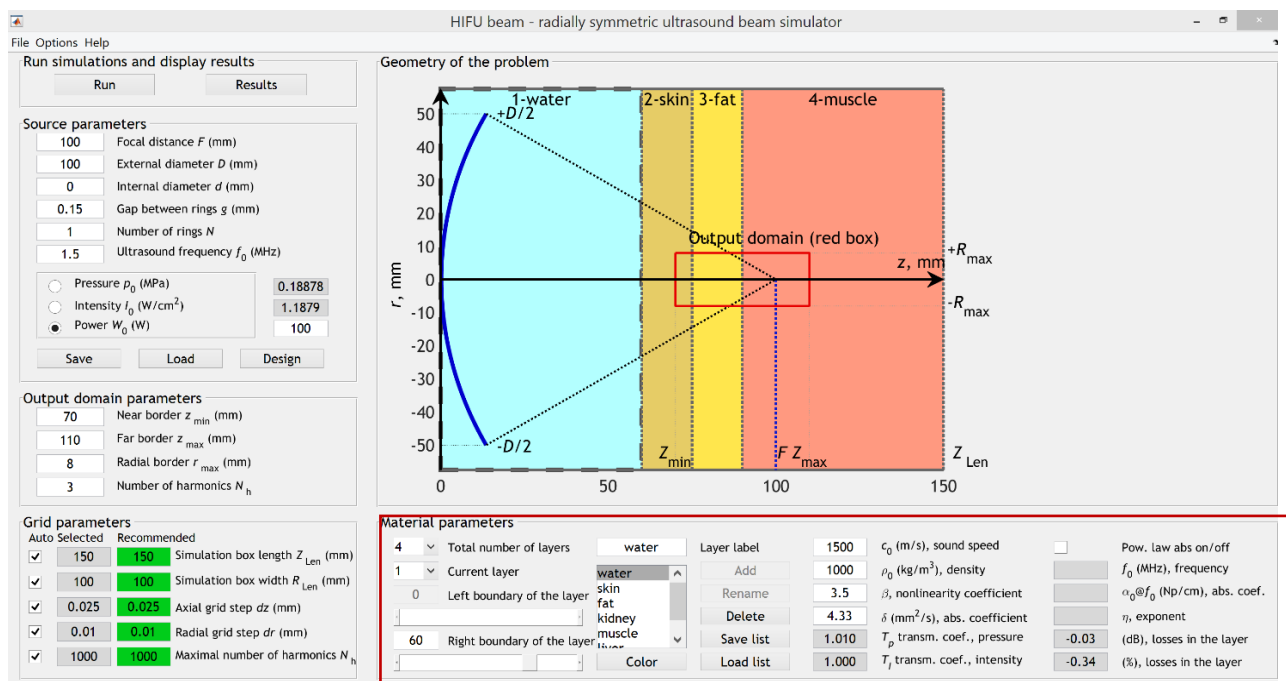
- ‘No phasing’. Phase of each element is zero, focusing occurs only due to the spherical shape of the surface.
- ‘Single steered focus’. Each element has additional phase shift so that focusing occurs in steered focus chosen by the user.
- ‘Interval of steered foci’. This option is used to obtain an elongated focal region of a given axial length determined by the user specified interval on the axis. This interval is split into  $(N-1)$  equal subintervals ( $N$  - number of the array elements), and the centers of each subinterval are considered as

electronic foci where portion of the field should be focused. The inner element (ring #1) phase is set to zero. The software calculates phases of the rest elements in such a way that each successive pair of the elements has a mutual phase shift corresponding to focusing at the center of the corresponding subinterval. In particular, the 2<sup>nd</sup> ring has an additional phase shift such that the interference of its field with the field of the 1<sup>st</sup> ring is constructive (in-phase) at the center of the 1<sup>st</sup> subinterval, which is closest to the source. Similarly, the combination of the (N-1)<sup>th</sup> and N<sup>th</sup> rings focuses field to the center of the distal subinterval.

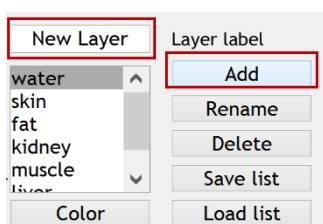
- ‘Manual setup in a table’. User manually sets the phases for each of array elements.

### Third step: Propagation in a multi-layer medium

The software “HIFU beam” allows a user to calculate the propagation of ultrasonic wave in a *flat-layered* medium. The number of layers can vary from one (a homogeneous medium) to ten. User can configure the parameters of the propagation medium in the box ‘Material parameters’ shown below.



Setting parameters of propagation medium in the box ‘Material parameters’.



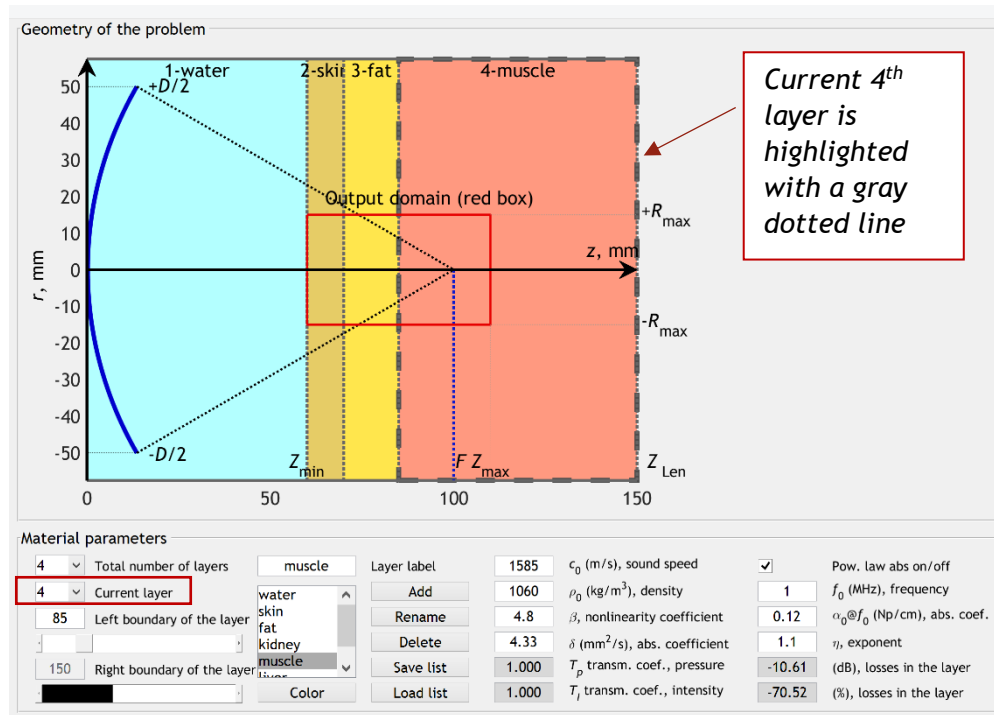
Setting user-defined layer. Enter layer name in ‘Layer Label’ field and click ‘Add’.

Default settings include seven materials with acoustic parameters given in a table below. The user can change these parameters or add a new material with the user-defined properties. To add a new user-defined layer, the user should enter material name in the field ‘Layer label’, click button ‘Add’, and indicate acoustic parameters of the created material. If specified material has a power law absorption with frequency, user should check the box ‘Pow. Law abs on/off’. User can also choose a color for the created layer by clicking to the push button ‘Color’.

	water	skin	fat	kidney	muscle	liver	blood
sound speed, $c_0$ (m/s)	1500	1500	1450	1570	1585	1580	1560
density, $\rho_0$ (kg/m <sup>3</sup> )	1000	1020	920	1050	1060	1050	1050
nonlinearity coef., $\beta$	3.5	5	6	4.7	4.8	4.9	4.1
thermoviscous absorption coef., $\delta$ (mm <sup>2</sup> /s)	4.33	4.33	4.33	4.33	4.33	4.33	4.33
absorption coef. at 1 MHz frequency, $\alpha_0$ (Np/cm)	off	0.2	0.065	0.1	0.12	0.046	0.016
exponent in the absorption law, $\eta$	off	0.6	1.1	1.1	1.1	1.15	1.21

Table with parameters of default materials which a user can choose for layers.

All manipulations with layer coordinates are immediately displayed graphically in the box ‘Geometry of the problem’. The user should indicate total number of layers and then for each current layer enter coordinates of its left and right boundaries. Coordinates can be set by entering numbers or by using sliders. When the user configures current layer, it is highlighted with a thick gray dotted line in the geometrical sketch.



Note that in calculations of the ultrasonic field, the transmission coefficient  $T_p$  for pressure from one layer to another one is accounted for by assuming normally incident plane waves (43). Both transmission coefficients for pressure  $T_p$  and intensity

$T_l$  are displayed in the settings in the box ‘Material parameters’. Also, for each layer power law, absorption losses are displayed in dB and in percentage.

In the software, user-defined list of materials can be saved by clicking the button ‘Save list’ and subsequently used by loading the list through ‘Load list’.

#### Fourth step: Setting the grid and output domain parameters

##### Grid parameters

For setting the numerical grid for simulation, five parameters should be specified in the box ‘Grid parameters’:

- ‘Simulation box length  $Z_{Len}$  (mm)’. Enter size of the calculation area along the axial coordinate.
- ‘Simulation box width  $R_{Len}$  (mm)’. Enter size of the calculation area along the radial coordinate.
- ‘Axial grid step  $dz$  (mm)’.
- ‘Radial grid step  $dr$  (mm)’.
- ‘Maximal number of harmonics  $N_h$ ’. This parameter is especially important for nonlinear calculations when shock fronts are formed.

Grid parameters		
Auto	Selected	Recommended
<input checked="" type="checkbox"/>	150	150
<input checked="" type="checkbox"/>	100	100
<input checked="" type="checkbox"/>	0.02	0.02
<input checked="" type="checkbox"/>	0.01	0.01
<input checked="" type="checkbox"/>	1000	1000

Setting grid parameters. Check ‘Auto’ column to set recommended parameters.

If user has no preferences about the grid parameters, the best option is to use recommended parameters displayed in the green column. They are automatically copied to the current-use parameter boxes after checking corresponding check-boxes ‘auto’ on the left.

##### Output domain parameters

In the box ‘Output domain parameters’ the size of the output area and number of output harmonics should be indicated:

- ‘Near border  $z_{min}$  (mm)’ (along the axial coordinate)
- ‘Far border  $z_{max}$  (mm)’ (along the axial coordinate)
- ‘Radial border  $r_{max}$  (mm)’ (along the radial coordinate)
- ‘Number of harmonics  $N_h$ ’

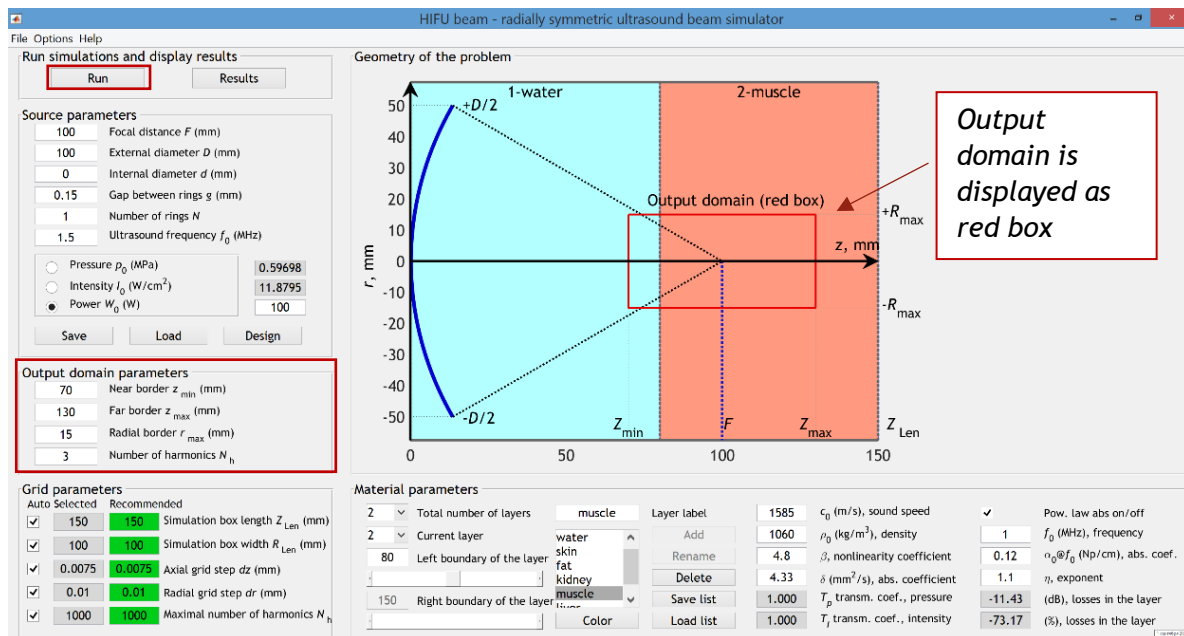
The output domain is displayed in the geometrical sketch by the red box. The area around the focus is most commonly used as the output area.

##### Run simulations

After settings all groups of parameters, calculations are started by clicking the button ‘Run’ in the upper left corner of the interface. After the simulation completes, the user can press the ‘Results’ button to get access to pressure waveforms in any chosen location along z-axis and along r-axis in the focal plane, at the distance  $z = F$ , and to four type of distributions (1D axial, 1D radial, 2D in the axial plane, 2D in the transverse plane) for peak positive pressure, peak negative pressure, shock amplitude,



intensity, heat sources, acoustic power, and harmonic amplitudes in the output domain. The results from previous simulations may be accessed in the ‘Results’ tab.



Setting output domain around the focus (shown as red box in the interface).  
 Simulations is ready to run!

# Examples of numerical simulations

In this section, numerical simulations for two representative laboratory ultrasonic transducers are presented. Simulations are shown for both 'KZK' and 'WAPE' modes. The sources are single element transducer and annular array, propagation in water as well as in a layered medium is considered.

## Single-element focused transducer, propagation in water

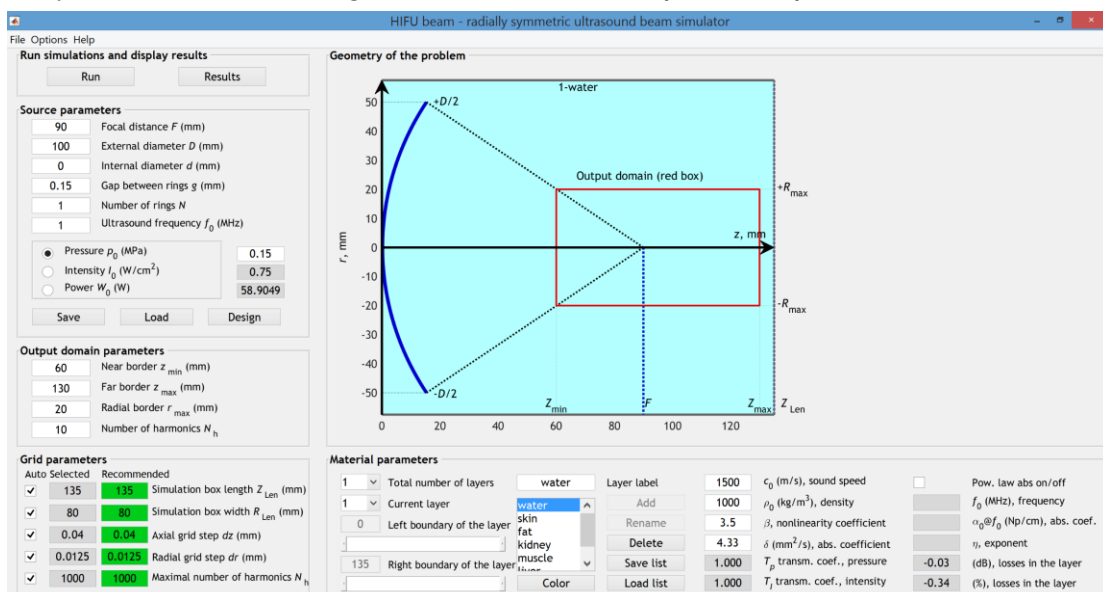
The first example is a single element spherical source of 1 MHz frequency with radius of 5 cm and focal distance of 9 cm. Calibration of its acoustic field in water is presented in papers [10,11,19]. Here, a detail description is provided on how to calculate acoustic field of this transducer in water for different initial pressure amplitudes at the source. Three cases will be considered below: quasilinear propagation ( $p_0 = 0.15$  MPa), developed shock formation ( $p_0 = 0.45$  MPa), and saturation regime of focusing ( $p_0 = 0.70$  MPa) with formation of two shocks in acoustic waveform close to the focus leading to specific double spike structure on the axial distribution of the peak positive pressure. Calculations are launched in the 'KZK' mode in order to show how equivalent source model works.



Single element spherical source of 1-MHz frequency ( $F = 90$  mm,  $D = 100$  mm) produced by Imasonic.

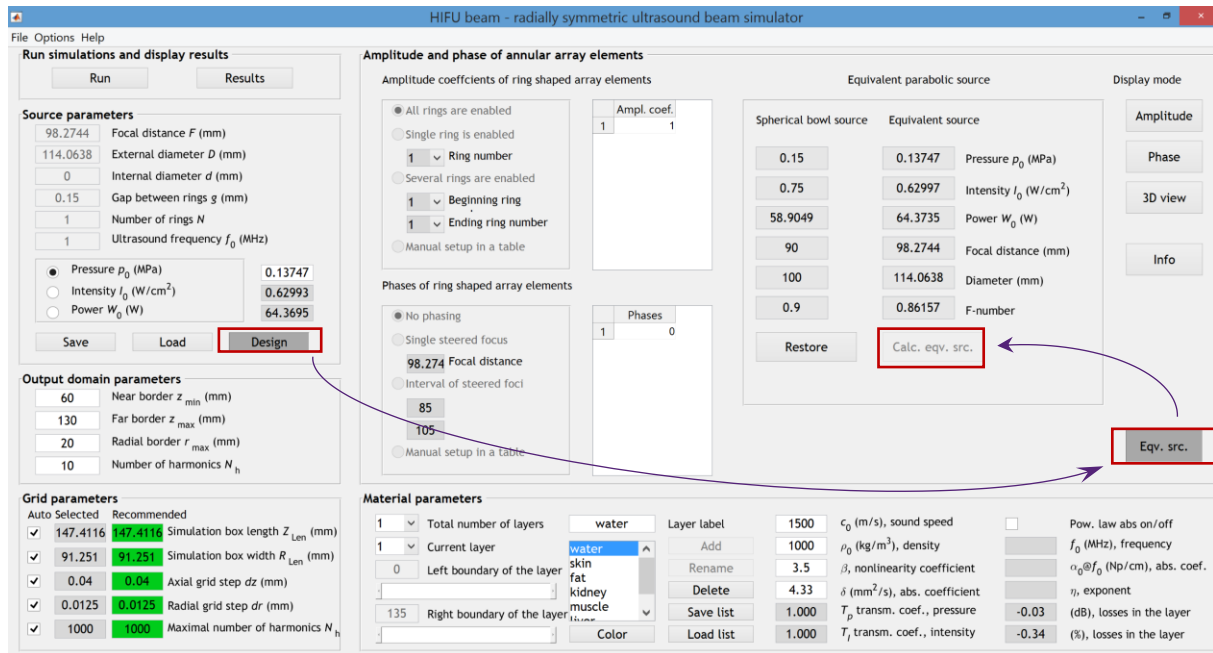
## Quasilinear case ( $p_0 = 0.15$ MPa)

A quasilinear waveform distortion is usually defined following the criterion that less than 10% of the wave intensity is distributed over harmonics above the fundamental frequency. For the chosen transducer, a limiting situation at which exactly 10% of the focal intensity is distributed at higher harmonics corresponds to  $p_0 = 0.15$  MPa.<sup>10</sup>



Step1: setting parameters of the single element spherical source in the 'KZK' mode.

The first step in calculations is to set parameters of the single-element spherical source in the 'KZK' mode. Since source parameters are known over a spherical surface, the equivalent source model should be applied to transfer correctly the boundary condition to the initial plane.

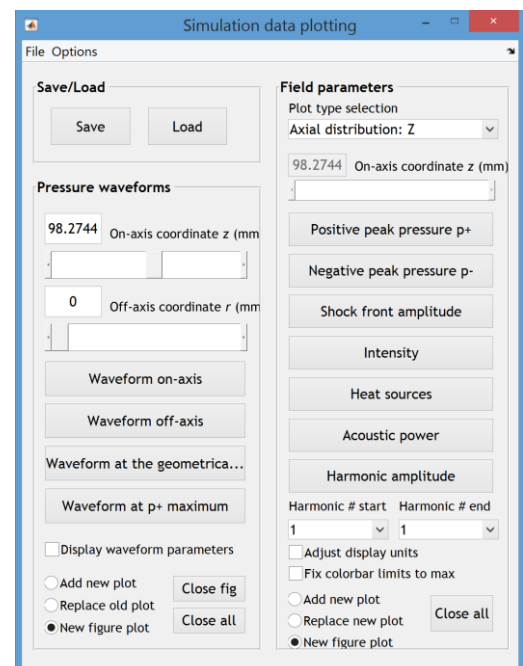


Step 2: applying equivalent source model ('Design' → 'Eqv.src.' → 'Calc.eqv.src.') in the 'KZK' mode.

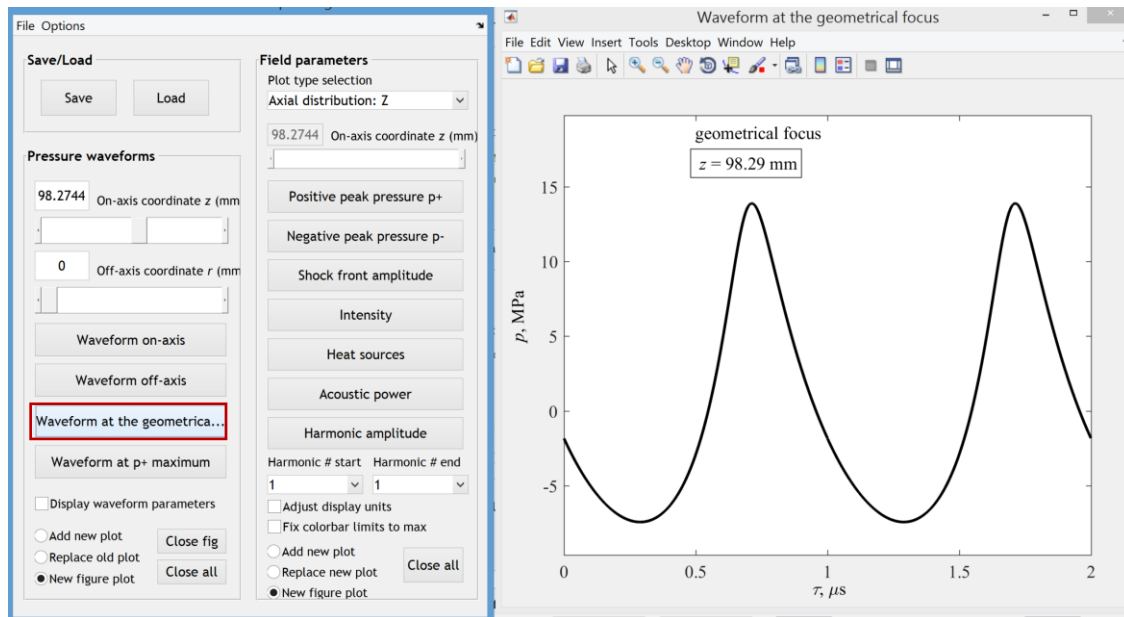
Now, in the box 'Source parameters', focal distance, external diameter, and pressure are recalculated:  $F = 98.2744$  mm (instead of 90 mm),  $D = 114.0638$  mm (instead of 100 mm), and  $p_0 = 0.13747$  MPa (instead of 0.15 MPa). Preliminary preparation of the source configuration is done, the user can run simulations.

After finishing the calculations, results are displayed by clicking the button 'Results'. In the pop-up window 'Simulation data plotting', the left half is dedicated to displaying pressure waveforms. The interface allows the user to display waveforms for on-axis coordinate  $z$  ( $r = 0$  mm) or off-axis coordinate  $r$  in the focal plane ( $z = 98.2744$  mm in the current case). Note that the axial coordinate  $z$  in the displayed results is tied to the parabolic source and is shifted relative to the real spherical one by 8.2744 mm.

The right column of 'Simulation data plotting' is for setting the output of the field parameters: peak positive pressure  $p_+$ , peak negative pressure  $p_-$ , shock front amplitude (in the Version 1.0 doesn't work 😞, it will be implemented in the next version), intensity, heat sources, acoustic power, and harmonic amplitude.

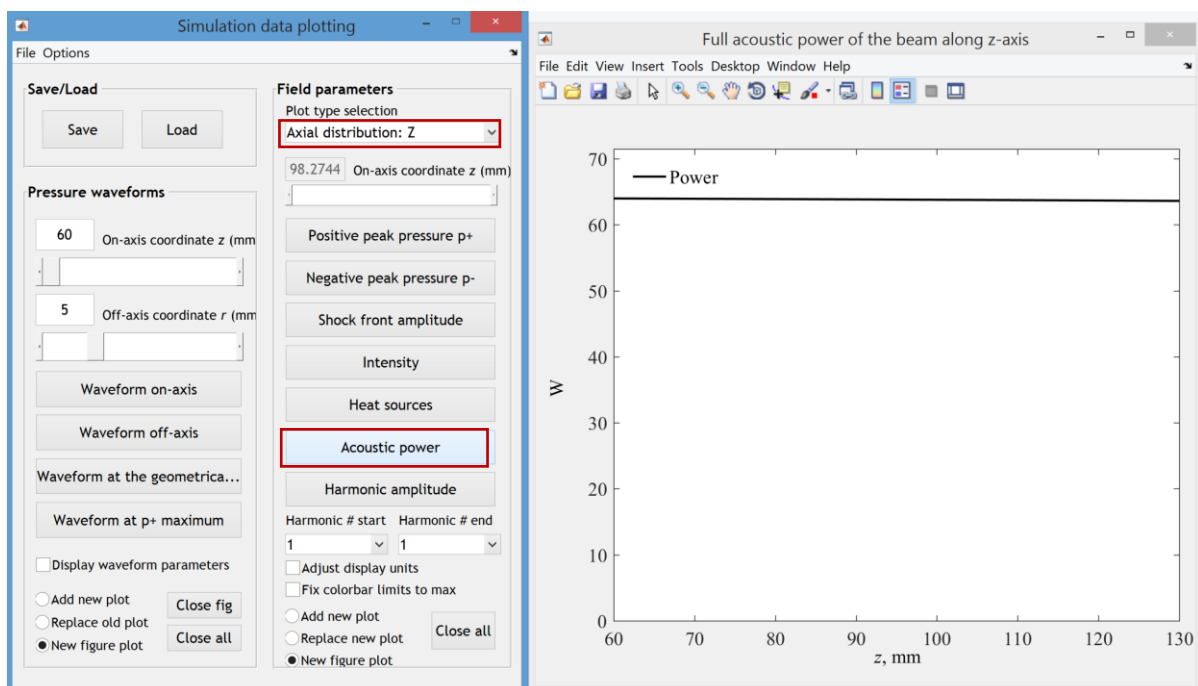


Interface for plotting results.



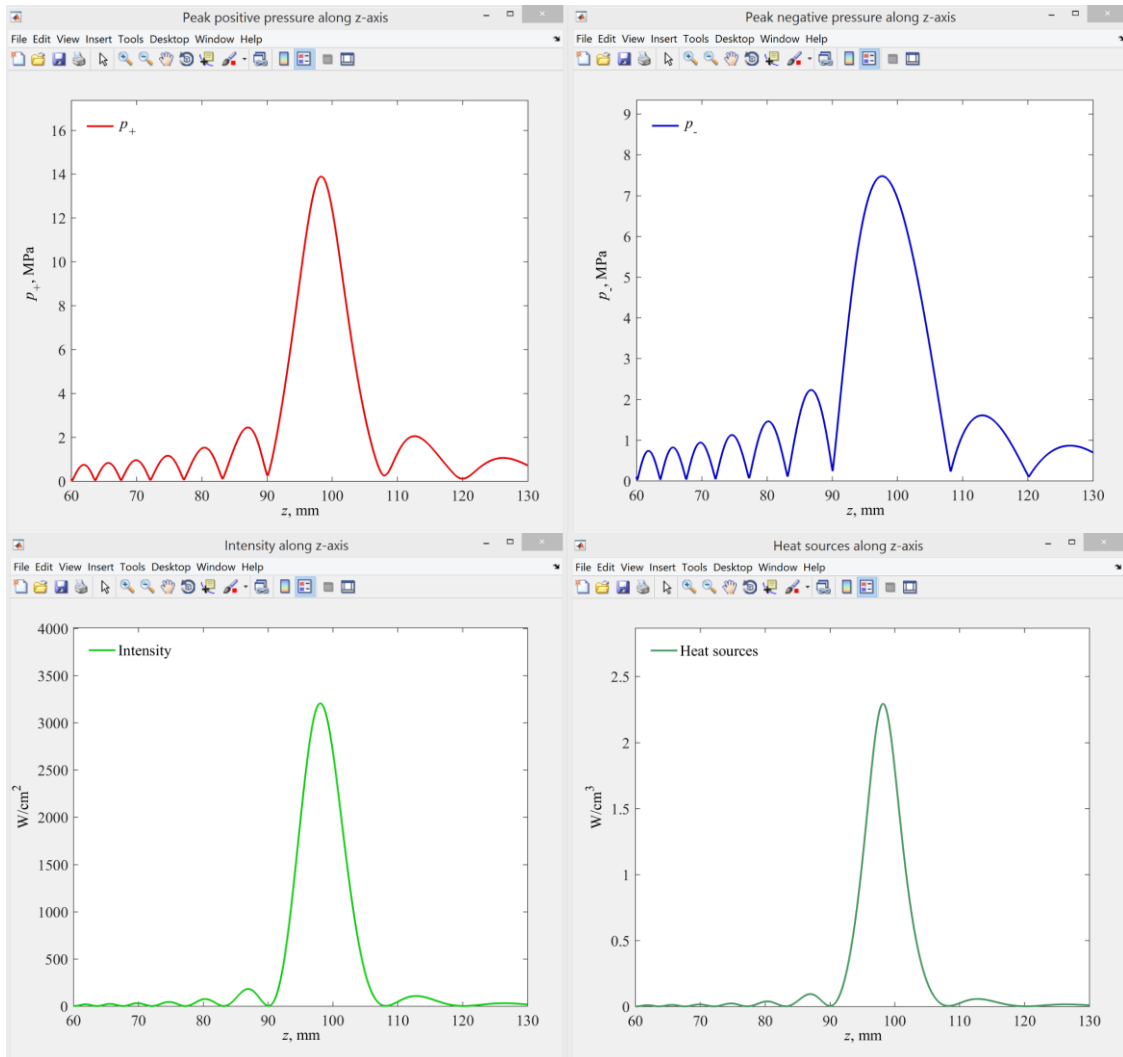
*Display results: waveform at the geometrical focus. This waveform corresponds to the quasilinear case: it is slightly distorted by nonlinear effects but only 10% of the wave intensity is distributed over harmonics of the fundamental frequency.*

Acoustic power is displayed only along the  $z$ -axis, so plotting the power distribution requires setting 'Axial distribution: Z' in the 'Plot type selection'. In this example propagation is in water, there are no shock fronts, thus absorption is negligible, and the beam power is almost constant:

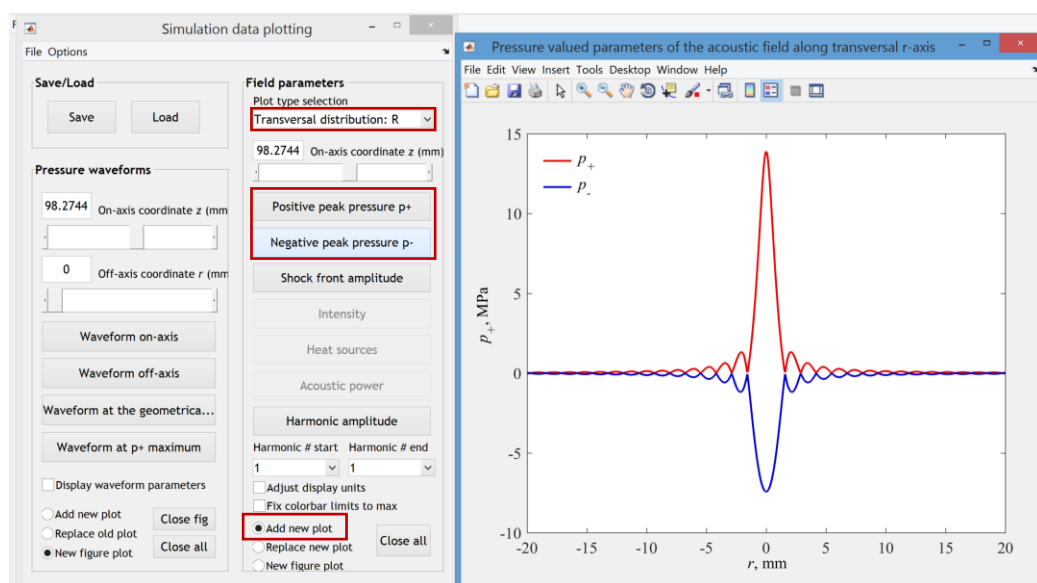


*Display results: Acoustic power of the beam along the  $z$ -axis.*

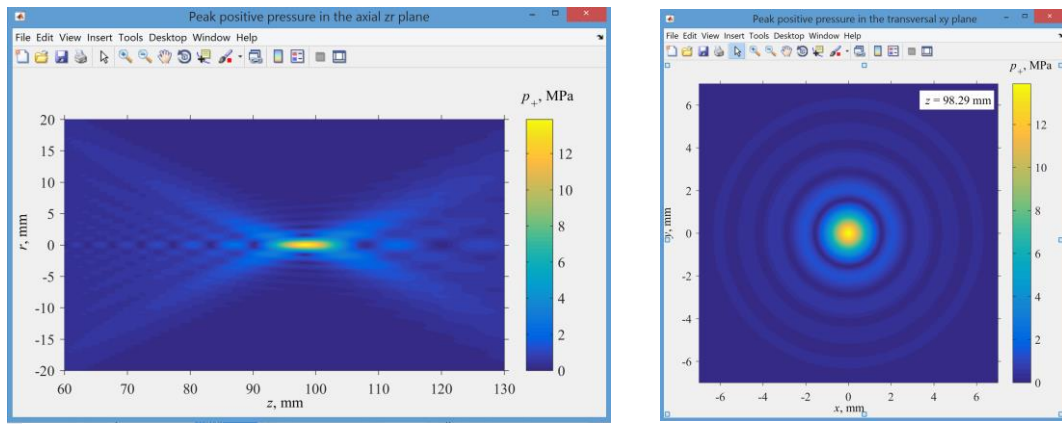
Other field parameters can be displayed as one-dimensional distributions along  $z$  or  $r$  axes (the latter one in the focal plane) and as two-dimensional distributions in the axial plane  $zr$  or in the focal plane  $xy$ . Several examples shown below illustrate how these distributions are displayed in the interface of the software "HIFU beam".



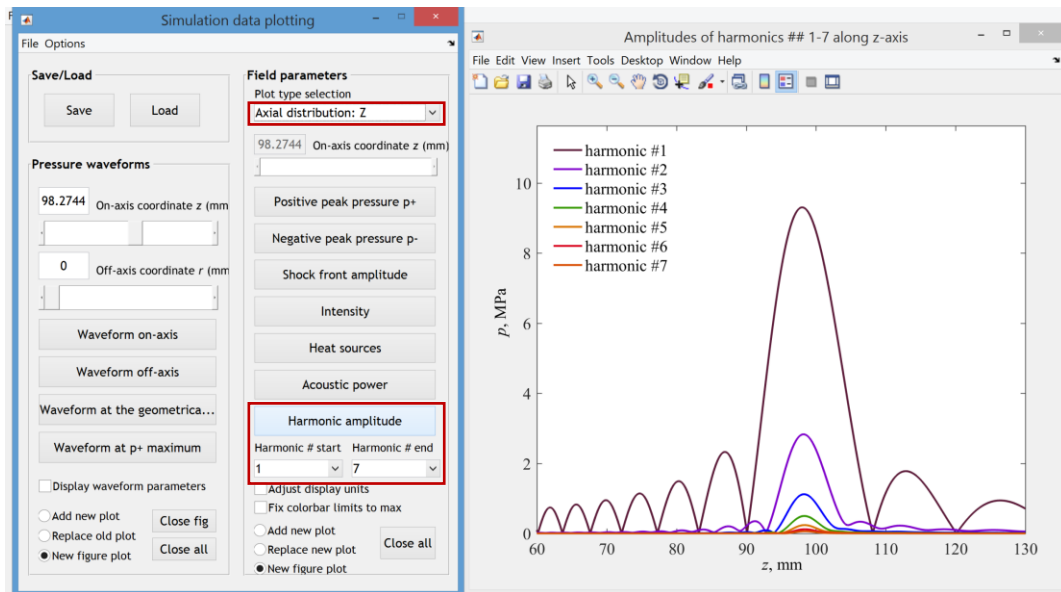
Display results: axial distributions (along the z-axis) of the peak positive pressure, peak negative pressure, intensity, and heat sources. Note, that axis z is shifted in 8.2744 mm since equivalent source model is applied.



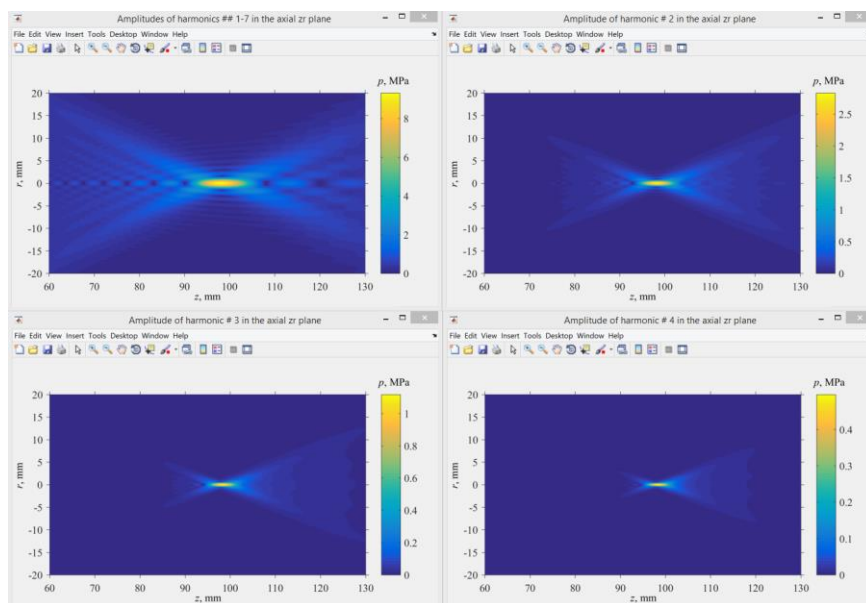
Display results: radial distributions (along the r-axis) of peak positive and peak negative pressures. Checking the box 'Add new plot' allows to plot both distributions on the same graph.



Display results: 2D distributions of the peak positive pressure in the axial plane  $zr$  (left) and at the focal plane  $xy$  (right).



Display results: Pressure amplitude of the first seven harmonics along the  $z$ -axis. Number of harmonics in displaying results can't be larger than indicated initially in the box 'Output domain parameters'.

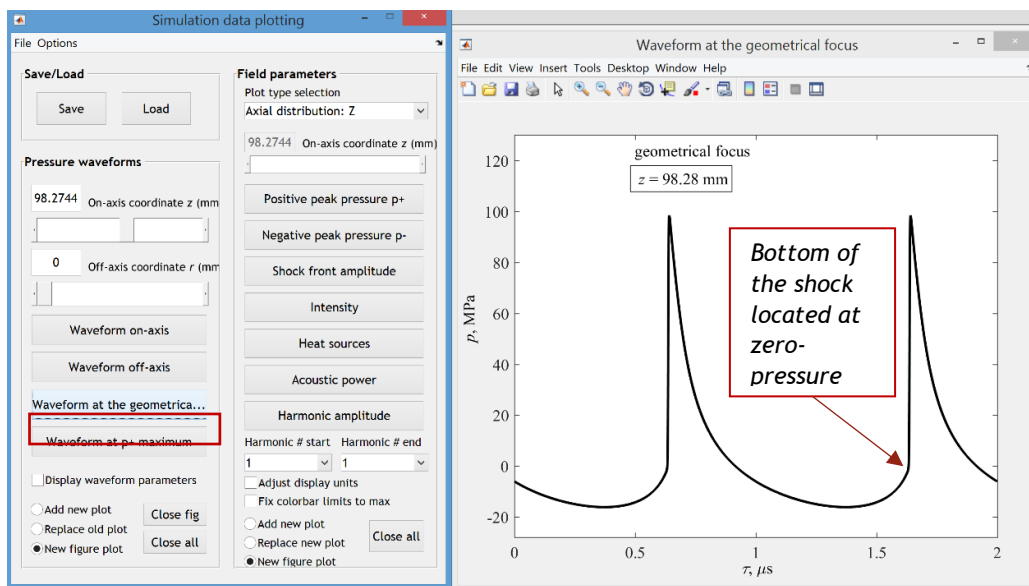


Display results: 2D pressure amplitude distributions are displayed for each of the harmonic separately. Here are the results for first four harmonics in the plane  $zr$ .

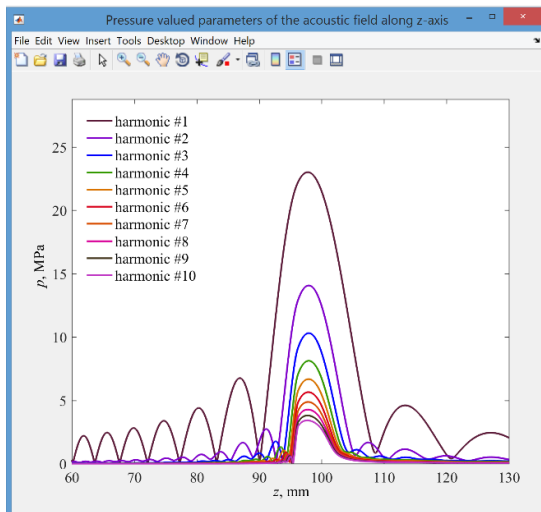


### Case corresponding to the developed shock formation ( $p_0 = 0.45$ MPa)

After increasing  $p_0$  beyond quasilinear condition ( $p_0 \leq 0.15$  MPa), formation of a shock front occurs at a certain pressure level. The shock initially forms near the positive peak of the waveform, and then, with further increase of  $p_0$ , the shock grows in amplitude so that its bottom edge moves down toward a level of zero pressure. The level of distortion, where the shock amplitude normalized to the source pressure  $p_0$  reaches a maximum, is termed as the level of developed shock formation.<sup>10</sup> At this level, the focusing gain for the shock amplitude relative to the source pressure reaches its maximum, thus, the focusing is most effective. To determine which level of  $p_0$  corresponds to the formation of the developed shock, a specific feature of this regime can be used: the bottom of the shock front in the focal waveform should be located at the zero-pressure level. For the chosen single-element transducer this occurs at  $p_0 = 0.45$  MPa, as shown below.



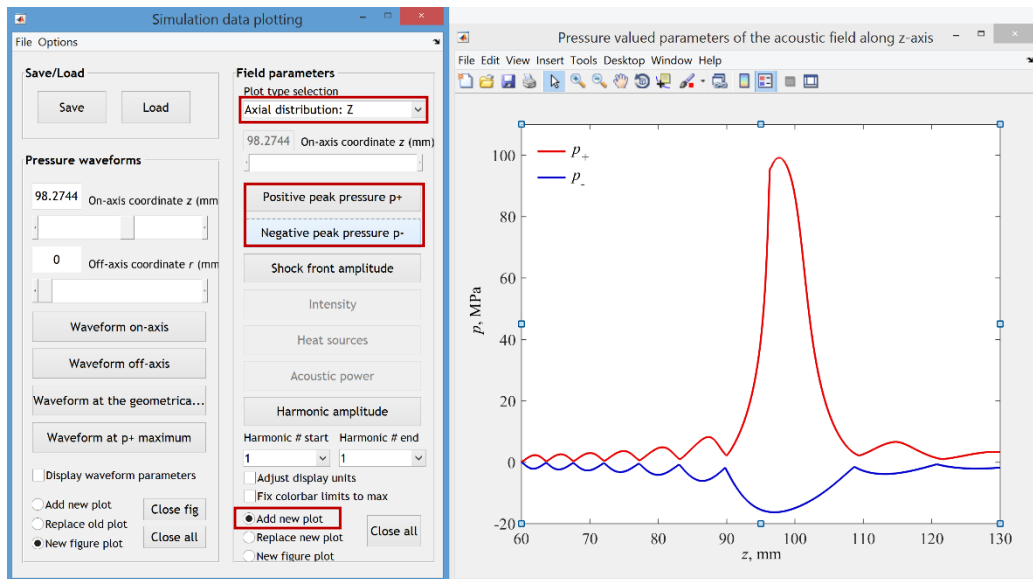
Display results: formation of the developed shock front in the focal pressure waveform (simulations in the 'KZK' mode, equivalent source model is applied).



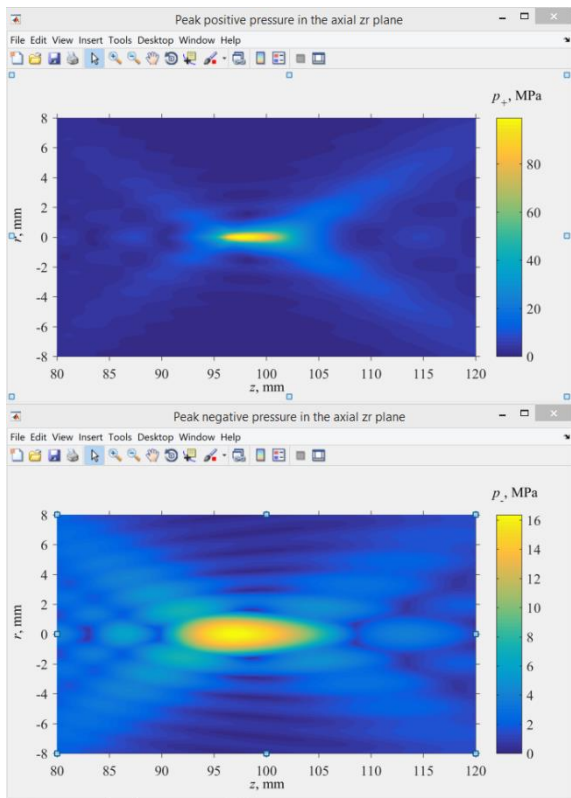
Display results: axial distribution of the pressure amplitude for first 10 harmonics.

Nonlinear effects are significant at this drive level and a large portion of the intensity is distributed over higher harmonics, as shown on the 1D axial distributions of the harmonics' amplitudes. While the amplitude of the shock front reaches almost 100 MPa, the amplitude of the fundamental harmonic (harmonic #1 in the figure) is only about 23 MPa.

The axial distributions of the peak positive and peak negative pressures become strongly asymmetric relative to each other. The focal spot for the peak positive pressure is about twice shorter along the z-axis than the focal spot for the peak negative pressure.



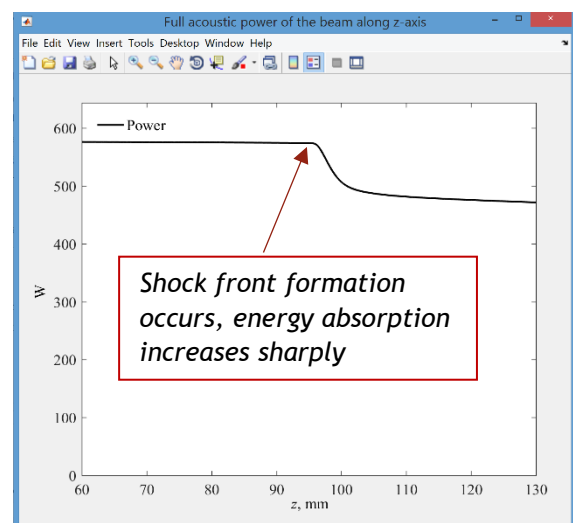
*Display results: axial distributions (along the z-axis) of the peak positive and peak negative pressures.*



*Display results: 2D distributions in the axial zr plane of the peak positive (upper inset) and peak negative (lower inset) pressures.*

The moment of the beginning of shock front formation corresponds to a sharp decrease of the beam power and is clearly seen in the figure with power dependence along z-axis.

The width of the focal spot for the peak positive pressure along the radial coordinate  $r$  (at -3 dB level) is only 0.5 mm which is comparable to the size of a hydrophone tip in experiments. This is why the peak positive pressures are sometimes underestimated in the hydrophone measurements at very high source pressures.<sup>31</sup> The corresponding width of the focal spot for the peak negative pressure is 1.8 mm, more than three times wider than for the peak positive pressure.

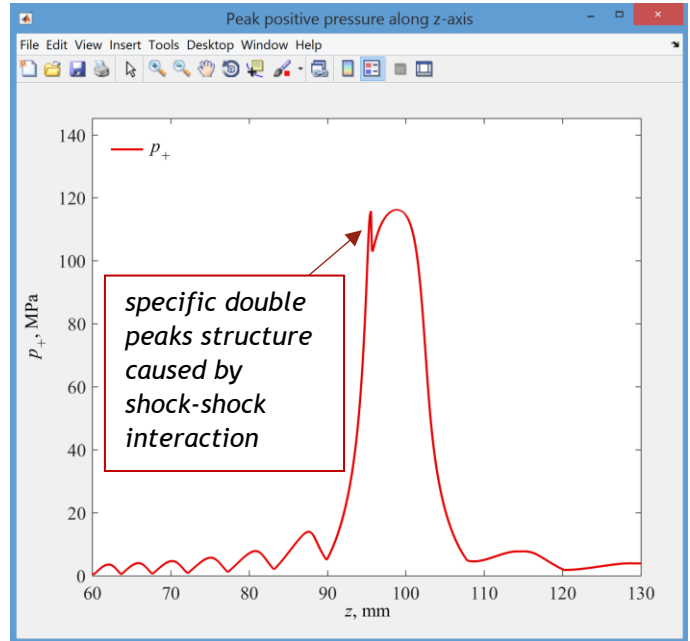


*Display results: power along the beam axis z.*



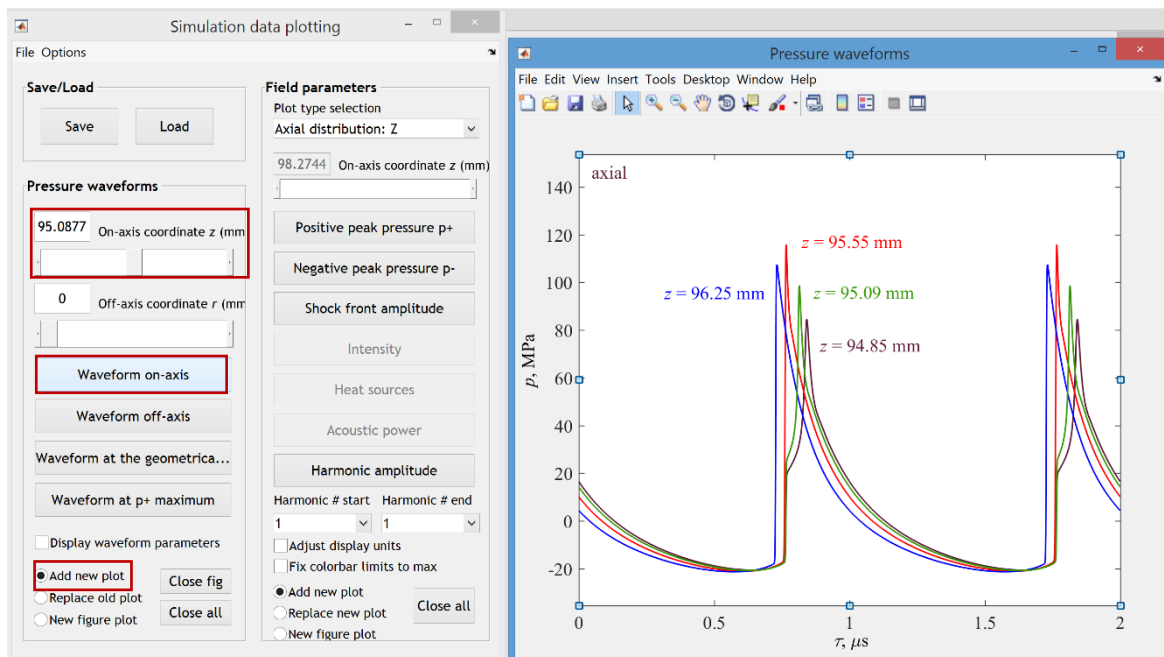
### Saturation regime ( $p_0 = 0.7$ MPa) with specific double spike structure on $p_+(z)$

With further increase in  $p_0$  beyond the level of the developed shock formation ( $p_0 = 0.45$  MPa), the bottom edge of the shock continues to move down below the zero-pressure level. However, the growth rate of the shock front becomes slower because of strong energy attenuation in the shocks which start to form prefocally. At these pressure levels, experienced users of the parabolic KZK model expect to see a specific double spike structure on the axial distribution of the peak positive pressure. <sup>1,32,33,34</sup> Indeed, such structure forms for the considered transducer and shown in the figure on the right for  $p_0 = 0.7$  MPa.



Display results: axial distribution of the peak positive pressure ('KZK' mode with eqv. source).

In order to identify the physical reasons for the formation of such a spike, pressure waveforms should be analyzed in its vicinity. In the prefocal region, just before the spike formation distance, the pressure waveform contains two shock fronts (see waveforms at  $z = 94.85$  and  $95.09$  mm in the figure below). The left (lower) shock in the waveform corresponds to the direct wave while right (upper) shock comes with the edge wave of the piston source. Since energy absorption at the shock front is proportional to the cube of the shock amplitude  $A_{sh}^3$ , energy absorption for a wave with two shocks is



Display results: axial pressure waveforms in the vicinity of the prefocal peak.

proportional to the sum of cubes of two shock amplitudes  $\left(A_{sh1}^3 + A_{sh2}^3\right)$ . Propagating closer to the focus, shock fronts of the direct and the edge waves merge at a certain distance. Exactly at this distance top of the peak is located ( $z = 95.55$  mm). After merging of the two shocks, energy absorption is proportional to  $\left(A_{sh1} + A_{sh2}\right)^3$  and increases sharply because of inequality  $\left(A_{sh1} + A_{sh2}\right)^3 > \left(A_{sh1}^3 + A_{sh2}^3\right)$ . Amplitude of the resulting shock decreases due to absorption (waveform at  $z = 96.25$  mm). Since this shock-shock interaction occurs in the prefocal area, decrease of  $p_+$  after the spike turns into its increase due to diffraction amplification near the focus.

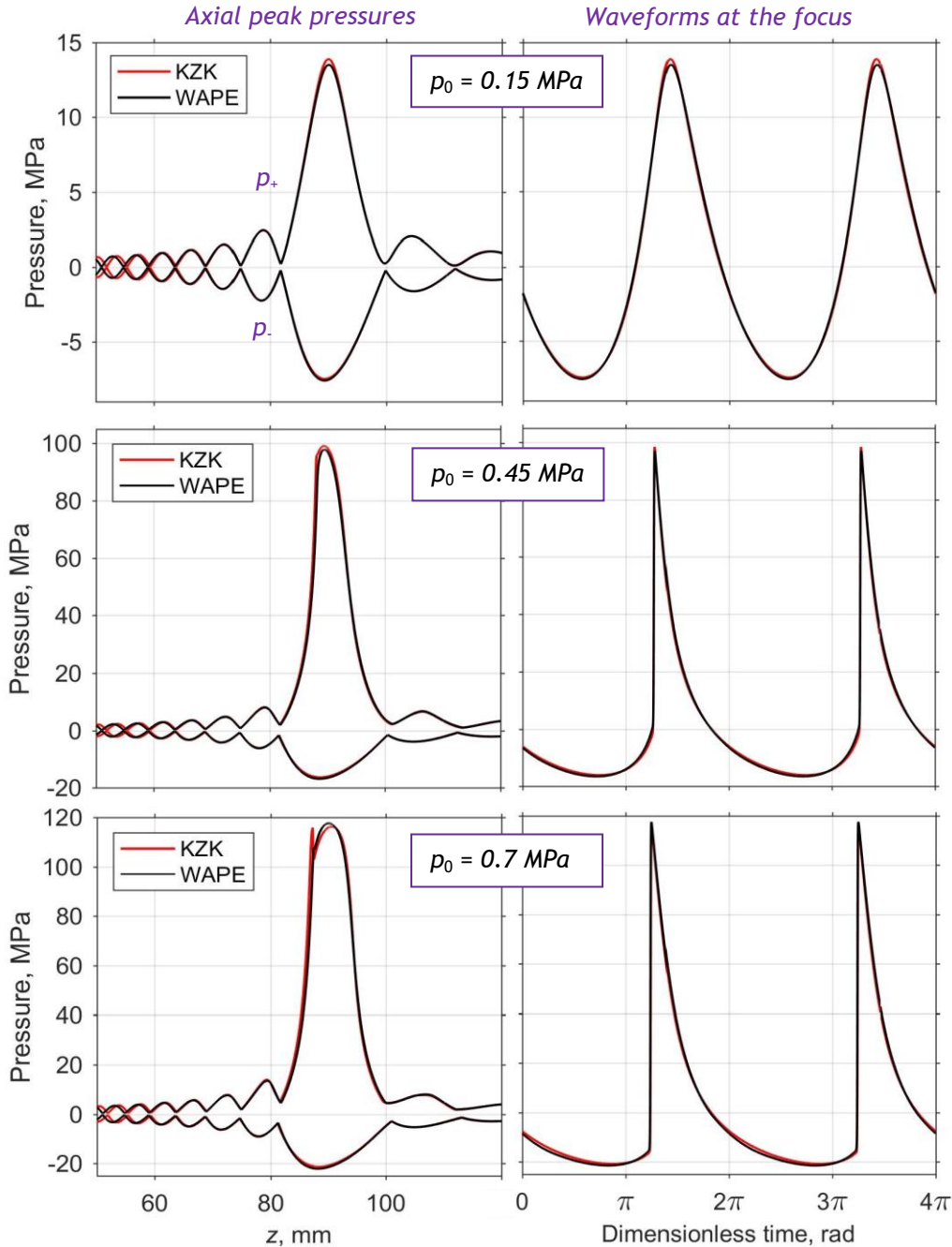
The physical mechanism behind the formation of two shocks at one wave period is diffraction, more specifically, it is related to the arrival of the edge waves. Phenomenon of shock-shock interaction is quite subtle to study. Fine structure of shock fronts should be analyzed for correct description and interpretation. The ‘KZK’ mode takes into account diffraction effects in a parabolic approximation and may underestimate or overestimate this effect. Comparison with the WAPE modeling and further discussion are given in the next section.

### *‘WAPE’ vs. ‘KZK’: certain differences in calculation details*

The ultrasound field of a single element spherical source of 1 MHz frequency ( $F = 90$  mm,  $D = 100$  mm) considered above was also characterized in the ‘WAPE’ mode. For both ‘KZK’ and ‘WAPE’ modes the numerical grids in the simulation were the same for the same values of  $p_0$  (auto grid parameters were chosen in the interface). Comparison of axial distributions of the peak positive and the peak negative pressures as well as comparison of waveforms at the geometrical focus ( $z = F = 90$  mm) are shown below in the figure for both ‘KZK’ and ‘WAPE’ modes. The  $z$ -axis for the ‘KZK’ results was shifted on 8.2744 mm to have it related to the real source, not to the parabolic equivalent one.

In general, the results are in a very good agreement for both models. For the quasilinear case ( $p_0 = 0.15$  MPa) maximal discrepancy between levels of focal pressure does not exceed 3%. For the level of  $p_0$  that corresponded to the developed shock formation ( $p_0 = 0.45$  MPa), the discrepancy between two models is less than 2%. At saturation level, for  $p_0 = 0.7$  MPa, the effect of shock-shock peak formation is slightly higher in the KZK model. The WAPE model also predicts a small peak on the  $p_+$  distribution, but it is less pronounced compared to the parabolic model. The reason for this discrepancy is most probably related to different accuracy of governing the diffraction effects. For small diffraction angles, shock-shock interaction is stronger since the shock fronts are less distant from each other and merge faster. The parabolic KZK model reduces the diffraction angle, which leads to an artificial enhancement of shock-shock interactions in the prefocal zone. Nevertheless, even in this case the maximal discrepancy between the two models is 7% in tiny vicinity of the prefocal peak only.

Note that a tenfold reduction in steps of the calculation grid halves the prefocal peak amplitude in the ‘KZK’ mode, but the calculation time increases significantly and the peak is still higher than in the WAPE model. Our recommendation is to use ‘WAPE’ mode if you don’t have specific preference to simulate the KZK equation and exclude this tiny extra peak when evaluating the peak positive pressure values.



Comparison of results obtained by using ‘KZK’ and ‘WAPE’ modes for a single-element spherical source of 1-MHz frequency ( $F = 90$  mm,  $D = 100$  mm).

### Examples of scripts to plot results directly from .mat files

Some users of “HIFU beam” may prefer to plot the results not through a graphical interface, but directly through MATLAB scripts, as it has been done with the last figure. For those who prefer their own plot scripts we give examples on how to plot axial

distributions of the peak pressures and waveform at the focus from the `.mat` file created by the software. At the end of the simulation, save the results and refer to the scripts shown here. The data are packed into a structure called `'simdata'`. Note that the pressures `'simdata.Pmax'` and `'simdata.Pmin'` are dimensionless and normalized to  $p_0$ . All axes are in `'simdata.Axes'`. Below is provided a possible script to plot results, just copy it to your MATLAB editor, change path and run after commenting unnecessary parts.

```
%----script to plot results obtained by HIFU beam software-----
clc;
clear all

path = 'G:\Projects_rus\HIFUbeam\'; %enter path to the folder 'MatlabLibrary'
GPath.lib = fullfile([path 'MatlabLibrary\']);
addpath(genpath([GPath.lib]));

datapath = 'G:\Projects_rus\HIFUbeam\Data_HIFUbeam\'; %enter path to folder where results were saved
load(fullfile(datapath,'D100_F90_P0_045.mat')); %load .mat file with data

%-----axial pressures (for KZK mode with eqv. source)-----
hf = figure;
Font = 10;
set(hf,'Units','centimeters','Position',[11 6 8 7]);
set(hf,'DefaultLineLineWidth',1.0,'DefaulttextFontSize',Font, 'DefaulttextFontName', 'Arial');
F = simdata.Source.RingP.F * 1e3; % focal distance in mm
shift = F - 90; % enter focal depth of the real source, 90 mm in given case
plot(simdata.Axes.Pmax.pt.zg-shift, simdata.Pmax.pt{1, 1}.*simdata.Phys.p0.*1e-6); hold on
plot(simdata.Axes.Pmin.pt.zg-shift, simdata.Pmin.pt{1, 1}.*simdata.Phys.p0.*1e-6); hold on
grid on
xlim([0 max(simdata.Axes.Pmax.pt.zg-shift)]);
set(gca,'fontSize',Font,'fontName','Arial', 'box','on','TickDir','out');
ylabel('\rmPressure, MPa');
xlabel('\itz\rm, mm');

%-----axial pressures (for WAPE mode)-----
hf = figure;
Font = 10;
set(hf,'Units','centimeters','Position',[11 6 8 7]);
set(hf,'DefaultLineLineWidth',1.0,'DefaulttextFontSize',Font, 'DefaulttextFontName', 'Arial');
plot(simdata.Axes.Pmax.pt.zg, simdata.Pmax.pt{1, 1}.*simdata.Phys.p0.*1e-6); hold on
plot(simdata.Axes.Pmin.pt.zg, simdata.Pmin.pt{1, 1}.*simdata.Phys.p0.*1e-6); hold on
grid on
xlim([0 max(simdata.Axes.Pmax.pt.zg)]);
set(gca,'fontSize',Font,'fontName','Arial', 'box','on','TickDir','out');
ylabel('\rmPressure, MPa');
xlabel('\itz\rm, mm');

%-----waveforms at the focus -----
hf = figure;
Font = 10;
set(hf,'Units','centimeters','Position',[11 6 8 7]);
set(hf,'DefaultLineLineWidth',1.0,'DefaulttextFontSize',Font, 'DefaulttextFontName', 'Arial');

% choose variant with ind - first for 'KZK', second for 'WAPE' (RingP or RingF)
%ind = find(simdata.Axes.Wf.pt.zg >= simdata.Source.RingP.F * 1e3,1); % index of z = F for KZK
ind = find(simdata.Axes.Wf.pt.zg >= simdata.Source.RingF.F * 1e3,1); % index of z = F for WAPE

% plotE is a function from the folder 'MatlabLibrary'
plotE(simdata.Axes.tg, simdata.Wf.pt{1,1}(:,1, ind).*simdata.Phys.p0.*1e-6,'t2'); hold on

grid on
set(gca,'fontSize',Font,'fontName','Arial', 'box','on','TickDir','out');
ylabel('\rmPressure, MPa');
xlabel('\rmDimensionless time, rad');
xlim([0 4*pi]);
set(gca,'XTick',0:pi:4*pi)
set(gca,'XTickLabel',{'0','\fontsize{13}\pi','\fontsize{10}2\fontsize{13}\pi',...
'\fontsize{10}3\fontsize{13}\pi','4\fontsize{13}\pi'});
```

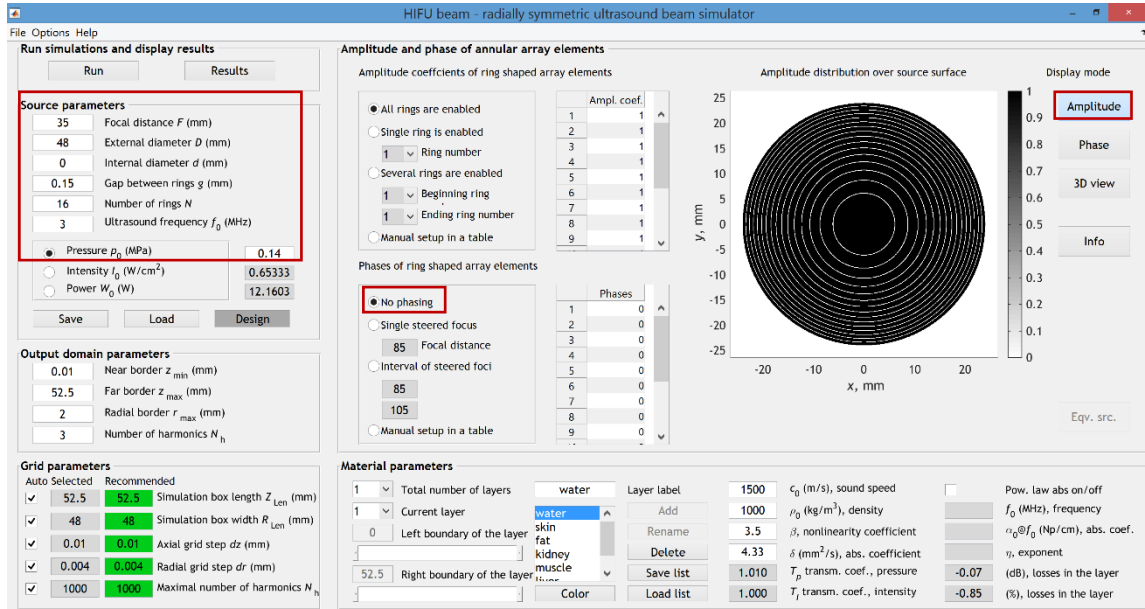
## Ring-shaped array, propagation in water

The next example of a representative ultrasound source is a ring-shaped array that has been used for developing thermal and mechanical methods of tissue ablation in mouse tumors.<sup>35</sup> The source is a 3 MHz 16-element annular array of 48 mm diameter, 35 mm radius of curvature, and the ring spacing is 0.15 mm. In calculations of its acoustic field in water, ‘WAPE’ mode is used.

Results of simulations shown here were performed for quasilinear, developed shock formation, and saturation cases. In the first series of simulations, there was no additional phasing of the array elements. When focusing at the geometrical focus, the quasilinear case corresponds to  $p_0 = 0.14$  MPa and developed shock forms at the focus at  $p_0 = 0.425$  MPa. The case that corresponded to saturation regime was simulated for  $p_0 = 0.75$  MPa.



Ring-shaped array of 3-MHz frequency ( $F = 35$  mm,  $D = 48$  mm, 16 elements). Photo is taken from [35] (fig. 1a).

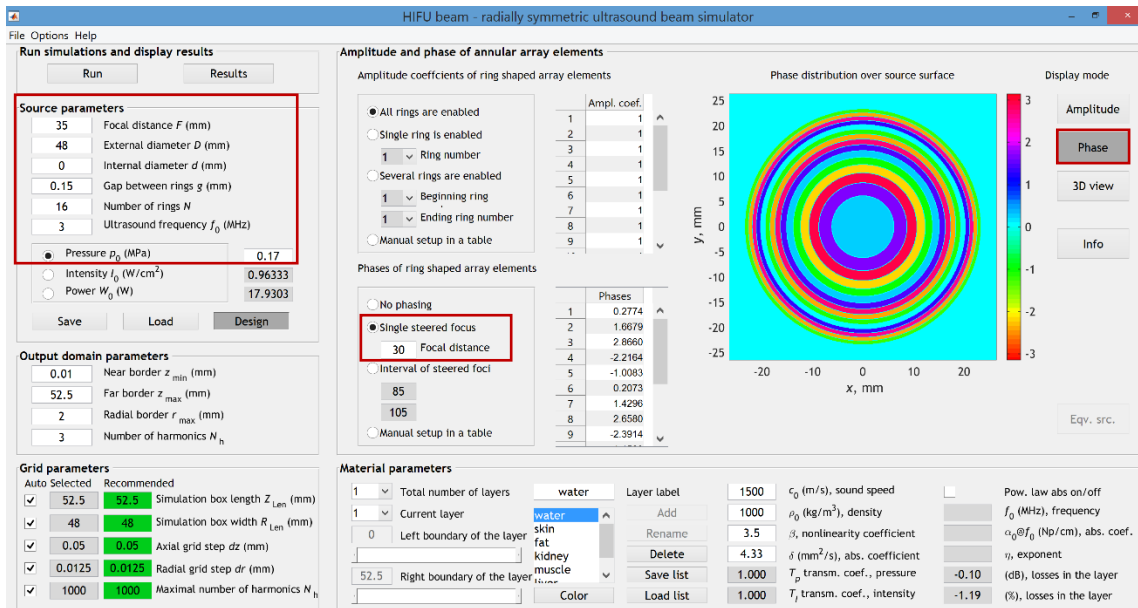


Setting parameters of 3 MHz 16-element ring-shaped array ( $F = 35$  mm,  $D = 48$  mm) in the ‘WAPE’ mode for  $p_0 = 0.14$  MPa (quasilinear case).

In the second series of calculations, the focus was steered to the location  $z = 30$  mm by adding phases to the array elements. In this case, the waveform at steered focus was quasilinear at  $p_0 = 0.17$  MPa and formation of a developed shock at steered focus occurred at  $p_0 = 0.525$  MPa. The saturation case was also simulated for  $p_0 = 0.75$  MPa to show the differences arising when source power  $W_0$  is the same but with and without steering. In order to compare the results of simulations for different values of  $p_0$ , we saved the data obtained with “HIFU beam” and plotted them by a MATLAB script without using the graphical interface of the software.

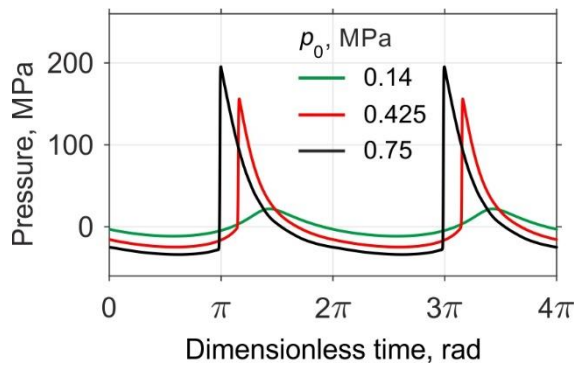
Shown below are pressure waveforms simulated for 3 cases (quasilinear, formation of the developed shock, and saturation) when focusing occurs at the geometrical focus (on the left) and steered 5 mm closer to the source (on the right).



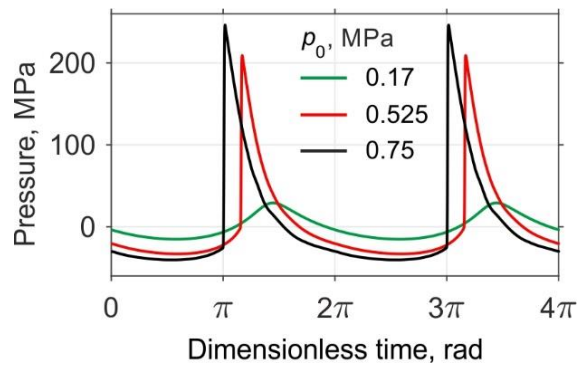


Setting parameters of 3 MHz 16-element ring-shaped array ( $F = 35$  mm,  $D = 48$  mm) in the 'WAPE' mode with focus steered at  $z = 30$  mm for  $p_0 = 0.17$  MPa (quasilinear case).

Small dimensions of the source and its quite high operation frequency (3 MHz) allow to obtain shock fronts of very high amplitude (about 200 MPa) at the focus.



Pressure waveforms at the focus  $z = F = 35$  mm for quasilinear ( $p_0 = 0.14$  MPa), developed shock formation ( $p_0 = 0.425$  MPa), and saturation ( $p_0 = 0.75$  MPa) cases.

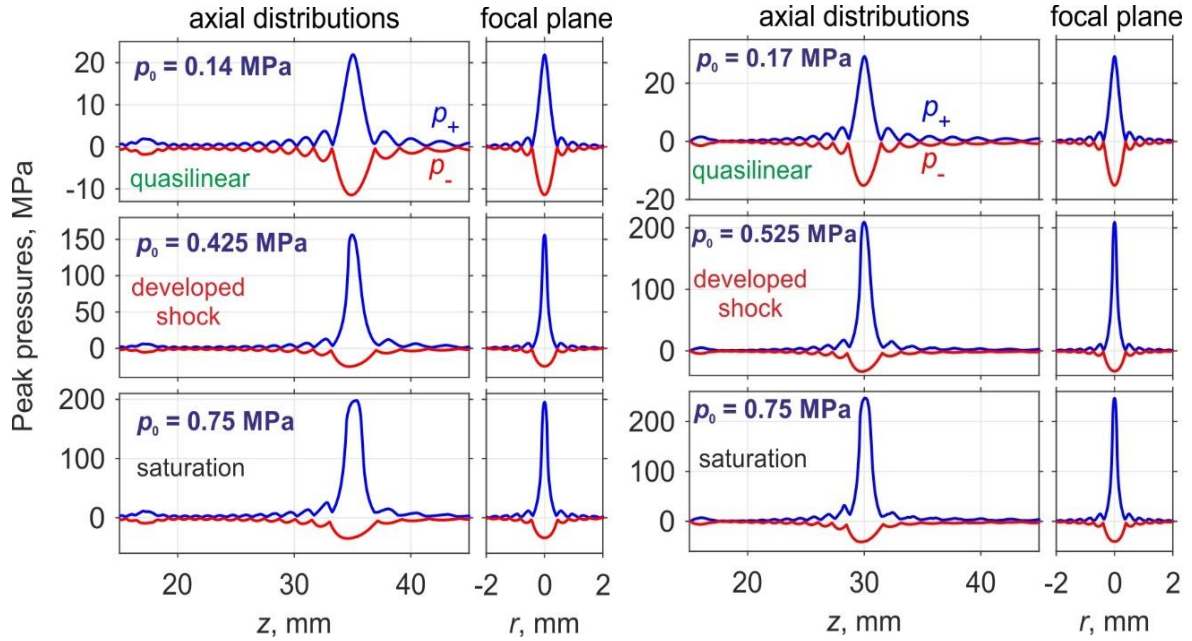


Pressure waveforms at steered focus  $z = 30$  mm for quasilinear ( $p_0 = 0.17$  MPa), developed shock formation ( $p_0 = 0.525$  MPa), and saturation ( $p_0 = 0.75$  MPa) cases.

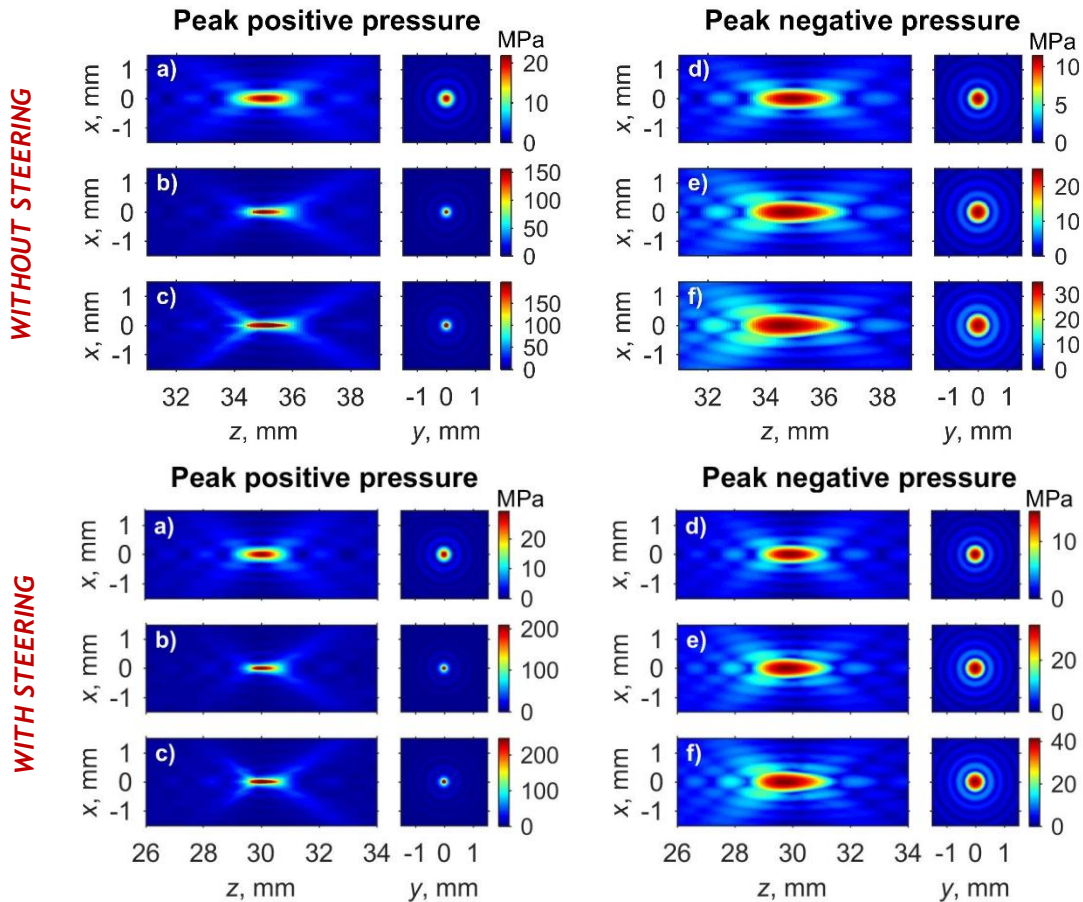
Steering the focus by phasing the array elements increases the focusing angle for comparing to the current geometry. In a publication discussing this data [12] it was shown that the most important parameter of the source that controls nonlinear effects is the focusing angle. It follows that focus steering can change manifestation of nonlinear effects. When the focus is steered at  $z = 30$  mm, the beam has higher focusing angle than without steering, developed shock forms at higher pressure levels  $p_0$  (0.525 MPa vs. 0.425 MPa) and has higher amplitude.

The size of the focal lobe also changes with changing focusing angle. Weakly focused beams have longer focal lobes. In 1D axial distributions of the peak positive and peak negative pressures (see figure below) it is clearly shown that focal lobe in the case of steering (right column) is narrower than in the case without steering (left column). Thus, for the considered 16-element array, steering the focus 5 mm closer to the source

leads to decrease of the length of the focal lobe, to formation of the developed shock front at higher array power and to higher pressure levels achievable at steered focus in saturation regime (see figures below).



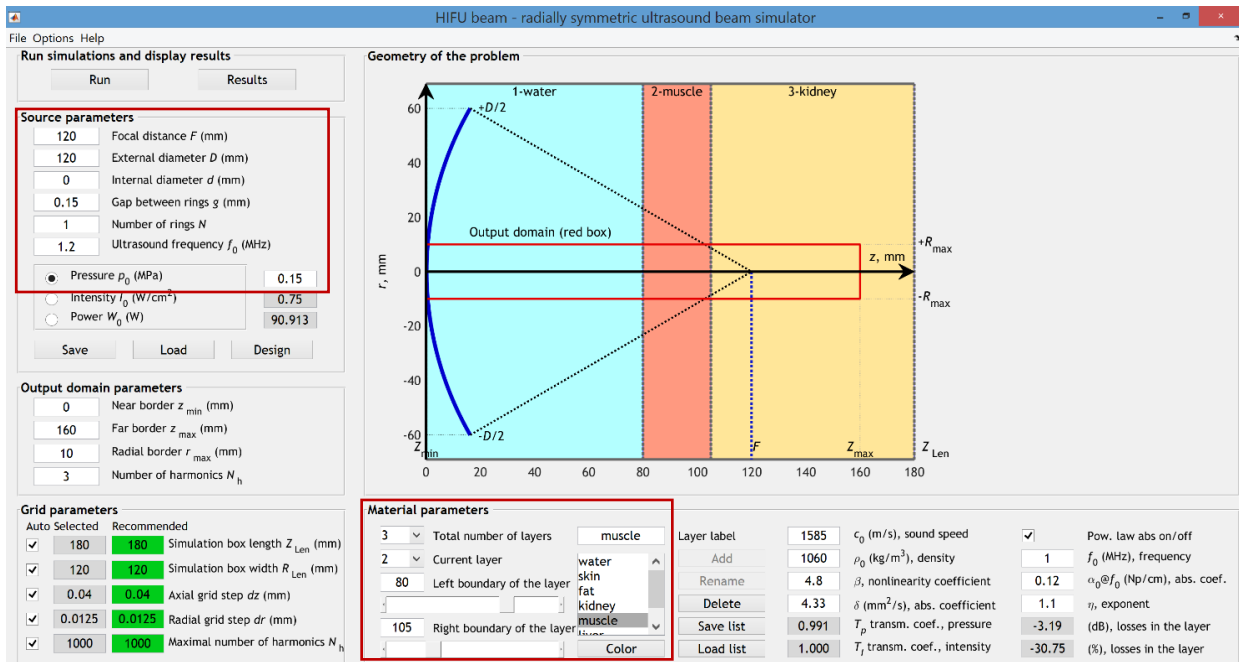
1D axial and radial distributions of the peak positive and the peak negative pressures. Left part corresponds to focusing at the focus  $z = F = 35$  mm, right part - to steering the focus at  $z = 30$  mm.



2D distributions of the peak positive (a,b,c) and the peak negative (d,e,f) pressures in cases without steering and with steering. a),d) corresponds to quasilinear case; b),e) -to developed shock formation; c),f)- to saturation case.

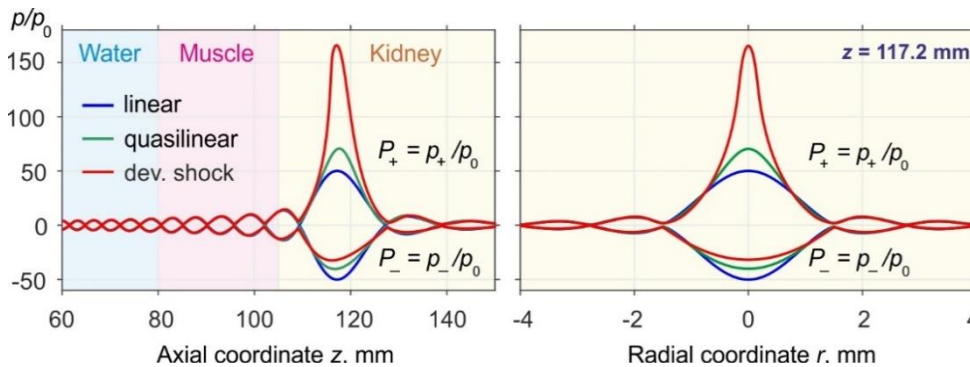
## Single-element spherical HIFU source, multi-layered medium

The last example is for a transducer with parameters typical for real HIFU transducer in a clinical setting. The source has the same operating frequency  $f_0 = 1.2$  MHz and the same focal distance  $F = 120$  mm as the array of the MRgHIFU Sonalleve system (Med. Profound, Canada).<sup>14</sup> The diameter  $D$  is 120 mm which provides  $F$ -number equal to unity. Propagation is in a layered medium consisting of water ( $0 \leq z \leq 80$  mm), muscle ( $80 \leq z \leq 105$  mm), and kidney ( $z \geq 105$  mm). Simulations are performed in the 'WAPE' mode for linear, quasilinear ( $p_0 = 0.15$  MPa), developed shock formation ( $p_0 = 0.375$  MPa), and saturation ( $p_0 = 0.75$  MPa) cases. The saturation case corresponds to the source power of 2273 W which is achievable in practice and the results for this case are presented to demonstrate how nonlinear effects develop further after shock formation.



Setting parameters for 1.2 MHz single-element spherical source ( $F = D = 120$  mm) in the 'WAPE' mode, propagation medium includes 3 layers (water, muscle, kidney),  $p_0 = 0.15$  MPa (quasilinear case).

In the presence of tissue layers, the maximum of  $p_+$  is reached closer to the source than it would be in water due to the refraction at layer interfaces: in the linear case the pressure maximum is shifted to  $z = 117.2$  mm while geometrical focus is at  $z = F = 120$  mm. The focal gain is about 50 for the linear propagation.



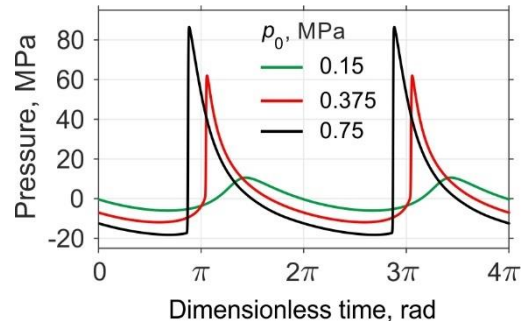
1D axial (on left) and radial (on right) distributions of normalized peak positive and peak negative pressures for linear, quasilinear ( $p_0 = 0.15$  MPa), and developed shock formation ( $p_0 = 0.375$  MPa) cases.



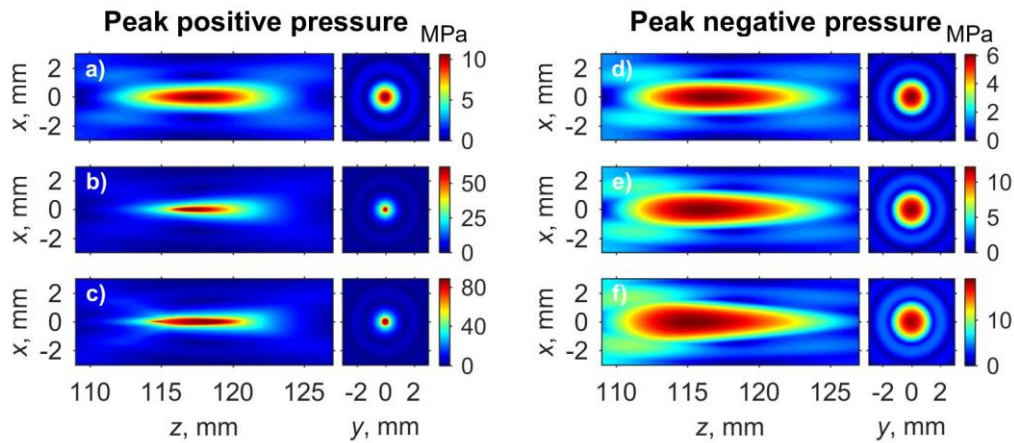
Nonlinear effects increase the focal gain for the peak positive pressure:<sup>6,11</sup> it reaches 70 already in quasilinear case although the pressure waveform is slightly distorted. When developed shock formation occurs, the focal gain is 165. However, the amplitude of the developed shock is only about 60 MPa because of significant absorption in muscle layer and in kidney.

When shock front starts to develop in the pressure waveform, the focusing efficiency increases, but at the same time the focal lobe becomes narrower. The smallest size of the focal lobe approximately corresponds to formation of the fully developed shock. In this case, the spectrum is dominated by higher harmonics which are focused very locally. The focal region of  $p_+$  has elongated shape: its axial length is about 6 mm while the transverse size is only 0.6 mm at -6 dB level. With further increase of  $p_0$ , shocks form not only close to the focus but also in adjacent area. The focusing efficiency decreases as compared to the case of the developed shock formation and the size of the focal area increases (see figure below, left column with 2D  $p_+$  distributions).

The focal lobe of the peak negative pressure  $p_-$  is extending in the axial direction with the increase of  $p_0$  and moves towards the source (see figure below, right column with 2D  $p_-$  distributions).



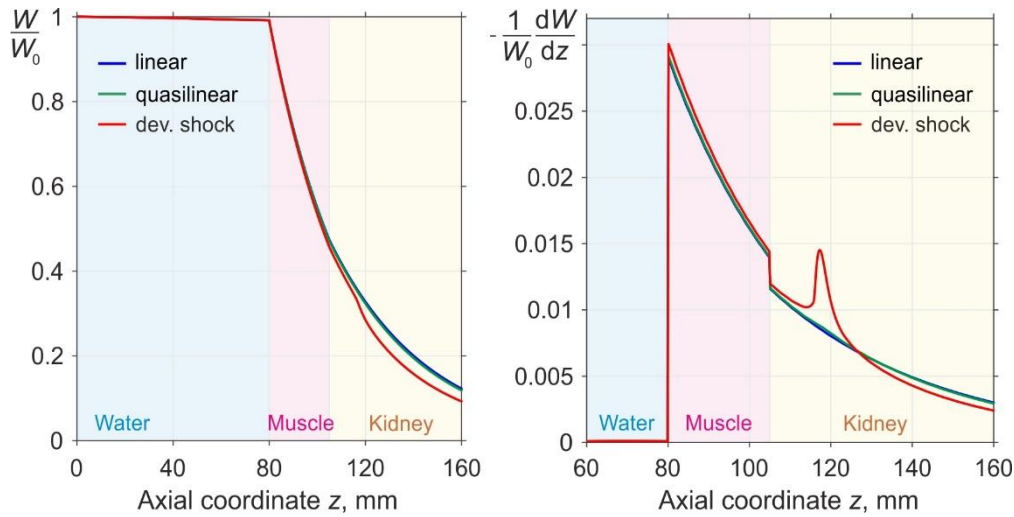
Pressure waveforms at  $z = 117.2$  mm for quasilinear ( $p_0 = 0.15$  MPa), developed shock formation ( $p_0 = 0.375$  MPa), and saturation ( $p_0 = 0.75$  MPa) cases.



2D distributions of the peak positive (a,b,c) and the peak negative (d,e,f) pressures. a),d) corresponds to quasilinear case; b),e) -to developed shock formation; c),f)- to saturation case.

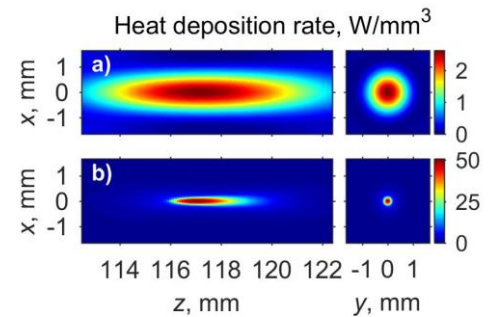
The software “HIFU beam” can also help users to evaluate the increase in the thermal effect caused by nonlinear focusing of ultrasound in tissue. Clicking ‘Acoustic power’, the user can visualize the change of the total acoustic beam power  $W$  with propagation distance. The button ‘heat sources’ is for 1D and 2D distributions of the heat deposition rate.

In the linear case, the total acoustic beam power decreases exponentially in tissue. Formation of the shock front leads to additional heat deposition proportional to the cube of the shock amplitude  $A_{sh}^3$ . As shown in the figure below, in the case of developed shock formation, the decrease of the total beam power deviates significantly from the exponential law after ‘muscle-kidney’ boundary in comparison to the quasilinear case. In a focal region, there is a sharp jump in power losses caused by formation of the shock.



*Total acoustic beam power (on the left) and losses of power  $dW/dz$  (on the right) normalized to the initial acoustic power  $W_0$  along the beam axis  $z$  for linear, quasilinear ( $p_0 = 0.15$  MPa), and developed shock formation ( $p_0 = 0.375$  MPa) cases.*

Despite the fact that normalized power losses  $-(1/W_0)dW/dz$  differ in the focus by only about two times between linear propagation and nonlinear with the developed shock formation, acoustic beam power is distributed over different volumes. In the linear case, calculated for the same power as for the developed shock formation (568 W,  $p_0 = 0.375$  MPa), the maximum of the heat deposition rate is  $2.6 \text{ W/mm}^3$  while for the nonlinear propagation it is about 20 times higher ( $50.6 \text{ W/mm}^3$ ). At the same time, axial and radial sizes of focal areas for heat sources differ in 3 times: it is smaller when the developed shock formation occurs (see figure with heat sources).



*Heat sources in axial  $zr$  and focal  $xy$  planes for the same power of 568 W when propagation is linear (a) and nonlinear with developed shock formation at the focus (b).*

In summary, shock-wave exposure protocols provide very fast heating of tissue in a localized volume. This effect is used in boiling histotripsy methods to liquefy tissue mechanically<sup>22,23</sup> and in developing methods of faster volumetric thermal tissue ablation by shock waves in existing clinical HIFU systems<sup>36</sup>.

## Appendix: numerical methods and algorithms

Numerical simulations of the KZK equation and WAPE are based on the method of fractional steps with an operator splitting procedure of the second-order accuracy. A combined time-and frequency-domain approach is used to describe different physical effects separately at each step of the grid along the beam axis from  $z$  to  $z + \Delta z$ . At each spatial point  $(r, z)$  the pressure is represented either as a temporal pressure waveform or in the form of a finite Fourier series expansion by harmonic components. An adaptive algorithm with varying number of harmonics included in simulations is used at each step over the coordinate  $z$ . The number of harmonics is increased with increasing distortion of the waveform and corresponding broadening of its spectrum. If the amplitude of the last currently used harmonic exceeds 1% of the source amplitude, then larger number of higher harmonics is added to the calculation up to the maximal number of 1000, which was found to be sufficient for accurate governing nonlinear propagation effects and evolution of high-amplitude shocks generated by HIFU single-element transducers and annular arrays in a flat-layered medium imitating biological tissues.

Since the nonlinear and absorption operators are the same for both the ‘KZK’ and ‘WAPE’ modes, identical methods to calculate them were used.

### *Boundary Conditions for the Radial Coordinate (PML)*

The waves radiated by the source propagate both in radial and axial directions. Eventually, they reach the radial boundary of the numerical domain  $R_{\text{Len}}$ . If no special care is taken, the waves reflect back to the beam axis  $r = 0$  and interfere with the primary acoustic field, which is typically observed as appearance of ripples. This effect can be mitigated by increasing  $R_{\text{Len}}$ , since for longer propagation distances the wave amplitude decreases at least due to geometrical spreading. However, it is not practical to take  $R_{\text{Len}}$  significantly larger than 1.5–2 of the source radius. In order to properly deal with reflections from radial boundary, the perfectly matched layer (PML) method is used. Here, details of the method are presented for radially symmetric case realized in the “HIFU beam” simulator.

A small boundary layer with thickness  $w = R_{\text{Len}} - r_{\text{PML}}$  is introduced, in which the radial coordinate  $r$  is transformed to the complex value  $\tilde{r}$  as:

$$\tilde{r} = r + \int_{r_{\text{PML}}}^r \frac{i\sigma(r')}{\omega} dr', \quad (\text{A1})$$

where  $\sigma(r)$  is a positive attenuation function which is non-zero only within PML; the PML begins at the spatial coordinate  $r_{\text{PML}}$  and continues up to the outer boundary  $R_{\text{Len}}$ . In simulations,  $R_{\text{Len}}$  was chosen equal to  $D$ , so the simulation box width is equal to twice the external diameter of the source.

The function for infinitesimal variations of complex spatial coordinate  $\tilde{r}$  gives  $d\tilde{r} = Sdr$ , where  $S(r) = 1 + \frac{i\sigma(r)}{\omega}$  has a meaning of complex stretch factor. Introducing a variable  $\bar{S}(r) = 1 + \frac{1}{r} \int_{r_{\text{PML}}}^r \frac{i\sigma(r')}{\omega} dr'$ , one obtains the relation between the coordinates  $\tilde{r}$  and  $r$ :  $\tilde{r} = r\bar{S}(r)$ .

As a result, differential operator  $\hat{L}$  within the layer is transformed as:

$$\begin{aligned} \frac{1}{k^2} \frac{1}{\tilde{r}} \frac{\partial}{\partial \tilde{r}} \left( \tilde{r} \frac{\partial}{\partial \tilde{r}} \right) &= \frac{1}{\bar{S}r} \frac{1}{S} \frac{\partial}{\partial r} \left[ \frac{\bar{S}}{S} r \frac{\partial}{\partial r} \right] = \frac{1}{\bar{S}r} \frac{1}{S} \frac{\bar{S}}{S} \frac{\partial}{\partial r} \left[ r \frac{\partial}{\partial r} \right] + \frac{1}{\bar{S}r} \frac{1}{S} \left[ \frac{\bar{S}'S - S'\bar{S}}{S^2} \right] r \frac{\partial}{\partial r} = \\ &= \frac{1}{S^2} \left[ \frac{1}{r} \frac{\partial}{\partial r} \left( r \frac{\partial}{\partial r} \right) + \frac{\bar{S}'S - S'\bar{S}}{\bar{S}S} \frac{\partial}{\partial r} \right], \end{aligned} \quad (\text{A2})$$

where  $S'(r)$  and  $\bar{S}'(r)$  denote their derivatives over the coordinate  $r$ . These functions differ from unity only within the PML; outside the PML, the differential operator  $\hat{L}$  has its original form.

In the simulator “HIFU beam” the attenuation function  $\sigma(r)$  is chosen following a power law as follows:

$$\sigma(r) = \sigma_0 \left( \frac{r - r_{\text{PML}}}{R_{\text{Len}} - r_{\text{PML}}} \right)^3. \quad (\text{A3})$$

The value of the coefficient  $\sigma_0$  and the PML thickness are usually chosen experimentally by minimizing the amplitude of the reflected waves. In the “HIFU beam”,  $\sigma_0$  is chosen exceeding the angular frequency  $\omega_0$  by a factor of 10. The layer width  $w$  is chosen equal to 10 mm. The amplitude of the reflected waves for such choice was less than -80 dB of the incident wave amplitude in typical cases that have been evaluated.

## Diffraction operator

### Diffraction operator in the 2D radially symmetric KZK equation (mode ‘KZK’)

The diffraction operator in the ‘KZK’ mode is calculated in the frequency domain independently for each harmonic component:

$$\frac{\partial p_n}{\partial z} = \frac{ic_0}{2n\omega_0} \Delta_{\perp} p_n. \quad (\text{A4})$$

At each splitting step, the diffraction operator is solved by finite difference schemes, either using a fully implicit backward differences scheme or a semi-implicit Crank-Nicolson scheme.<sup>37</sup> The fully implicit backward differences scheme is the more

absorptive of the two and it is used at the initial stage of the wave propagation. In the software, it is applied up to the distance of  $0.05F$  in order to suppress field oscillations caused by sharp edges of the pressure distribution in the source plane. Especially, oscillations can occur in the case of the piston source with sharp edges. The finite difference equations for the backward differences scheme are:

$$\begin{aligned} p_{n,j}^{m+1} - p_{n,j}^m &= \frac{i(\Delta z)c_0}{2n\omega_0(\Delta r)^2} \left[ p_{n,j+1}^{m+1} - 2p_{n,j}^{m+1} + p_{n,j-1}^{m+1} + \frac{p_{n,j+1}^m - p_{n,j-1}^m}{2(j-1)} \right], \quad j = 2 \dots N_r - 1, \\ p_{n,1}^{m+1} - p_{n,1}^m &= \frac{2i(\Delta z)c_0}{n\omega_0(\Delta r)^2} [p_{n,2}^{m+1} - p_{n,1}^{m+1}], \quad j = 1 \quad (r = 0), \\ p_{n,N_r}^{m+1} - p_{n,N_r}^m &= \frac{i(\Delta z)c_0}{n\omega_0(\Delta r)^2} [p_{n,N_r-1}^{m+1} - p_{n,N_r}^{m+1}], \quad j = N_r \quad (r = R_{\text{Len}}). \end{aligned} \quad (\text{A5})$$

The scheme (A5) is of second order of accuracy over the radial coordinate  $r$  (step  $\Delta r$ , index of the spatial grid node  $j$ ) and of first order of accuracy over the axial coordinate  $z$  (step  $\Delta z$ , index of the spatial grid node  $m$ ). For the axial node  $j = 1$  the discrete

equation is obtained based on the radial symmetry  $\left. \frac{\partial p_\omega}{\partial r} \right|_{r=0} = 0$ , and for the outer

boundary node  $j = N_r$  rigid wall condition is chosen  $\left. \frac{\partial p_\omega}{\partial r} \right|_{r=r_{\text{max}}} = 0$ . Finally, equations of

the system (A5) are represented in a tridiagonal matrix form, which is then solved using the Thomas algorithm.<sup>37</sup>

A semi-implicit Crank-Nicolson scheme is applied at larger ( $z > 0.05F$ ) distances.

The discrete equations for each harmonic component  $p_n$  are:

$$\begin{aligned} p_{n,j}^{m+1} - p_{n,j}^m &= \frac{i\Delta z c_0}{4n\omega_0(\Delta r)^2} \left[ p_{n,j+1}^m - 2p_{n,j}^m + p_{n,j-1}^m + \frac{p_{n,j+1}^{m+1} - p_{n,j-1}^{m+1}}{2(j-1)} + \right. \\ &\quad \left. + p_{n,j+1}^{m+1} - 2p_{n,j}^{m+1} + p_{n,j-1}^{m+1} + \frac{p_{n,j+1}^m - p_{n,j-1}^m}{2(j-1)} \right], \quad j = 2 \dots N_r - 1, \\ p_{n,1}^{m+1} - p_{n,1}^m &= \frac{i\Delta z c_0}{n\omega_0(\Delta r)^2} [p_{n,2}^m - p_{n,1}^m + p_{n,2}^{m+1} - p_{n,1}^{m+1}], \quad j = 1 \quad (r = 0), \\ p_{n,N_r}^{m+1} - p_{n,N_r}^m &= \frac{i\Delta z c_0}{2n\omega_0(\Delta r)^2} [p_{n,N_r-1}^m - p_{n,N_r}^m + p_{n,N_r-1}^{m+1} - p_{n,N_r}^{m+1}], \quad j = N_r \quad (r = R_{\text{Len}}). \end{aligned} \quad (\text{A6})$$

The boundary conditions on the axis and on the edge of the spatial window are the same as they were described for the backward differences scheme. The approximations (A6) are of second order of accuracy over both coordinate  $r$  and  $z$ . The system is solved similarly to the backward differences scheme using the Thomas algorithm.

Note that the splitting step of the diffraction operator is appropriately divided into smaller substeps to maintain necessary accuracy of the numerical method.<sup>13</sup>

### *Diffraction operator in the wide angle parabolic approximation (mode ‘WAPE’)*

For the WAPE, the diffraction operator (35) is solved iteratively for each harmonic component  $p_n$ :

$$\prod_{m=1}^N (1 + \nu_m \hat{L}) p_n(z + \Delta z) = \prod_{m=1}^N (1 + \mu_m \hat{L}) p_n(z), \quad (\text{A7})$$

where  $N = 3$  iterations were used:

$$\begin{aligned} (1 + \nu_m \hat{L}) \tilde{p}_n^m(z + \Delta z) &= (1 + \mu_m \hat{L}) \tilde{p}_n^m(z), \\ \tilde{p}_n^1(z) &= p_n(z), \\ &\dots \\ \tilde{p}_n^{m+1}(z) &= \tilde{p}_n^m(z + \Delta z), \\ &\dots \\ \tilde{p}_n^N(z + \Delta z) &= p_n(z + \Delta z). \end{aligned} \quad (\text{A8})$$

The discrete equations for each iteration are:

$$\begin{aligned} \tilde{p}_{n,j}^{m+1} + \frac{\nu_m c_0^2}{n^2 \omega_0^2 (\Delta r)^2} \left( \tilde{p}_{n,j+1}^{m+1} - 2\tilde{p}_{n,j}^{m+1} + \tilde{p}_{n,j-1}^{m+1} + \frac{\tilde{p}_{n,j+1}^{m+1} - \tilde{p}_{n,j-1}^{m+1}}{2(j-1)} \right) &= \\ = \tilde{p}_{n,j}^m + \frac{\mu_m c_0^2}{n^2 \omega_0^2 (\Delta r)^2} \left( \tilde{p}_{n,j+1}^m - 2\tilde{p}_{n,j}^m + \tilde{p}_{n,j-1}^m + \frac{\tilde{p}_{n,j+1}^m - \tilde{p}_{n,j-1}^m}{2(j-1)} \right), \quad j = 2 \dots N_r - 1, \\ \tilde{p}_{n,1}^{m+1} + \frac{4\nu_m c_0^2}{n^2 \omega_0^2 (\Delta r)^2} (\tilde{p}_{n,2}^{m+1} - \tilde{p}_{n,1}^{m+1}) &= \tilde{p}_{n,1}^m + \frac{4\mu_m c_0^2}{n^2 \omega_0^2 (\Delta r)^2} (\tilde{p}_{n,2}^m - \tilde{p}_{n,1}^m), \quad j = 1 \quad (r = 0), \quad (\text{A9}) \\ \frac{2\nu_m c_0^2}{n^2 \omega_0^2 (\Delta r)^2} \tilde{p}_{n,N_r-1}^{m+1} + \left( 1 - \frac{2\nu_m c_0^2}{n^2 \omega_0^2 (\Delta r)^2} \right) \tilde{p}_{n,N_r}^{m+1} &= \\ = \frac{2\mu_m c_0^2}{n^2 \omega_0^2 (\Delta r)^2} \tilde{p}_{n,N_r-1}^m + \left( 1 - \frac{2\mu_m c_0^2}{n^2 \omega_0^2 (\Delta r)^2} \right) \tilde{p}_{n,N_r}^m, \quad j = N_r \quad (r = R_{\text{Len}}). \end{aligned}$$

The system (A9) is similar to the equation obtained for the semi-implicit Crank-Nicolson scheme (A6) and it is also solved using the Thomas algorithm. Within the PML layer, the finite-difference schemes presented above were modified following the transformation of the operator  $\hat{L}$ .

## Nonlinear operator

To calculate the nonlinear operator, both frequency- and time-domains are used. At small distances from the source, a set of coupled equations for the harmonic amplitudes

$$\frac{\partial p_n}{\partial z} = \frac{i\beta n\omega_0}{2\rho_0 c_0^3} \left( 2 \sum_{m=1}^{\infty} p_m^* p_{n+m} + \sum_{m=1}^{n-1} p_m p_{n-m} \right) \quad (\text{A10})$$

is solved using the fourth-order accuracy Runge-Kutta method.<sup>37</sup> When the amplitude of the 10-th harmonic exceeds the amplitude of the fundamental frequency by 1%, a conservative Godunov-type scheme in the time domain is applied.<sup>6,13,38</sup>

## Absorption

The absorption term is calculated in the spectral domain based on exact analytic solution for each of the harmonics. The term includes thermoviscous absorption of the medium and the power law absorption, Eq. (43), with corresponding dispersion, Eq. (44), in biological tissue:

$$p_n(z + \Delta z) = p_n(z) \exp\left(-\frac{\delta n^2 \omega_0^2}{2c_0^3} \Delta z\right) \exp\left(in\omega_0 \frac{\Delta c(n\omega_0)}{c_0^2} \Delta z - \alpha(n\omega_0) \Delta z\right). \quad (\text{A11})$$



## References and links

---

- [1] V.A. Khokhlova, R. Souchon, J. Tavakkoli, O.A. Sapozhnikov, and D. Cathignol. Numerical modeling of finite amplitude sound beams: Shock formation in the nearfield of a cw plane piston source. *J. Acoust. Soc. Am.*, 2001, v.110, N1, pp. 95-108.
- [2] S.S. Kashcheeva, O.A. Sapozhnikov, V.A. Khokhlova, M.A. Averkiou, and L.A. Crum. Nonlinear distortion and attenuation of intense acoustic waves in lossy media obeying a frequency power law. *Acoustical Physics*, 46(2):170-177, 2000.
- [3] E.A. Filonenko and V.A. Khokhlova. Effect of acoustic nonlinearity on heating of biological tissue by high-intensity focused ultrasound. *Acoustical Physics*, 47(4):468-475, 2001.
- [4] V.A. Khokhlova, A.E. Ponomarev, M.A. Averkiou, and L.A. Crum. Nonlinear pulsed ultrasound beams radiated by rectangular focused diagnostic transducers. *Acoustical Physics*, 52(4):481-489, 2006.
- [5] O.V. Bessonova and V.A. Khokhlova. Spatial structure of high intensity focused ultrasound beams of various geometry. *Physics of Wave Phenomena*, 17(1):45-49, 2009.
- [6] O.V. Bessonova, V.A. Khokhlova, M.R. Bailey, M.S. Canney, and L.A. Crum. Focusing of high power ultrasound beams and limiting values of shock wave parameters. *Acoustical Physics*, 55(4-5): 463-473, 2009.
- [7] O.V. Bessonova, V.A. Khokhlova, M.S. Canney, M.R. Bailey, and L.A. Crum. A derating method for therapeutic applications of high intensity focused ultrasound. *Acoust. Phys.*, 2010, v. 56, No. 3, pp. 376-385.
- [8] M.V. Averiyarov, V.A. Khokhlova, O.A. Sapozhnikov, Ph. Blanc-Benon, and R.O. Cleveland. Parabolic equation for nonlinear acoustic wave propagation in inhomogeneous moving media. *Acoustical Physics*, 52(6):623-632, 2006.
- [9] M.M. Karzova, M.V. Averiyarov, O.A. Sapozhnikov, and V.A. Khokhlova. Mechanisms for saturation of nonlinear pulsed and periodic signals in focused acoustic beams. *Acoustical Physics*, 58(1):81-89, 2012.
- [10] P.B. Rosnitskiy, P.V. Yuldashev, B.A. Vysokanov, and V.A. Khokhlova. Setting boundary conditions to the Khokhlov-Zabolotskaya equation for modeling ultrasound fields generated by strongly focused transducers. *Acoustical Physics*, 62(2):151-159, 2016.
- [11] P.B. Rosnitskiy, P.V. Yuldashev, O.A. Sapozhnikov, A.D. Maxwell, W. Kreider, M.R. Bailey, and V.A. Khokhlova. Design of HIFU transducers for generating specified nonlinear ultrasound fields. *IEEE Transactions on Ultrasonics, Ferroelectrics, and Frequency Control*, 64(2):374-390, 2017.
- [12] P.B. Rosnitskiy, P.V. Yuldashev, and V.A. Khokhlova. Effect of the angular aperture of medical ultrasound transducers on the parameters of nonlinear ultrasound field with shocks at the focus. *Acoust. Phys.* 61(3):301-307, 2015.
- [13] P.V. Yuldashev and V.A. Khokhlova. Simulation of three-dimensional nonlinear fields of ultrasound therapeutic arrays. *Acoustical Physics*, 57(3):334-343, 2011.
- [14] C. Perez, H. Chen, T.J. Matula, M.S. Karzova, V.A. Khokhlova. Acoustic field characterization of the Duolith: Measurements and modeling of a clinical shockwave therapy device. *J. Acoust. Soc. Am.*, 2013, 134(2), Pt.2, pp. 1663-1674.
- [15] W. Kreider, P.V. Yuldashev, O.A. Sapozhnikov, N. Farr, A. Partanen, M.R. Bailey, and V.A. Khokhlova. Characterization of a multi-element clinical HIFU system using acoustic holography and nonlinear modeling. *IEEE Transactions on Ultrasonics, Ferroelectrics, and Frequency Control*, 60(8):1683-1698, 2013.
- [16] A.D. Maxwell, P.V. Yuldashev, W. Kreider, T.D. Khokhlova, G.R. Schade, T.L. Hall, O.A. Sapozhnikov, M.R. Bailey, and V.A. Khokhlova. A prototype therapy system for transcutaneous application of boiling histotripsy. *IEEE Trans. Ultrason., Ferroelect., Freq. Contr.*, 2017, v. 64(10), pp. 1542 - 1557.
- [17] M.M. Karzova, P.V. Yuldashev, O.A. Sapozhnikov, V.A. Khokhlova, B.W. Cunitz, W. Kreider, M.R. Bailey. Shock formation and nonlinear saturation effects in the ultrasound field of a diagnostic curvilinear probe, *J. Acoust. Soc. Am.*, 2017, v. 141(4), pp. 2327-2337.
- [18] C. R. Bawiec, T. D. Khokhlova, O. A. Sapozhnikov, P.B. Rosnitskiy, B.W. Cunitz, M.A. Ghanem, C. Hunter, W. Kreider, G.R. Schade, P.V. Yuldashev, V.A. Khokhlova. A prototype therapy system for boiling histotripsy in abdominal targets based on a 256 element spiral array. *IEEE Trans. Ultrason., Ferroelect., Freq. Contr.*, 2021, v. 68(5), pp.1496-1510.

- 
- [19] P.V. Yuldashev, I.S. Mezdokhin, and V.A. Khokhlova. Wide-angle parabolic approximation for modeling high-intensity fields from strongly focused ultrasound transducers. *Acoustical Physics*, 64(3):309-319, 2018.
- [20] V.A. Khokhlova, M.R. Bailey, J.A. Reed, B.W. Cunitz, P.J. Kaczkowski, and L.A. Crum. Effects of nonlinear propagation, cavitation, and boiling in lesion formation by high intensity focused ultrasound in a gel phantom. *J. Acoust. Soc. Am.*, 2006, 119(3), 1834 - 1848.
- [21] M.S. Canney, M.R. Bailey, L.A. Crum, V.A. Khokhlova, and O.A. Sapozhnikov. Acoustic characterization of high intensity focused ultrasound fields: A combined measurement and modeling approach. *J. Acoust. Soc. Am.*, 2008, v.124(4), pp. 2406-2420.
- [22] M. Canney, V. Khokhlova, O. Bessonova, M. Bailey, L. Crum. Shock-induced heating and millisecond boiling in gels and tissue due to high intensity focused ultrasound, *Ultrasound in Medicine & Biology*, 2010, v.36(2), pp. 250-267.
- [23] T.D. Khokhlova, M.S. Canney, V.A. Khokhlova, O.A. Sapozhnikov, L.A. Crum, M. R. Bailey. Controlled tissue emulsification produced by high intensity focused ultrasound shock waves and millisecond boiling. *J. Acoust. Soc. Am.*, 2011, v.130(5), pp. 3498-3510.
- [24] T.D. Khokhlova, P.B. Rosnitskiy, C. Hunter, A. Maxwell, W. Kreider, G. ter Haar, M. Costa, O. Sapozhnikov, V. Khokhlova. Dependence of inertial cavitation induced by high intensity focused ultrasound on transducer  $F$ -number and nonlinear waveform distortion. *J. Acoust. Soc. Am.*, 2018, v. 144 (3), pp. 1160-1169.
- [25] H.T. O'Neil. Theory of focusing radiators. *Journal of the Acoustical Society of America*, 21: 516 (1949).
- [26] O.A. Sapozhnikov, S.A. Tsysar, V.A. Khokhlova, W. Kreider. Acoustic holography as a metrological tool for characterizing medical ultrasound sources and fields. *J. Acoust. Soc. Am.* 138, 3, 1515-1532 (2015).
- [27] V.M. Levin, O.I. Lobkis, and R.G. Maev. Sound field of the spherical transducer of arbitrary aperture. *Akusticheskij Zhurnal*, 33 (1): 140-143 (1987).
- [28] P.V. Yuldashev, S.M. Shmeleva, S.A. Ilyin, O.A. Sapozhnikov, L.R. Gavrilov, and V.A. Khokhlova. The role of acoustic nonlinearity in tissue heating behind the rib cage using high intensity focused ultrasound phased array. *Physics in Medicine and Biology*, 58(8):2537-2559, 2013.
- [29] K.R. Waters, J. Mobley, and J. G. Miller. Causality-imposed (Kramers-Kronig) relationships between attenuation and dispersion. *IEEE Transactions on Ultrasonics, Ferroelectrics, and Frequency Control*, 52(5): 822-823, 2005.
- [30] D.A. Nikolaev, S.A. Tsysar, V.A. Khokhlova, W. Kreider, and O.A. Sapozhnikov. Holographic extraction of plane waves from an ultrasound beam for acoustic characterization of an absorbing layer of finite dimensions, 2021, *Journal of the Acoustical Society of America*, v. 149(1), pp. 386-404.
- [31] M.M. Karzova, P.V. Yuldashev, O.A. Sapozhnikov, V.A. Khokhlova, B.W. Cunitz, W. Kreider, and M.R. Bailey. Shock formation and nonlinear saturation effects in the ultrasound field of a diagnostic curvilinear probe. *J. Acoust. Soc. Am.* 141(4): 2327-2337, 2017.
- [32] O.A. Sapozhnikov, V.A. Khokhlova, and D. Cathignol. Nonlinear waveform distortion and shock formation in the near field of a continuous wave piston source, *J. Acoust. Soc. Am.*, 2004, vol. 115(5), Pt. 1, pp. 1982-1987.
- [33] B. Sturtevant, V. A. Kulkarny, The focusing of weak shock waves, *J. Fluid Mech.*, 1976, vol. 73(4), pp. 651-671.
- [34] M. M. Karzova, V. A. Khokhlova, E. Salze, S. Ollivier, Ph. Blanc-Benon, "Mach stem formation in reflection and focusing of weak shock acoustic pulses," *J. Acoust. Soc. Am.*, 2015, v. 137(6), pp. EL436-442.
- [35] V.A. Khokhlova, P. Yuldashev, P. Rosnitskiy, O. Sapozhnikov, E. Dumont, M. Hoogenboom, M. den Brok, J. Futterer, G. Adema. Reconstruction of nonlinear ultrasound field of an annular therapeutic array from acoustic holograms of its individual elements. *Proc. Mtgs. Acoust.* 32(1): 020013/1-020013/4, 2017.
- [36] Y.S. Andriyakhina, M. M. Karzova, P. V. Yuldashev, and V. A. Khokhlova. Accelerated thermal ablation of biological tissue volumes using HIFU beams with shock fronts. *Acoustical Physics*, 2019, v. 65(2), pp. 141-150.

- 
- [37] W.H. Press, S.A. Teukolsky, W.T. Vetterling, and B. P. Flannery, *Numerical Recipes in FORTRAN. The Art of Scientific Computing*, Cambridge, UK: Cambridge University Press, 2nd ed., 1992.
- [38] A. Kurganov and E. Tadmor. New high-resolution central schemes for nonlinear conservation laws and convection-diffusion equations. *J. Comput. Phys.*, 160(1): 241-282, 2000.